Lithos 178 (2013) 96–127

Contents lists available at ScienceDirect

Lithos

journal homepage: www.elsevier.com/locate/lithos

Invited review article

Geochemistry of subduction zone serpentinites: A review

Fabien Deschamps [a,*], Marguerite Godard [a], Stéphane Guillot [b], Kéiko Hattori [c]

[a] Géosciences Montpellier, Université Montpellier 2, CNRS, cc 060, Place E. Bataillon, 34095 Montpellier, France
[b] ISTerre, Université Grenoble I, CNRS, 1381 rue de la Piscine, 38400 Grenoble Cedex 09, France
[c] Department of Earth Sciences, University of Ottawa, Ottawa, Ontario K1N 6N5, Canada

ARTICLE INFO

Article history:
Received 5 October 2012
Accepted 31 May 2013
Available online 11 June 2013

Keywords:
Subducted serpentinites
Mantle wedge serpentinites
Abyssal peridotites
Serpentine phases
Subduction zones
Geochemistry

ABSTRACT

Over the last decades, numerous studies have emphasized the role of serpentinites in the subduction zone geodynamics. Their presence and role in subduction environments are recognized through geophysical, geochemical and field observations of modern and ancient subduction zones and large amounts of geochemical database of serpentinites have been created. Here, we present a review of the geochemistry of serpentinites, based on the compilation of ~900 geochemical data of abyssal, mantle wedge and exhumed serpentinites after subduction. The aim was to better understand the geochemical evolution of these rocks during their subduction as well as their impact in the global geochemical cycle.

When studying serpentinites, it is essential to determine their protoliths and their geological history before serpentinization. The geochemical data of serpentinites shows little mobility of compatible and rare earth elements (REE) at the scale of hand-specimen during their serpentinization. Thus, REE abundance can be used to identify the protolith for serpentinites, as well as magmatic processes such as melt/rock interactions before serpentinization. In the case of subducted serpentinites, the interpretation of trace element data is difficult due to the enrichments of light REE, independent of the nature of the protolith. We propose that enrichments are probably not related to serpentinization itself, but mostly due to (*sedimentary-derived*) fluid/rock interactions within the subduction channel after the serpentinization. It is also possible that the enrichment reflects the geochemical signature of the mantle protolith itself which could derive from the less refractory continental lithosphere exhumed at the ocean–continent transition.

Additionally, during the last ten years, numerous analyses have been carried out, notably using in situ approaches, to better constrain the behavior of fluid-mobile elements (FME; e.g. B, Li, Cl, As, Sb, U, Th, Sr) incorporated in serpentine phases. The abundance of these elements provides information related to the fluid/rock interactions during serpentinization and the behavior of FME, from their incorporation to their gradual release during subduction. Serpentinites are considered as a reservoir of the FME in subduction zones and their role, notably on arc magma composition, is underestimated presently in the global geochemical cycle.

Contents

* Corresponding author.
E-mail address: fabien.deschamps@gm.univ-montp2.fr (F. Deschamps).

0024-4937/$ – see front matter © 2013 Elsevier B.V. All rights reserved.
http://dx.doi.org/10.1016/j.lithos.2013.05.019

1. Introduction

Serpentinites (hydrated ultramafic rocks) and the processes of serpentinization have attracted much attention over the last two decades, and interest in these rocks continues unabated. It has recently been posited that the occurrence of serpentinites, specifically in subduction zones, could have important implications for the Earth's dynamic and global geochemical cycle (e.g. Hattori and Guillot, 2003; Hilairet et al., 2007). However, deciphering the origin of the serpentinites and the causalities of serpentinization remains a challenge as the onset of this particular process mostly occurs at the seafloor (near mid-ocean ridges, MOR) and continues during subduction of abyssal serpentinites and peridotites; moreover mantle wedge serpentinites are produced by fluids released from the subducting slab. A large number of high quality bulk rock compositions, as well as in situ geochemical data on serpentine phases, have now become available and hence correspond to a fully representative set of serpentinite compositions worldwide (see references through the text; Section 2.4). In this context, the present manuscript attempts to review the available geochemical data of abyssal peridotites and subduction zone-related serpentinites, including subducted and metamorphosed serpentinites and mantle wedge–forearc serpentinites. This review paper will emphasize the role of serpentinites on chemical cycling in subduction zones, and in doing so perhaps broach new concerns for the forthcoming studies.

This paper aims: (i) to review and to provide comprehensive geochemical compositions of serpentinites, as well as serpentine phases, in order to depict the influence and significance of protolith; (ii) to evaluate the role of fluid-mobile element (FME) compositions as tracers of fluid/rock interactions in geodynamic contexts and processes (temperature (T), pressure (P), redox conditions); and finally, (iii) to discuss the active role of serpentinites upon the global geochemical cycle in subduction zones. Notably, we summarize observations about interactions between various lithologies in the subducted slab and serpentinites into the subduction channel, and the fluids and fluid-mobile elements released during their metamorphism. We are fully aware about the non-exhaustive review of this synthesis and we refer the reader to the many outstanding studies cited below.

1.1. Subduction zones

Subduction zones are one of the most challenging geological contexts in Earth sciences. Since the first reference to these particular environments six decades ago (Amstutz, 1951), numerous studies have been undertaken in order to constrain their geophysical and geochemical signatures (see Stern, 2002, for a review). Subduction zones and oceanic convergent boundaries represent a total length of around 67,500 km (Bird, 2003; Lallemand, 1999). As a weak and buoyant mineral, and its broad P–T stability field, a serpentine mineral can play a key role in the dynamics of subduction zone, notably on the triggering of earthquakes, exhumation of HP to UHP rocks, and probably initiation of subduction itself (Hirth and Guillot, 2013). One of the most important features of subduction zones is the recycling of hydrated lithologies back into the mantle, the so called “subduction factory” (Tatsumi, 2005). This recycling mechanism has important consequences into the global geochemical cycling as well as on the dynamics of the Earth. Due to the downgoing movement of the hydrated oceanic lithosphere and its heating related to prograde metamorphism, fluids are progressively released from the slab. These fluids are considered to trigger partial melting within mantle wedge leading to arc magmatism (e.g. Green, 2007; Tatsumi et al., 1986). In this context, subduction-related metamorphism will play a major role in the dynamics, chemistry and rheology of subduction zones. Numerous studies were conducted in order to determine the water budget of the subducting lithosphere and the timing of water released (e.g. Rüpke et al., 2002; Schmidt and Poli, 1998; Van Keken et al., 2011). Dehydration mostly occurs during the first 100 to 170 km of subduction, depending on the geothermal gradient, and is related to the stability of key hydrous phases such as amphiboles (Pawley and Holloway, 1993; Poli and Schmidt, 1995) and serpentines (Ulmer and Trommsdorff, 1995; Wunder and Schreyer, 1997; Fig. 1a).

1.2. Water: an important component in subduction zone

Water is one of the most important components in subduction zone and its geochemical cycle. Water can be transported, and recycled, at different depths when it is stored into subducted sediments, and to a lesser extent in the oceanic lithosphere. Under the effect of subduction-related prograde metamorphism, water can also be released into the overlying mantle wedge and react with mantle peridotites to form hydrous minerals. Water is present in different forms: (1) molecular (H_2O) in magmas and/or silicate fluids released from the slab, (2) hydroxyl (OH^-) as part of hydrous phases (e.g. chlorite, amphibole, serpentine), (3) hydrogen as point defects in nominally

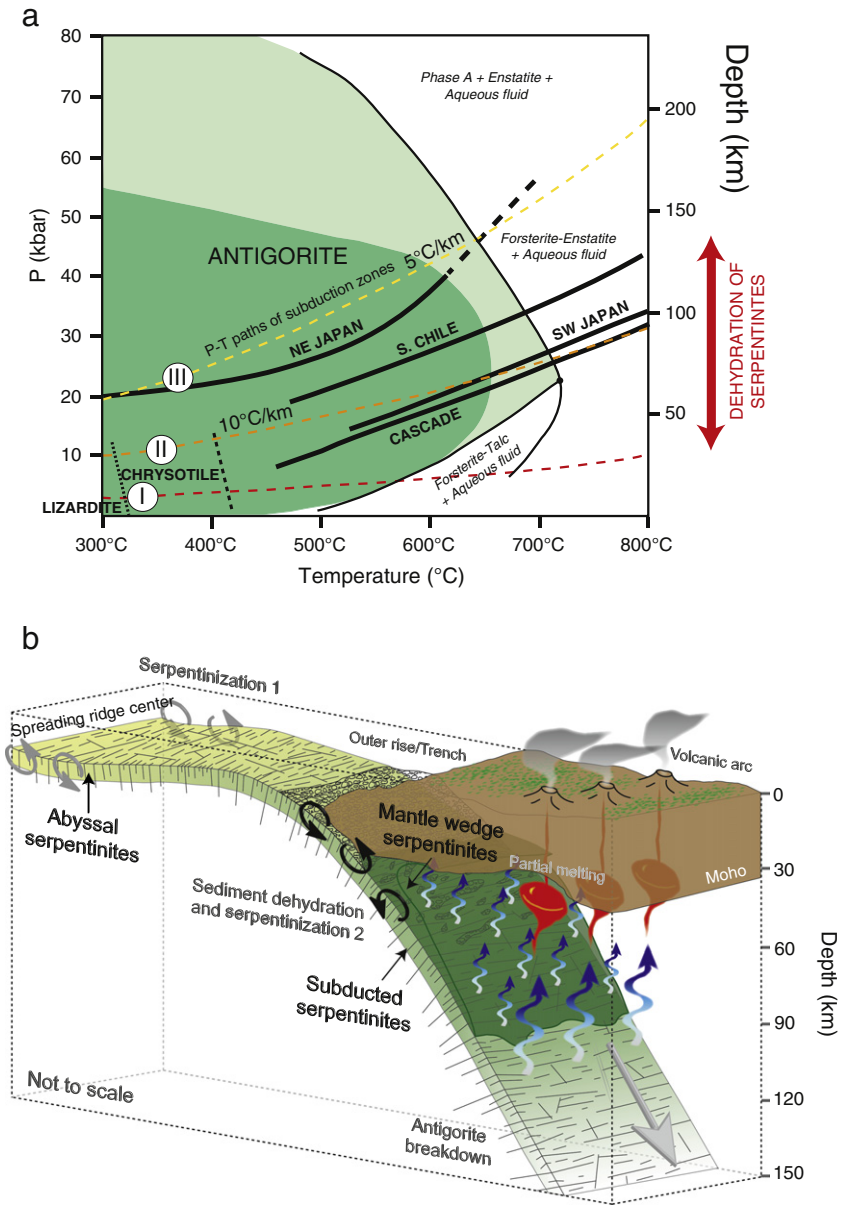

Fig. 1. a.) Stability fields of serpentine minerals after experimental observations in a P–T–depth diagram. Stability fields of antigorite was determined by studies of Wunder and Schreyer (1997) and Bromiley and Pawley (2003) (dark green field) and Ulmer and Trommsdorff (1995) (light green field). Thick solid curves represent different P–T paths of subduction zones (data sources are from Fukao et al., 1983; Furukawa, 1993; Peacock and Wang, 1999). Dashed curves are theoretical P–T paths for a subducted oceanic crust having different ages (Peacock, 1990). Theoretical depth where "antigorite breakdown" occurs is indicated by an arrow on the right part of the diagram. Modified after Hattori and Guillot (2003). b.) Schematic sketch illustrating the geological environment during subduction-related serpentinization as well as the geological impact of serpentinites in the subduction context.

anhydrous minerals such as olivine, pyroxene or garnet, or (4) supercritical fluids at high pressure (HP)–high temperature (HT) conditions. Behavior of water in subduction zone is relatively well constrained, notably through studies concerning the mineralogical changes associated to HP–LT (low temperature) metamorphism characteristics of subduction context and related dehydration reactions (e.g. Peacock, 1990; Schmidt and Poli, 1998). Experimental petrology on subduction zone lithologies has contributed significantly toward clarifying the influence of water (in its different forms) in various petrological processes during subduction. It results into phase diagrams that constrained stability field and water content for most common minerals in this context (e.g. Hacker et al., 2003). Nearly all metamorphic facies in subduction zones are able to transport significant quantity of water, despite dehydration processes. Taking the example of the oceanic crust, the average amount of water varies from 7 wt.% in the zeolite facies to 0.09 wt.% in the eclogite facies (Hacker et al., 2003). Thus, it seems that a very small amount of water is recycled back into the asthenospheric mantle.

The majority of subducted water is released from the slab lithologies and percolates through the mantle wedge. The main dewatering takes place by compaction at temperatures between 300 and 600 °C and at a pressure lower than 1.5 GPa (Rüpke et al., 2004). In mantle wedges, water is hosted by serpentine minerals, chrysotile (ctl)/lizardite (lz) and antigorite (atg), which can hold on an average of 13 wt.% of water until isotherms 600–700 °C (Ulmer and Trommsdorff, 1995; Wunder and Schreyer, 1997; Fig. 1a). Then, other hydrous minerals such as amphibole, chlorite, talc, mica, or phase A can bring water deeper but in less important quantity (Hacker et al., 2003; Schmidt and Poli, 1998). Above the 800 °C isotherm and 2 GPa, mantle peridotites cannot host water under hydroxyl form anymore (Ulmer and Trommsdorff, 1995).

Above the mantle wedge serpentinite layer, water percolates into the anhydrous mantle and can trigger partial melting, a process

which is at the heart of arc magmatism (e.g. Morris et al., 1990; Plank and Langmuir, 1993; Tatsumi, 1986). This theory is reinforced by observations of high concentrations of water in the arc magmas (on average 1.7 wt.%; Sobolev and Chaussidon, 1996) compared to those observed in primitive magmas from oceanic ridge (0.1–0.5 wt.%). Concerning the modality of water migration into the anhydrous mantle wedge, several possible scenarios are proposed (Stern, 2002): (1) for a cold lithosphere having a sufficient porosity, water is present under its molecular form, causing pore pressure to increase, which can subsequently trigger seismic rupture (Davies, 1999), (2) water circulation is also possible between mineral pores using an interconnected network, facilitating interaction between fluid and minerals, and (3) a third type, highlighted by numerical models, presents formation of cold plumes of serpentinites from the serpentinite layer to the mantle wedge (Gerya and Yuen, 2003).

1.3. Subduction-related serpentinites: water and fluid-mobile element carriers

Serpentinites are hydrated ultramafic rocks (with H_2O content up to 15–16 wt.%, average of 13 wt.%) which form through the alteration of olivine- and pyroxene-dominated protoliths at temperatures lower than 650–700 °C (e.g. Evans et al., 2013; Hemley et al., 1977; Janecky and Seyfried, 1986; O'Hanley, 1996). Water-rich and stable over a relatively important P–T range as demonstrated by experimental works (Bromiley and Pawley, 2003; Ulmer and Trommsdorff, 1995; Wunder and Schreyer, 1997; Fig. 1a), serpentinites are among the most efficient lithology to carry great amount of water at relatively great depths (120 to 170 km depth). Largely underestimated in the past (compared to metasediments and eclogites) in subduction zone models, an increasing number of studies on serpentinites were conducted over the last 20 years. It appears that serpentinites are widespread on oceanic floor (e.g. Cannat et al., 2010). In this context, it appeared that subducted serpentinites, and those resulting from the hydration of the mantle wedge, represent a particularly significant water reservoir influencing arc magmatism (Hattori and Guillot, 2003, 2007; Savov et al., 2005a; Scambelluri et al., 2001a, 2004a,b; Ulmer and Trommsdorff, 1995). In parallel, some studies on the trace element and isotope compositions of arc magmas have shown geochemical evidence for fluids released after dehydration of subduction-related serpentinites (e.g. Barnes et al., 2008; Singer et al., 2007; Tonarini et al., 2007). Additionally, serpentinites present strong enrichments in fluid-mobile elements (FME; e.g. B, Li, Cl, As, Sb, Pb, U, Cs, Sr, Ba; e.g. Bonatti et al., 1984; Deschamps et al., 2010, 2011, 2012; Hattori and Guillot, 2003, 2007; Kodolányi et al., 2012; Lafay et al., 2013; O'Hanley, 1996; Scambelluri et al., 2001a,b, 2004a, b; Tenthorey and Hermann, 2004; Vils et al., 2008, 2011). These enrichments result from fluid/rock interactions occurring for example at mid-ocean ridges after percolation of seawater and/or hydrothermal fluids, during subduction by percolation of fluids released from different lithologies from the slab, or also by interactions (mechanical, diffusive and/or fluid assisted) with metasediments during subduction.

During their subduction, serpentinites experience prograde metamorphism until their dehydration, the so-called antigorite breakdown (up to 600–700 °C; Fig. 1a). Fluids released from dehydrating serpentinites are rich in fluid-mobile elements as demonstrated by the experimental work of Tenthorey and Hermann (2004). These fluids are enriched in FME (such as B, Cs, As, Sb, Pb, Li, Ba); in parallel, Ryan et al. (1995) shown that FME are also enriched in arc magmas. Yet, despite considerable progress for characterizing the geochemistry of serpentinites in different geological contexts, little is known about the real impact they might have on the geochemistry of arc magmas. First, the trace-element fingerprint of the protolith, as well as primary minerals, upon the geochemistry of bulk serpentinites and mineral phases starts to become clearer. Second, the sequence of enrichment in FME and its relation to geological contexts are still unclear and need further clarifications since FME are a powerful tool to discriminate serpentinites (e.g. De Hoog et al., 2009; Deschamps et al., 2010, 2011, 2012; Kodolányi et al., 2012). Additionally, recent studies have emphasized geochemical interactions between serpentinites and metasediments in the accretionary prism and subduction channel (Deschamps et al., 2010, 2011, 2012; Lafay et al., 2013). Third, the role of serpentinite-derived fluids in subduction zone is not perfectly understood and no geochemical tracers (elements or isotopes) are discriminating enough to highlight the role of serpentinites upon arc magma geochemical signature, as it is the case for sediments.

2. Nature, formation and location of subduction-related serpentinites

The geochemistry of serpentinites is influenced by the geodynamic setting in which they were formed. Their composition is a function of the temperature of formation and the nature of hydrating fluids; the last parameters being controlled by the geological settings. We distinguish three groups of serpentinites present in subduction zone: abyssal, mantle wedge, and subducted serpentinites (Fig. 1b). Abyssal serpentinites represent hydration of oceanic peridotites by seafloor hydrothermal activity/seawater alteration. Mantle wedge serpentinites are hydrated mantle peridotites by fluid released from the subducted slabs. Subducted serpentinites are more heterogeneous in terms of timing of serpentinization: they are found mostly in suture zones and associated with HP–LT metamorphic rocks. They can originate either from abyssal peridotites hydrated at ridges, trenches or within the subduction channel or from the oceanic–continent transition zone (OCT).

2.1. Abyssal serpentinites

In this paper, we will focus our review on oceanic lithosphere formed at slow (1 to 5 $cm \cdot yr^{-1}$) to ultraslow (<2 $cm \cdot yr^{-1}$) spreading ridges, which represent about one third of the 55,000 km of global ridge system (Dick et al., 2003). Such ridges are characterized by episodic magmatic and tectonic activities causing exposure of the sub-oceanic mantle during amagmatic periods (Cannat, 1993; Cannat et al., 1995; Karson et al., 2006). The relatively thin oceanic crust (1 to 7 km), and the presence of numerous normal faults on the flank of the ridge axis, induce deep fluid circulation and serpentinization of the oceanic lithosphere (Epp and Suyenaga, 1978; Francis, 1981; Mével, 2003). The formation of secondary low-pressure/low-temperature minerals such as prehnite, amphibole, chlorite, and clay minerals are a good sink for water. Hence, basalts from the upper part of the oceanic lithosphere could carry 2 to 6 wt.% of water (Hacker et al., 2003; Peacock, 1990; Schmidt and Poli, 1998), but the majority of water in the oceanic lithosphere is in serpentinites since they can hold on an average of 13 wt.% of H_2O. In addition, they are representing 5 to 25% for the Atlantic seafloor (Cannat et al., 1995, 2010; Carlson, 2001; Mével, 2003). This makes serpentinite an important host of water in oceanic lithosphere formed at slow spreading ridges.

Abyssal serpentinites and hydrated peridotites (both terms are commonly used in the literature) are observed mostly at slow to ultraslow spreading ridges (Fig. 2) where (a) oceanic mantle peridotites are commonly exposed on the seafloor, (b) along normal fault related to crustal thinning and extension, (c) on the seafloor warping oceanic core complexes (e.g. Cannat, 1993; Escartin et al., 2003; MacLeod et al., 2009; Michael et al., 2003), and (d) along major scarps and transform faults (Bideau et al., 1991; Bonatti, 1976; Epp and Suyenaga, 1978; Francis, 1981; Karson and Lawrence, 1997; Morishita et al., 2009; O'Hanley, 1991; for a review, refer to Mével, 2003). Previous studies have shown that seawater is the main fluid responsible for the hydration of abyssal peridotites based on oxygen and hydrogen isotope compositions (it appears that serpentinization occurs for temperature

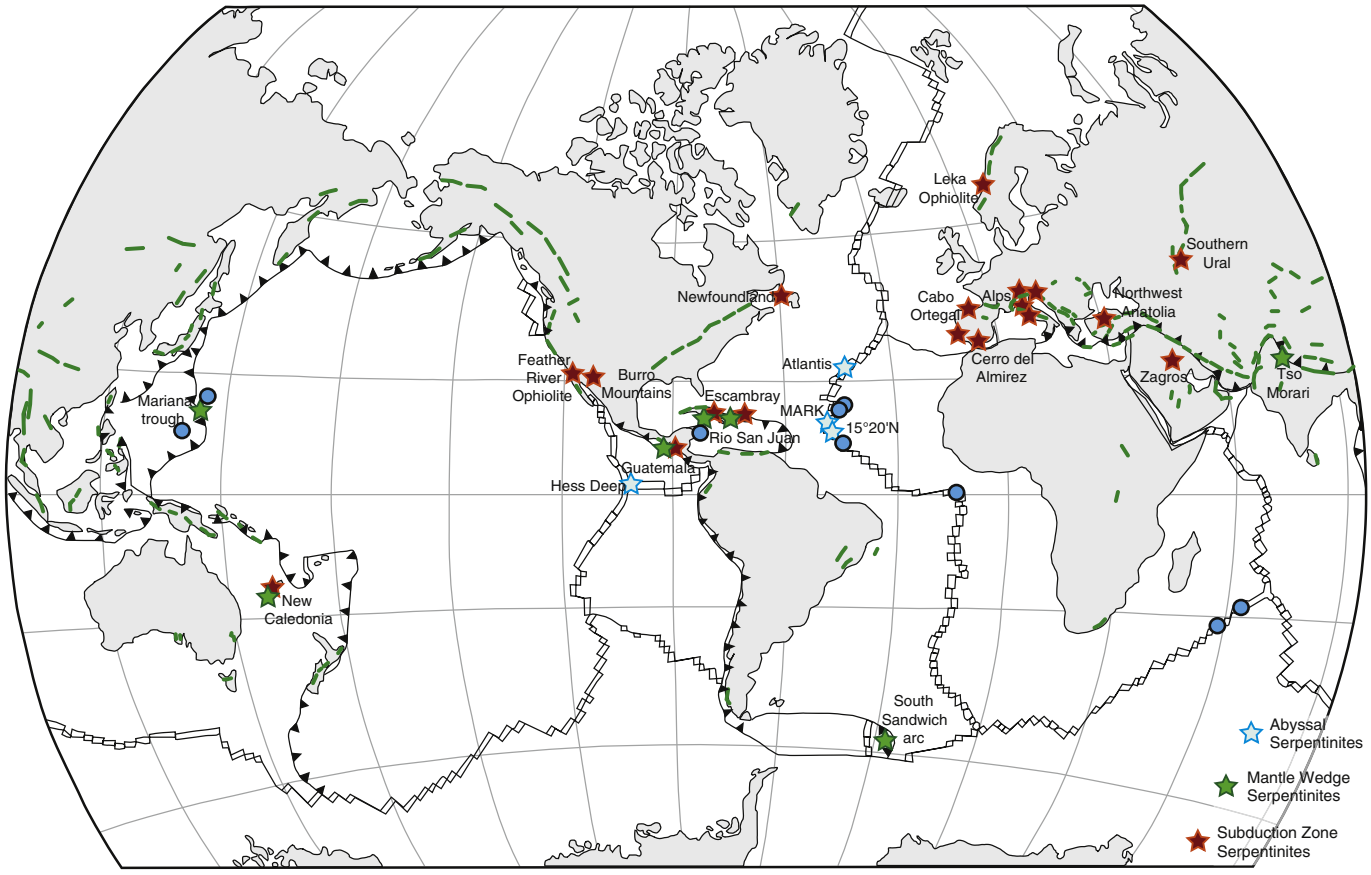

Fig. 2. Worldwide occurrences of serpentinite outcrops and massifs used for this compilation. Three types of serpentinites are distinguished: abyssal (blue star), subducted (red star) and mantle wedge serpentinites (green star). Abyssal serpentinites are represented by samples from MARK Zone-ODP Leg 209 (Jöns et al., 2010; Kodolányi et al., 2012; Paulick et al., 2006), Atlantis Massif-IODP Exp. 304–305 (Delacour et al., 2008), Logatchev hydrothermal field (Augustin et al., 2012) and Hess Deep (Kodolányi et al., 2012). Mantle wedge serpentinites are after studies from the Mariana forearc-ODP Legs 125 and 195 (Ishii et al., 1992; Kodolányi et al., 2012; Lagabrielle et al., 1992; Parkinson and Pearce, 1998; Savov et al., 2005a,b, 2007), Tso Morari massif Himalaya (Deschamps et al., 2010; Guillot et al., 2001; Hattori and Guillot, 2007), Dominican Republic (Deschamps et al., 2012; Saumur et al., 2010), Cuba (Mayarí massif, Marchesi et al., 2006; Blanco-Quintero et al., 2011), South Sandwich arc (Pearce et al., 2000) and New Caledonia (Marchesi et al., 2009; Ulrich et al., 2010). Subducted and subduction-related serpentinites are compiled from the studies of the European Alps (Chenaillet: Chalot-Prat et al., 2003; Queyras: Hattori and Guillot, 2007; Lafay et al., 2013; Erro–Tobbio massif: Scambelluri et al., 2001b; Zermatt-Saas ophiolite: Li et al., 2004; Elba, Monti Livornesi and Murlo: Anselmi et al., 2000; Viti and Mellini, 1998; Slovenska Bistrica ultramafic complex in Slovenia; De Hoog et al., 2009), the Greater Antilles (Blanco-Quintero et al., 2011; Deschamps et al., 2012; Hattori and Guillot, 2007; Saumur et al., 2010), Cerro del Almirez ultramafic complex (Spain; Garrido et al., 2005), Cabo Ortegal massif (Spain; Pereira et al., 2008), Leka ophiolite complex (Norway; Iyer et al., 2008), Zagros suture zone (Iraq; Aziz et al., 2011), ophiolite complexes of Northwest Anatolia (Turkey, Aldanmaz and Koprubasi, 2006), Feather River ophiolite (California, U.S.A.; Li and Lee, 2006; Agranier et al., 2007), and Burro mountain (California, U.S.A.; Coleman and Keith, 1971). We report also major occurrences of serpentinites on continents (green lines; after Coleman, 1977) and major seafloor sites where serpentinites were recognized (blue circles).

lower than 450–500 °C in this context; Agrinier and Cannat, 1997; Früh-Green et al., 1996). In contrast to slow spreading ridges, fast spreading ridges (>9 cm·yr^{-1} of opening) present a more important magmatic activity, leading to the formation of a thick oceanic crust (7–10 km in thickness). Abyssal peridotites in this context cannot outcrop on the seafloor (Sinton and Detrick, 1992), preventing the serpentinization effect. To our knowledge, the only evidence of serpentinized peridotites in this context is documented at rare tectonic windows (e.g. Hess Deep; Mével and Stamoudi, 1996).

Oceanic serpentinization is mostly controlled by fractures ranging in size from the grain to the metric scale (Andreani et al., 2007), but mechanisms of fluid transfer and their depth extension are not yet well constrained. Nevertheless, stability field of observed serpentine phases (essentially lizardite and chrysotile), coupled to stable isotope studies indicate that serpentinization is present down to a depth of around 7 km (Escartin et al., 1997) and for a maximum temperature of 450–500 °C (Evans et al., 1976). Similar conclusions were reached in the study of the microseismicity recorded on the seafloor, which revealed the presence of faults with a vertical extent from 2 to 9 km (Kong et al., 1992); such faults allow seawater to penetrate to such depths. Abyssal serpentinites are characterized by pseudomorphic texture suggesting a static serpentinization by pervasive fluids infiltration (Aumento and Loubat, 1971; Prichard, 1979; Wicks and Whittaker, 1977). Some authors have described an initial high-temperature stage (~400 °C) marked by relict textures of orthopyroxene replaced by tremolite and talc (Mid-Atlantic Ridge, Sites 1270 and 1271; Allen and Seyfried, 2003; Bach et al., 2004; Paulick et al., 2006). Low temperature alteration, the so-called seafloor alteration, is also recorded in serpentinites and is documented by the formation and/or precipitation of aragonite veinlets, Fe-oxyhydroxides, and clay minerals (Paulick et al., 2006).

2.2. Mantle wedge serpentinites

Mantle wedge is generally described as the part of mantle between the upper part of subducting lithosphere and lower part of the overriding plate. We include under this term forearc serpentinites having a mantle wedge affinity (e.g. Marianas). Forearc sensu stricto is located between trench and an associated volcanic arc; it could be filled with sediments, oceanic crustal material and mantle peridotites hydrated at the base of the mantle wedge by fluids from the slab. Mantle wedge serpentinites s.s. are located in deepest and hotter parts of the supra-subduction mantle and defined as a km-thick layer along the subduction plane, while the forearc serpentinites are

located in the coldest parts of the top-slab mantle, closer to the slab (the cold nose, e.g. Guillot et al., 2009). We are fully aware that absysal serpentinites could be also incorporated into the forearc and a distinction was made for this compilation. Since forearc serpentinites historically refer to rocks having a mantle wedge affinity (e.g. Marianas), we decide to combine both type of serpentinites (forearc and mantle wedge) throughout this manuscript.

The mantle wedge has complex geochemical characteristics due to the continual input from the underlying subducted slab, and the output of melt for arc volcanoes. Seismic tomography shows abnormal low seismic zone correlated to strong seismic attenuation and interpreted as a witness of a hot and ductile mantle (Stern, 2002). However, this low viscosity area could also be explained by the presence of fluids and magmas resulting from the slab dehydration (Currie et al., 2004; Hyndman et al., 2005; Kelemen et al., 2003). Some authors propose that the mantle flow induced by the downwelling slab is able to create an upwelling of asthenospheric mantle toward the surface, and then create a thinning of the overlying lithosphere which will contribute to hot temperature for partial melting (Eberle et al., 2002). Additionally, numerical models using thermo-mechanical-dependent rheology indicate that shear heating could increase the temperature within the mantle wedge and create melting by adiabatic decompression (Cagnioncle et al., 2007; van Keken et al., 2002). Presence of fluids and melts will also reduce the viscosity of the mantle (Hirth and Kohlstedt, 1996; Korenaga and Karato, 2008) and possibly control the geodynamics of the mantle wedge (Arcay et al., 2005).

Rare occurrence of xenoliths from mantle wedges indicates relatively high degree of partial melting leading to their depletion (Arai, 1994; Dick and Bullen, 1984). Mantle wedge xenoliths are also characterized by higher oxygen fugacity than abyssal peridotites (Ballhaus et al., 1991; Parkinson and Arculus, 1999). Back arc peridotites are often harzburgites with chromian spinel having high Cr# (= atomic ratio of $Cr/(Cr + Al) > 0.4$; Arai and Ishimaru, 2008). Mg# (= atomic ratio of $Mg \times 100/(Mg + Fe^{2+})$) of spinels is in general lower than in abyssal peridotites for a given Cr# (Arai and Ishimaru, 2008; Ishii et al., 1992). Na_2O content of clinopyroxene is typically low, and associated hydrous phases (such as clinochlore, amphibole, phlogopite) are characterized by low Ti content (Arai and Ishimaru, 2008). Studies of xenoliths have also shown the strong influence of metasomatism and its consequences, such as strong Si enrichments and formation of hydrated phases and sulfides (Arai and Ishimaru, 2008). Si-enrichment of some depleted harzburgites from mantle wedge results in the formation of secondary orthopyroxene, replacing olivine (Wang et al., 2008). Moreover, aqueous fluids in equilibrium with peridotites are also enriched in SiO_2 compared to MgO (Mibe et al., 2002; Nakamura and Kushiro, 1974), although this point remains controversial (Canil, 1992; Kelemen et al., 1998; Melekhova et al., 2007; Stalder and Ulmer, 2001). Formation of secondary hydrous minerals, such as clinochlore, pargasite and phlogopite, is common and results from the percolation of metasomatic agents (Wang et al., 2007). These hydrous phases are sometimes characterized by low TiO_2 content (western Pacific: Arai et al., 2007; Colorado Plateau: Smith, 1979; Smith et al., 1999; Wyoming Craton: Downes et al., 2004). These observations are in agreement with the percolation of a Ti-poor fluid coming from the slab as described by Keppler (1996).

The mantle wedge is continually percolated by fluids released from the dehydration of subducted lithologies such as sediments, altered basalts and gabbros, and serpentinites. The depth of dehydration depends on the stability field of hydrous phases and on the local geotherm: this point will be discussed in Section 4. Water released from the slab will percolate upward by buoyancy, induce the hydration of the mantle wedge, and in particular serpentinize when its temperature is lower than 700 °C (Bebout and Barton, 1989; Bostock et al., 2002; DeShon and Schwartz, 2004; Fryer et al., 1985; Gill, 1981; Guillot et al., 2000; Hattori and Guillot, 2003; Hyndman and Peacock, 2003; Kamiya and Kobayashi, 2000; Mottl et al., 2004; Peacock, 1987a,b, 1993). Serpentinites play an important role on the dynamics of mantle wedge. Due to the strong contrast in density and viscosity between newly formed serpentinites (2.6 g/cm^3) and anhydrous peridotites (3.2 g/cm^3), they can facilitate exhumation of high pressure subducted rocks often observed in accretionary prism (Guillot et al., 2000, 2001, 2009; Hermann et al., 2000; Schwartz et al., 2001). This process is well recognized today in the Mariana subduction zone with the formation of serpentinite seamounts in forearc position (Fryer, 1992; Fryer and Fryer, 1987; Fryer and Salisbury, 2006; Sakai et al., 1990; Savov et al., 2005a,b, 2007).

2.3. Subduction zone-related serpentinites

Subducted serpentinites represent serpentinites which were incorporated into subduction zone, subducted, and then exhumed in the accretionary complex or suture zone. Two main protoliths are possible for these serpentinites: (1) subducted oceanic peridotites and (2) continental peridotites exhumed and hydrated by seawater during rifting at the OCT (Boillot et al., 1980; Skelton and Valley, 2000). However, it is generally impossible to identify and distinguish these two groups on the field since all serpentinites appear very similar.

During subduction, sediments and altered oceanic crust are progressively dehydrated and interact with the subducted abyssal serpentinites and partially hydrate peridotites (e.g. Deschamps et al., 2012; van Keken et al., 2011). Here, apparent sink of fluid system emplaced at the top of the subduction plan is geophysically imaged in active subduction zone (Kawakatsu and Watada, 2007). Thus, a second serpentinization occurs along faults when the slab bends near the trench (e.g. Kerrick, 2002). This process allows the penetration of seawater-derived fluids, physically contaminated by sediments, along cracks and crustal normal faults (Contreras-Reyes et al., 2007; Ranero et al., 2003, 2005). As this process occurs at relatively shallow depth (<20 km), chrysotile mostly recrystallizes to lizardite, while oceanic lizardite is still stable. Thus serpentinites are dominated by lizardite-type. Downward, with increasing P–T conditions, lizardite is progressively transformed into antigorite around 400 °C and interacts with surrounding partly hydrated sediments (Deschamps et al., 2011, 2012; Lafay et al., 2013). Interactions between sediments and serpentinites favored the transfer of FME to serpentinites producing a specific signature of subducted abyssal antigorite-type serpentinites (see Section 4).

Additionally, serpentine minerals are generally thought to form at the subduction plan interface a relatively thin layer. This zone, at the interface between the relatively dry slab and the relatively dry wedge, is considered to be 5 to 10 km thick extending from ca. 20 to 80 km depth (Hilairet and Reynard, 2009; Schwartz et al., 2001) and define the so-called serpentinite subduction channel (Guillot et al., 2000, 2001, 2009). Such a layer has been geophysically observed with receiver function imaging on the top of the subducting plate of Japan at depth comprising between 80 and 140 km (Kawakatsu and Watada, 2007). In parallel, numerical simulations (Gerya and Stöckhert, 2002; Gerya et al., 2002; Gorczyk et al., 2007) suggest that this serpentinite channel is able to incorporate abundant subducted abyssal serpentinites, high pressure rocks from subducting slabs, and serpentinized peridotites from the overlying mantle wedge. All these units and/or fragments of rocks can be decoupled from the crust or mantle wedge and subsequently exhumed within the channel and accreted to form the accretionary wedge. Evidence of such mélange zone is observed in many locations (e.g. Blanco-Quintero et al., 2011; Deschamps et al., 2012; Saumur et al., 2010), notably the association of serpentinites with eclogitic rocks; almost 30% of Phanerozoic eclogitic massifs are associated with serpentinites (Guillot et al., 2009).

Table 1
Average compositions, standard deviation, and maximum and minimum values for abyssal, mantle wedge, and subducted compiled serpentinites (after dunite and harzburgite). Note that talc-dominated serpentinites observed in abyssal context were removed, as well as serpentinite muds observed in mantle wedge setting. Refertilized samples are serpentinites which experienced melt/rock interactions prior to serpentinization (see text).

	Abyssal serpentinites				Abyssal serpentinites				Abyssal serpentinites				Abyssal serpentinites			
Protolith	Dunite				Dunite–refertilized				Harzburgite				Harzburgite–refertilized			
# samples	n = 20				n = 5				n = 48				n = 30			
	Average	*Std. Dev.*	*Max.*	*Min.*	Average	*Std. Dev.*	*Max.*	*Min.*	Average	*Std. Dev.*	*Max.*	*Min.*	Average	*Std. Dev.*	*Max.*	*Min.*
Major elements (wt.%)																
SiO_2	36.09	*4.05*	*41.83*	*26.74*	36.47	*2.95*	*40.65*	*33.08*	38.59	*1.60*	*42.56*	*35.60*	40.17	*2.64*	*44.58*	*35.53*
TiO_2	0.02	*0.01*	*0.03*	*0.01*	0.02	*0.01*	*0.03*	*0.01*	0.01	*0.00*	*0.02*	*0.00*	0.03	*0.02*	*0.06*	*0.01*
Al_2O_3	0.40	*0.23*	*0.74*	*0.04*	0.62	*0.29*	*0.96*	*0.19*	0.60	*0.15*	*0.99*	*0.13*	0.86	*0.30*	*1.34*	*0.26*
Cr_2O_3	0.45	*0.09*	*0.55*	*0.39*	–	–	–	–	0.35	*0.11*	*0.51*	*0.19*	–	–	–	–
Fe_2O_3 (t)	8.56	*2.03*	*12.95*	*4.96*	8.79	*0.61*	*9.72*	*8.08*	7.21	*0.49*	*8.35*	*6.08*	7.92	*1.36*	*11.53*	*6.14*
MnO	0.10	*0.03*	*0.18*	*0.05*	0.10	*0.01*	*0.12*	*0.08*	0.09	*0.02*	*0.13*	*0.05*	0.11	*0.02*	*0.16*	*0.07*
NiO	0.24	*0.03*	*0.27*	*0.20*	–	–	–	–	0.28	*0.02*	*0.30*	*0.26*	–	–	–	–
MgO	38.26	*4.30*	*42.64*	*26.60*	39.50	*1.71*	*40.95*	*36.57*	39.68	*1.24*	*42.64*	*36.56*	37.34	*1.68*	*39.94*	*34.60*
CaO	0.18	*0.16*	*0.55*	*0.03*	0.40	*0.54*	*1.20*	*0.03*	0.39	*0.59*	*3.78*	*0.03*	0.60	*0.83*	*2.85*	*0.04*
Na_2O	0.10	*0.06*	*0.22*	*0.00*	0.12	*0.04*	*0.17*	*0.06*	0.08	*0.05*	*0.18*	*0.00*	0.11	*0.05*	*0.20*	*0.01*
K_2O	0.02	*0.01*	*0.03*	*0.01*	0.01	*0.00*	*0.01*	*0.01*	0.01	*0.00*	*0.03*	*0.01*	0.03	*0.02*	*0.06*	*0.01*
P_2O_5	0.02	*0.01*	*0.04*	*0.01*	0.01	*0.01*	*0.02*	*0.01*	0.01	*0.00*	*0.01*	*0.01*	0.01	*0.01*	*0.03*	*0.01*
L.O.I.	14.21	*2.99*	*22.76*	*11.66*	13.31	*1.91*	*15.20*	*10.28*	12.96	*1.48*	*15.43*	*7.61*	12.48	*0.96*	*13.79*	*9.98*
Total	99.53	*0.61*	*100.35*	*97.84*	99.26	*0.92*	*100.58*	*98.26*	99.71	*0.66*	*100.76*	*97.81*	99.60	*0.45*	*100.68*	*98.73*
Trace elements (ppm)																
B	–	–	–	–	–	–	–	–	44.56	*28.08*	*111.96*	*14.89*	–	–	–	–
Li	0.82	*0.91*	*2.38*	*0.09*	11.00	–	*11.00*	*11.00*	0.63	*0.41*	*1.57*	*0.06*	8.01	*6.05*	*27.60*	*2.20*
Be	0.00	*0.00*	*0.01*	*0.00*	–	–	*0.00*	*0.00*	0.00	*0.00*	*0.01*	*0.00*	–	–	–	–
Cl	–	–	–	–	–	–	–	–	2802	*2035*	*6640*	*1280*	–	–	–	–
Co	111	*18*	*152*	*74*	95	*28*	*112*	*45*	97	*7*	*112*	*80*	101	*39*	*219*	*9*
Ni	2193	*446*	*3760*	*1330*	1762	*864*	*2273*	*253*	2062	*112*	*2390*	*1880*	1598	*704*	*2430*	*36*
Zn	44	*14*	*84*	*18*	48	*12*	*61*	*38*	41	*4*	*50*	*34*	258	*488*	*1870*	*40*
Cr	1734	*1026*	*3967*	*37*	2046	*373*	*2450*	*1716*	2066	*1040*	*5180*	*640*	2274	*1804*	*10033*	*41*
Cu	11	*9*	*35*	*1*	7	*8*	*21*	*3*	9	*10*	*50*	*1*	1500	*5184*	*26921*	*2*
As	0.42	*0.10*	*0.71*	*0.32*	0.68	*0.50*	*1.26*	*0.36*	0.50	*0.28*	*1.46*	*0.26*	5.52	*4.51*	*12.34*	*0.70*
Sb	0.10	*0.08*	*0.15*	*0.00*	–	–	–	–	0.01	*0.01*	*0.03*	*0.00*	1.25	*1.61*	*4.10*	*0.01*
Rb	0.11	*0.12*	*0.43*	*0.00*	0.07	*0.01*	*0.08*	*0.06*	0.05	*0.04*	*0.19*	*0.01*	0.92	*1.62*	*6.80*	*0.06*
Sr	353.04	*1251.45*	*5274*	*0.44*	27.11	*58.34*	*131.46*	*0.39*	11.90	*70.56*	*463.77*	*0.26*	118.60	*333.75*	*1631.00*	*1.56*
Y	0.14	*0.15*	*0.50*	*0.01*	0.96	*1.09*	*2.89*	*0.35*	0.08	*0.12*	*0.83*	*0.01*	1.86	*1.98*	*9.27*	*0.35*
Zr	0.52	*0.83*	*3.59*	*0.03*	3.06	*3.86*	*9.38*	*0.29*	0.11	*0.13*	*0.58*	*0.01*	4.39	*5.92*	*20.80*	*0.04*
Nb	0.05	*0.06*	*0.24*	*0.00*	0.13	*0.15*	*0.39*	*0.04*	0.01	*0.01*	*0.05*	*0.00*	0.75	*1.00*	*3.94*	*0.01*
Cd	0.04	*0.04*	*0.09*	*0.00*	–	–	–	–	0.01	*0.00*	*0.01*	*0.00*	–	–	–	–
Cs	0.01	*0.01*	*0.02*	*0.00*	0.01	*0.01*	*0.02*	*0.00*	0.00	*0.00*	*0.02*	*0.00*	0.13	*0.25*	*0.83*	*0.00*
Ba	1.750	*1.762*	*7.852*	*0.037*	4.184	*3.979*	*8.955*	*0.128*	0.812	*1.112*	*3.548*	*0.022*	20.988	*37.334*	*136.000*	*0.360*
La	0.100	*0.132*	*0.461*	*0.002*	0.160	*0.155*	*0.421*	*0.025*	0.023	*0.057*	*0.308*	*0.000*	0.700	*0.718*	*2.590*	*0.070*
Ce	0.144	*0.195*	*0.715*	*0.003*	0.515	*0.576*	*1.517*	*0.089*	0.044	*0.115*	*0.644*	*0.001*	1.466	*1.586*	*5.980*	*0.070*
Pr	0.015	*0.018*	*0.056*	*0.000*	0.082	*0.094*	*0.245*	*0.014*	0.006	*0.016*	*0.092*	*0.000*	0.191	*0.210*	*0.905*	*0.010*
Nd	0.056	*0.071*	*0.220*	*0.002*	0.437	*0.527*	*1.359*	*0.081*	0.028	*0.077*	*0.447*	*0.000*	0.837	*0.939*	*4.340*	*0.080*
Sm	0.013	*0.015*	*0.043*	*0.001*	0.123	*0.152*	*0.389*	*0.021*	0.008	*0.022*	*0.135*	*0.000*	0.218	*0.246*	*1.190*	*0.030*
Eu	0.037	*0.049*	*0.186*	*0.000*	0.031	*0.020*	*0.064*	*0.014*	0.020	*0.066*	*0.401*	*0.000*	0.152	*0.254*	*1.370*	*0.011*
Gd	0.015	*0.016*	*0.047*	*0.001*	0.161	*0.195*	*0.504*	*0.040*	0.008	*0.025*	*0.163*	*0.000*	0.256	*0.288*	*1.370*	*0.010*
Tb	0.003	*0.003*	*0.007*	*0.000*	0.027	*0.034*	*0.086*	*0.007*	0.001	*0.004*	*0.025*	*0.000*	0.048	*0.051*	*0.235*	*0.007*
Dy	0.019	*0.018*	*0.054*	*0.002*	0.192	*0.228*	*0.594*	*0.059*	0.012	*0.025*	*0.167*	*0.001*	0.302	*0.324*	*1.490*	*0.020*
Ho	0.005	*0.004*	*0.014*	*0.000*	0.041	*0.049*	*0.127*	*0.014*	0.003	*0.005*	*0.033*	*0.000*	0.068	*0.069*	*0.313*	*0.010*
Er	0.017	*0.014*	*0.046*	*0.001*	0.117	*0.139*	*0.364*	*0.040*	0.012	*0.012*	*0.086*	*0.002*	0.191	*0.192*	*0.869*	*0.030*
Tm	0.003	*0.002*	*0.007*	*0.000*	0.018	*0.021*	*0.054*	*0.006*	0.003	*0.002*	*0.013*	*0.001*	0.030	*0.029*	*0.127*	*0.005*
Yb	0.027	*0.021*	*0.081*	*0.004*	0.122	*0.131*	*0.352*	*0.044*	0.022	*0.012*	*0.081*	*0.006*	0.208	*0.191*	*0.822*	*0.040*
Lu	0.007	*0.007*	*0.029*	*0.001*	0.020	*0.022*	*0.058*	*0.007*	0.005	*0.002*	*0.013*	*0.002*	0.032	*0.028*	*0.121*	*0.008*
Hf	0.019	*0.035*	*0.090*	*0.000*	0.152	*0.126*	*0.267*	*0.018*	0.003	*0.004*	*0.017*	*0.000*	0.158	*0.206*	*0.730*	*0.000*
Ta	0.011	*0.010*	*0.039*	*0.000*	0.013	*0.007*	*0.019*	*0.002*	0.005	*0.007*	*0.035*	*0.000*	0.056	*0.068*	*0.234*	*0.000*
W	–	–	–	–	–	–	–	–	–	–	–	–	0.055	*0.018*	*0.082*	*0.035*
Pb	0.220	*0.234*	*0.978*	*0.003*	0.243	*0.167*	*0.508*	*0.068*	0.388	*1.346*	*7.789*	*0.003*	9.548	*33.690*	*162.000*	*0.033*
Th	0.009	*0.018*	*0.068*	*0.000*	0.033	*0.038*	*0.060*	*0.006*	0.001	*0.002*	*0.010*	*0.000*	0.167	*0.367*	*1.850*	*0.000*
U	0.375	*0.336*	*1.069*	*0.001*	0.362	*0.380*	*0.741*	*0.007*	0.157	*0.329*	*1.287*	*0.000*	1.420	*1.864*	*7.600*	*0.020*
S	0.16	*0.14*	*0.65*	*0.04*	0.12	*0.06*	*0.20*	*0.05*	0.25	*0.41*	*2.09*	*0.04*	0.05	*0.01*	*0.05*	*0.04*
V	16.07	*8.83*	*34.94*	*1.00*	25.46	*12.57*	*39.66*	*15.76*	23.63	*5.74*	*32.92*	*5.68*	45.43	*36.02*	*174.00*	*14.00*
Ga	0.41	*0.15*	*0.58*	*0.31*	–	–	–	–	0.58	*0.21*	*0.84*	*0.18*	2.30	*2.58*	*12.10*	*0.45*
Mo	–	–	–	–	–	–	–	–	–	–	–	–	0.62	*0.11*	*0.76*	*0.45*
Sc	4.40	*1.28*	*6.42*	*2.14*	9.16	*7.88*	*23.16*	*4.94*	6.53	*1.31*	*10.39*	*3.38*	9.85	*7.46*	*36.90*	*3.60*
Sn	–	–	–	–	–	–	–	–	–	–	–	–	0.22	*0.08*	*0.31*	*0.09*
Ti	53.34	*49.01*	*134.87*	*11.34*	142.87	–	*142.87*	*142.87*	28.23	*20.31*	*103.87*	*3.68*	342.87	–	*342.87*	*342.87*

N.B.: Provenance of compiled serpentinites is indicated in Fig. 2.

Mantle wedge serpentinites				Mantle wedge serpentinites				Mantle wedge serpentinites				Mantle wedge serpentinites			
Dunite				Dunite–refertilized				Harzburgite				Harzburgite–refertilized			
n = 88				n = 7				n = 73				n = 2			
Average	*Std. Dev.*	*Max.*	*Min.*	Average	*Std. Dev.*	*Max.*	*Min.*	Average	*Std. Dev.*	*Max.*	*Min.*	Average	*Std. Dev.*	*Max.*	*Min.*
37.38	*2.05*	*39.91*	*32.51*	38.60	*3.08*	*40.59*	*35.05*	39.82	*2.23*	*44.85*	*35.31*	–	–	–	–
0.02	*0.02*	*0.12*	*0.00*	0.02	*0.01*	*0.03*	*0.02*	0.01	*0.01*	*0.03*	*0.00*	–	–	–	–
0.60	*0.62*	*3.09*	*0.01*	0.56	*0.20*	*0.77*	*0.37*	0.54	*0.30*	*1.14*	*0.12*	–	–	–	–
0.32	*0.08*	*0.43*	*0.23*	–	–	–	–	0.41	*0.11*	*0.54*	*0.31*	–	–	–	–
7.52	*1.34*	*9.90*	*3.81*	7.32	*0.43*	*7.59*	*6.83*	7.65	*0.54*	*9.00*	*6.58*	–	–	–	–
0.11	*0.02*	*0.16*	*0.05*	0.11	*0.02*	*0.13*	*0.09*	0.11	*0.01*	*0.14*	*0.08*	–	–	–	–
0.28	*0.03*	*0.32*	*0.25*	–	–	–	–	0.29	*0.01*	*0.30*	*0.28*	–	–	–	–
41.26	*3.58*	*47.41*	*31.58*	39.48	*2.62*	*41.82*	*36.65*	40.16	*3.47*	*46.77*	*33.71*	–	–	–	–
0.52	*0.94*	*6.54*	*0.01*	0.66	*0.38*	*1.05*	*0.29*	0.29	*0.18*	*0.76*	*0.02*	–	–	–	–
0.07	*0.06*	*0.25*	*0.00*	–	–	–	–	0.03	*0.02*	*0.07*	*0.01*	–	–	–	–
0.02	*0.02*	*0.05*	*0.00*	–	–	–	–	0.02	*0.01*	*0.04*	*0.01*	–	–	–	–
0.03	*0.04*	*0.11*	*0.01*	0.01	*0.01*	*0.01*	*0.00*	0.06	*0.06*	*0.15*	*0.00*	–	–	–	–
13.01	*3.37*	*18.40*	*6.19*	13.30	*3.60*	*17.00*	*9.80*	10.81	*5.53*	*18.15*	*0.13*	–	–	–	–
99.60	*0.69*	*100.74*	*98.27*	100.57	*0.18*	*100.70*	*100.36*	99.68	*0.66*	*100.79*	*98.17*	–	–	–	–
19.83	*19.68*	*80.80*	*2.60*	–	–	–	–	33.30	*27.78*	*71.68*	*5.40*	–	–	–	–
3.57	*3.59*	*18.90*	*0.04*	–	–	–	–	2.66	*3.28*	*12.76*	*0.23*	–	–	–	–
0.00	*0.00*	*0.00*	*0.00*	–	–	–	–	0.00	*0.00*	*0.01*	*0.00*	–	–	–	–
1610	*453*	*1930*	*1290*	–	–	–	–	1833	*1440*	*3790*	*472*	–	–	–	–
108	*10*	*125*	*86*	113	*10*	*121*	*92*	104	*7*	*118*	*82*	97	*4*	*99*	*94*
2241	*526*	*3603*	*373*	2472	*273*	*2777*	*1998*	2343	*229*	*2986*	*1882*	2081	*30*	*2102*	*2059*
42	*15*	*80*	*12*	41	*8*	*48*	*30*	39	*8*	*74*	*33*	53	*17*	*65*	*41*
2780	*1551*	*8300*	*368*	2272	*539*	*2850*	*1560*	2673	*782*	*6700*	*1140*	2270	*192*	*2405*	*2134*
4	*3*	*11*	*1*	6	*4*	*14*	*1*	5	*4*	*14*	*1*	23	*0*	*23*	*23*
8.84	*39.39*	*275.00*	*0.10*	50.56	*38.72*	*79.86*	*6.66*	55.42	*54.15*	*145.00*	*2.10*	–	–	–	–
0.02	*0.04*	*0.26*	*0.00*	–	–	–	–	0.01	*0.01*	*0.04*	*0.00*	–	–	–	–
0.47	*0.36*	*1.40*	*0.01*	0.30	*0.22*	*0.70*	*0.01*	0.23	*0.28*	*1.09*	*0.01*	0.32	*0.08*	*0.38*	*0.26*
17.01	*54.74*	*451.49*	*0.08*	13.32	*10.43*	*29.58*	*2.52*	11.04	*39.59*	*271.00*	*0.02*	796.00	*135.76*	*892.00*	*700.00*
0.05	*0.05*	*0.28*	*0.00*	0.33	*0.17*	*0.65*	*0.11*	0.10	*0.27*	*1.59*	*0.00*	0.34	*0.13*	*0.43*	*0.24*
0.27	*0.57*	*3.80*	*0.01*	0.29	*0.15*	*0.46*	*0.10*	0.12	*0.21*	*1.52*	*0.02*	0.07	*0.01*	*0.08*	*0.06*
0.04	*0.08*	*0.40*	*0.00*	0.22	*0.26*	*0.58*	*0.02*	0.01	*0.02*	*0.13*	*0.00*	–	–	–	–
0.02	*0.02*	*0.06*	*0.00*	0.01	*0.01*	*0.02*	*0.01*	0.00	*0.00*	*0.01*	*0.00*	–	–	–	–
0.17	*0.19*	*1.20*	*0.00*	0.23	*0.29*	*0.56*	*0.03*	0.16	*0.24*	*1.20*	*0.00*	–	–	–	–
3.937	*13.193*	*104.396*	*0.087*	1.538	*1.647*	*5.092*	*0.153*	2.062	*2.159*	*8.052*	*0.081*	2.595	*0.219*	*2.750*	*2.440*
0.011	*0.021*	*0.159*	*0.001*	0.079	*0.057*	*0.164*	*0.018*	0.016	*0.023*	*0.107*	*0.000*	0.007	*0.000*	*0.007*	*0.007*
0.036	*0.074*	*0.470*	*0.002*	0.109	*0.106*	*0.318*	*0.008*	0.029	*0.049*	*0.196*	*0.001*	0.016	*0.001*	*0.017*	*0.015*
0.003	*0.006*	*0.051*	*0.000*	0.017	*0.014*	*0.039*	*0.004*	0.004	*0.006*	*0.027*	*0.000*	0.003	*0.001*	*0.003*	*0.002*
0.022	*0.065*	*0.440*	*0.001*	0.074	*0.059*	*0.172*	*0.017*	0.015	*0.027*	*0.194*	*0.000*	0.012	*0.001*	*0.013*	*0.011*
0.008	*0.024*	*0.140*	*0.000*	0.019	*0.015*	*0.047*	*0.004*	0.008	*0.016*	*0.093*	*0.000*	0.007	*0.004*	*0.010*	*0.004*
0.004	*0.011*	*0.059*	*0.000*	0.007	*0.005*	*0.014*	*0.001*	0.002	*0.005*	*0.038*	*0.000*	0.004	*0.001*	*0.005*	*0.003*
0.012	*0.037*	*0.200*	*0.000*	0.028	*0.018*	*0.059*	*0.004*	0.007	*0.019*	*0.145*	*0.000*	0.016	*0.008*	*0.022*	*0.010*
0.002	*0.007*	*0.037*	*0.000*	0.005	*0.003*	*0.011*	*0.001*	0.001	*0.004*	*0.029*	*0.000*	0.005	*0.003*	*0.007*	*0.003*
0.015	*0.046*	*0.260*	*0.000*	0.041	*0.024*	*0.078*	*0.007*	0.010	*0.027*	*0.225*	*0.000*	0.044	*0.021*	*0.059*	*0.029*
0.004	*0.011*	*0.059*	*0.000*	0.010	*0.006*	*0.019*	*0.002*	0.003	*0.006*	*0.053*	*0.000*	0.011	*0.006*	*0.015*	*0.007*
0.012	*0.029*	*0.170*	*0.001*	0.032	*0.017*	*0.059*	*0.009*	0.011	*0.020*	*0.161*	*0.000*	0.039	*0.016*	*0.050*	*0.028*
0.004	*0.007*	*0.026*	*0.000*	0.006	*0.003*	*0.010*	*0.002*	0.002	*0.004*	*0.028*	*0.000*	0.008	*0.004*	*0.010*	*0.005*
0.019	*0.031*	*0.180*	*0.003*	0.040	*0.018*	*0.070*	*0.014*	0.019	*0.024*	*0.190*	*0.002*	0.054	*0.019*	*0.067*	*0.040*
0.004	*0.005*	*0.032*	*0.001*	0.007	*0.003*	*0.013*	*0.003*	0.004	*0.004*	*0.033*	*0.001*	0.010	*0.003*	*0.012*	*0.008*
0.007	*0.020*	*0.140*	*0.000*	0.008	*0.005*	*0.014*	*0.005*	0.004	*0.009*	*0.062*	*0.000*	–	–	–	–
0.001	*0.001*	*0.003*	*0.000*	0.004	*0.005*	*0.011*	*0.001*	0.001	*0.001*	*0.002*	*0.000*	–	–	–	–
0.003	–	*0.003*	*0.003*	1.400	*1.711*	*2.610*	*0.190*	–	–	–	–	–	–	–	–
0.135	*0.353*	*2.493*	*0.001*	3.423	*1.137*	*4.688*	*2.487*	0.239	*0.206*	*0.830*	*0.001*	–	–	–	–
0.002	*0.008*	*0.061*	*0.000*	0.015	*0.012*	*0.033*	*0.002*	0.001	*0.001*	*0.004*	*0.000*	0.004	*0.002*	*0.005*	*0.002*
0.002	*0.005*	*0.041*	*0.000*	1.088	*0.416*	*1.689*	*0.311*	0.037	*0.176*	*1.066*	*0.000*	0.799	*0.187*	*0.931*	*0.666*
–	–	–	–	–	–	–	–	–	–	–	–	–	–	–	–
27.20	*18.40*	*69.60*	*2.10*	34.00	*10.36*	*48.00*	*23.00*	30.11	*11.23*	*55.00*	*10.00*	43.50	*7.78*	*49.00*	*38.00*
0.31	*0.17*	*0.72*	*0.00*	0.32	*0.15*	*0.48*	*0.18*	0.57	*0.34*	*1.84*	*0.18*	0.87	*0.21*	*1.01*	*0.72*
–	–	–	–	–	–	–	–	–	–	–	–	–	–	–	–
6.20	*2.08*	*12.20*	*2.10*	3.83	*0.10*	*3.90*	*3.70*	5.27	*2.38*	*10.30*	*1.50*	9.00	*2.26*	*10.60*	*7.40*
–	–	–	–	–	–	–	–	–	–	–	–	–	–	–	–
15.76	*9.04*	*31.54*	*4.54*	16.10	*7.91*	*27.00*	*8.40*	32.08	*72.83*	*390.00*	*2.75*	85.50	*31.82*	*108.00*	*63.00*

(*continued on next page*)

Table 1 (*continued*)

	Subducted serpentinites				Subducted serpentinites			
Protolith	Dunite				Harzburgite			
# samples	n = 39				n = 109			
	Average	*Std. Dev.*	*Max.*	*Min.*	Average	*Std. Dev.*	*Max.*	*Min.*
Major elements (wt.%)								
SiO_2	37.73	*2.68*	*43.75*	*33.59*	40.84	*2.33*	*45.58*	*31.09*
TiO_2	0.01	*0.02*	*0.08*	*0.00*	0.05	*0.08*	*0.73*	*0.00*
Al_2O_3	0.46	*0.57*	*3.44*	*0.02*	1.71	*1.04*	*7.33*	*0.17*
Cr_2O_3	0.50	*0.23*	*1.02*	*0.26*	0.33	*0.05*	*0.42*	*0.25*
Fe_2O_3 (t)	8.03	*1.27*	*10.29*	*4.88*	7.93	*1.24*	*13.25*	*4.12*
MnO	0.12	*0.03*	*0.22*	*0.06*	0.12	*0.04*	*0.35*	*0.05*
NiO	0.32	*0.02*	*0.35*	*0.29*	0.27	*0.02*	*0.30*	*0.23*
MgO	41.29	*3.08*	*46.25*	*32.38*	38.13	*3.03*	*44.03*	*28.19*
CaO	0.62	*1.23*	*6.11*	*0.00*	1.24	*2.01*	*13.09*	*0.02*
Na_2O	0.02	*0.03*	*0.15*	*0.00*	0.03	*0.03*	*0.12*	*0.00*
K_2O	0.02	*0.01*	*0.06*	*0.00*	0.02	*0.01*	*0.05*	*0.00*
P_2O_5	0.00	*0.01*	*0.03*	*0.00*	0.02	*0.03*	*0.12*	*0.00*
L.O.I.	10.92	*3.06*	*16.78*	*3.62*	10.90	*3.44*	*20.61*	*2.66*
Total	99.46	*1.12*	*102.87*	*97.54*	98.29	*2.74*	*101.10*	*92.16*
Trace elements (ppm)								
B	167.03	*2.97*	*170.00*	*164.05*	21.83	*36.61*	*149.00*	*6.40*
Li	13.72	*13.51*	*30.04*	*0.27*	2.22	*4.43*	*23.51*	*0.05*
Be	0.24	*0.32*	*0.69*	*0.01*	0.04	*0.07*	*0.27*	*0.01*
Cl	2337	*654*	*2990*	*1683*	2310	*495*	*3010*	*1940*
Co	100	*31*	*151*	*66*	110	*18*	*149*	*53*
Ni	2393	*369*	*2836*	*1551*	2325	*898*	*7427*	*516*
Zn	47	*27*	*146*	*24*	53	*26*	*181*	*23*
Cr	2900	*1130*	*5208*	*234*	2907	*556*	*4291*	*1650*
Cu	18	*19*	*80*	*0*	16	*15*	*67*	*0*
As	0.22	*0.00*	*0.22*	*0.22*	0.87	*1.36*	*6.38*	*0.04*
Sb	0.02	*0.01*	*0.03*	*0.01*	0.91	*3.77*	*20.40*	*0.00*
Rb	0.71	*0.65*	*2.66*	*0.11*	0.45	*0.61*	*3.39*	*0.03*
Sr	12.63	*17.17*	*75.18*	*0.42*	4.07	*6.26*	*45.72*	*0.00*
Y	0.87	*0.53*	*2.10*	*0.20*	1.46	*2.46*	*22.04*	*0.05*
Zr	2.89	*1.99*	*9.58*	*0.07*	1.35	*2.41*	*21.70*	*0.00*
Nb	0.19	*0.21*	*0.83*	*0.01*	0.27	*1.02*	*8.91*	*0.00*
Cd	0.01	*0.00*	*0.01*	*0.01*	0.03	*0.02*	*0.08*	*0.01*
Cs	0.01	*0.01*	*0.04*	*0.00*	0.17	*0.47*	*3.03*	*0.00*
Ba	5.715	*3.360*	*13.000*	*0.243*	7.083	*17.336*	*136.000*	*0.044*
La	0.758	*1.821*	*6.510*	*0.056*	0.382	*1.072*	*7.970*	*0.000*
Ce	0.835	*1.413*	*5.260*	*0.127*	0.658	*2.151*	*19.000*	*0.000*
Pr	0.081	*0.101*	*0.390*	*0.016*	0.113	*0.322*	*2.600*	*0.002*
Nd	0.292	*0.261*	*1.040*	*0.088*	0.533	*1.556*	*12.500*	*0.008*
Sm	0.059	*0.036*	*0.150*	*0.020*	0.158	*0.439*	*3.200*	*0.003*
Eu	0.057	*0.124*	*0.450*	*0.010*	0.063	*0.171*	*1.130*	*0.003*
Gd	0.059	*0.028*	*0.120*	*0.020*	0.202	*0.481*	*3.200*	*0.005*
Tb	0.012	*0.006*	*0.020*	*0.005*	0.040	*0.095*	*0.610*	*0.001*
Dy	0.062	*0.031*	*0.110*	*0.010*	0.266	*0.611*	*3.900*	*0.006*
Ho	0.016	*0.007*	*0.030*	*0.009*	0.063	*0.131*	*0.850*	*0.002*
Er	0.044	*0.019*	*0.080*	*0.020*	0.183	*0.356*	*2.300*	*0.006*
Tm	0.008	*0.002*	*0.010*	*0.005*	0.032	*0.062*	*0.400*	*0.001*
Yb	0.049	*0.021*	*0.090*	*0.020*	0.204	*0.361*	*2.200*	*0.012*
Lu	0.010	*0.004*	*0.020*	*0.006*	0.034	*0.057*	*0.350*	*0.002*
Hf	0.041	*0.030*	*0.100*	*0.002*	0.038	*0.067*	*0.578*	*0.001*
Ta	0.011	*0.010*	*0.030*	*0.000*	0.026	*0.106*	*0.900*	*0.000*
W	–	–	–	–	0.124	*0.262*	*1.041*	*0.011*
Pb	0.829	*1.598*	*4.989*	*0.036*	1.064	*3.712*	*33.800*	*0.014*
Th	0.546	*0.656*	*1.800*	*0.002*	0.094	*0.359*	*3.030*	*0.000*
U	0.398	*0.767*	*2.710*	*0.009*	0.055	*0.169*	*1.220*	*0.001*
S	163.93	*16.91*	*178.40*	*136.40*	151.27	*24.19*	*182.60*	*113.80*
V	25.62	*9.07*	*39.00*	*8.00*	44.21	*13.49*	*69.00*	*11.10*
Ga	0.94	*0.56*	*2.16*	*0.14*	2.09	*1.32*	*6.34*	*0.14*
Mo	0.14	*0.11*	*0.25*	*0.03*	0.23	*0.21*	*0.83*	*0.02*
Sc	6.29	*1.81*	*9.00*	*3.36*	10.30	*2.73*	*20.81*	*4.83*
Sn	–	–	–	–	0.54	*0.36*	*1.32*	*0.12*
Ti	23.28	*10.06*	*33.33*	*13.22*	152.43	*105.60*	*540.00*	*25.69*

2.4. Compilation of serpentinites geochemistry

The locations of the serpentinites reviewed in this paper are summarized in Fig. 2. Average compositions, standard deviation, and maximum and minimum values of compiled serpentinites are reported in Table 1.

(i) *Abyssal serpentinites*: the compilation of abyssal serpentinites data is essentially representative of Mid-Atlantic Ridge. Among the selected sites, a majority of data is from MARK (MAR 23°N) and ODP Leg 209 (MAR 15°20′N; Jöns et al., 2010; Kodolányi et al., 2012; Paulick et al., 2006) and represents peridotites hydrated on the seafloor. Other sites are the Atlantis Massif-IODP Exp. 304–305 (Delacour et al., 2008) and Logatchev hydrothermal field (Augustin et al., 2012). The only record of serpentinites from a fast spreading ridge in this compilation is from the particular geological setting of Hess Deep (Kodolányi et al., 2012).

(ii) *Mantle wedge serpentinites*: collected data on serpentinites representative of hydrated mantle wedge are mostly from the Mariana forearc-ODP Legs 125 and 195 (Torishima, Conical and South Chamorro seamounts; Ishii et al., 1992; Kodolányi et al., 2012; Lagabrielle et al., 1992; Parkinson and Pearce, 1998; Savov et al., 2005a, b, 2007). In the same context (i.e. oceanic subduction), an analogous site is represented by the South Sandwich arc in southernmost Atlantic (dredged samples: Pearce et al., 2000). Other occurrences of mantle wedge serpentinites are from the Indus Suture Zone in Himalaya (Tso Morari massif; Deschamps et al., 2010; Guillot et al., 2001; Hattori and Guillot, 2007) and from the paleo-subduction channel preserved in the Greater Antilles (Cuba and Dominican Republic) where serpentinites protruded along major faults (Saumur et al., 2010), and fragments of mantle wedge occur in the matrix of subducted serpentinites (Marchesi et al., 2006 (Mayarí massif); Blanco-Quintero et al., 2011; Deschamps et al., 2012). Lastly, mantle wedge serpentinites are present as ultra depleted peridotites in New Caledonia (Marchesi et al., 2009; Ulrich et al., 2010).

(iii) *Subducted (and subduction zones-related) serpentinites*: geochemical compositions of subducted serpentinites are compiled from a number of studies that mostly dealt with ophiolitic complexes and accretionary zones around the world. Quite a few studies have been conducted in the European Alps such as the Chenaillet ophiolite in France (Chalot-Prat et al., 2003), Queyras in France (Hattori and Guillot, 2007; Lafay et al., 2013), Erro–Tobbio massif in Italy (Scambelluri et al., 2001b), Zermatt-Saas ophiolite in Switzerland (Li et al., 2004), Elba island, Monti Livornesi and Murlo massifs in Italy (Anselmi et al., 2000; Viti and Mellini, 1998), and Slovenska Bistrica ultramafic complex in Slovenia (De Hoog et al., 2009). Other massifs in Europe include the Cerro del Almirez ultramafic complex in Spain (Garrido et al., 2005), Cabo Ortegal massif in Spain (Pereira et al., 2008), Leka ophiolite complex in Norway (Iyer et al., 2008), and those throughout the world are Zagros suture zone in Iraq (Aziz et al., 2011), ophiolite complexes of Northwest Anatolia in Turkey (Aldanmaz and Koprubasi, 2006), the Greater Antilles extinct arc in Cuba and Dominican Republic (Blanco-Quintero et al., 2011; Deschamps et al., 2012; Hattori and Guillot, 2007; Saumur et al., 2010), Feather River ophiolite in California, U.S.A. (Agranier et al., 2007; Li and Lee, 2006), and Burro Mountain in California, U.S.A. (Coleman and Keith, 1971).

(iv) *Caveats in the compilation*: the petrological characterization of serpentinites remains controversial since, depending on the percentage of serpentine, some authors deal with hydrated peridotites and others with serpentinites s.s. As we will see in Section 3.1.1, it is quite difficult to define serpentinites only using the percentage of serpentinization or the loss on ignition (L.O.I.) content. So we choose data on samples with strong evidences of hydration, and significant amount of serpentine minerals. Moreover we considered only studies addressing serpentinite massifs, and we excluded veins of serpentinites. We choose serpentinites from peridotite protoliths, such as dunite, harzburgite, and lherzolite; in doing so we eliminated volumetrically less significant lithologies such as serpentinized pyroxenite, websterite, wehrlite, or olivine-rich gabbro. Another issue in establishing a compiled database is the quality of data. During the last decades, the quality of analytical methods has improved, but varied among different laboratories. Moreover, this advance in analytical technique lowered detection limits which facilitate notably the acquisition of data from depleted to highly depleted rocks, such as serpentinites deriving from dunite or harzburgite. Outliers appear in some cases, and this is particularly evident for trace elements. When such samples were really different from the bulk of the compiled data, diagrams focus only on the main dataset. However, we did not take the decision to discriminate between "good" and more "controversial" data; all analyses provide constructive information and we choose to use the greatest amount of published data in order to have a global view on the geochemical role of serpentinites in subduction contexts. For more details about each geological setting, we refer readers to the cited studies.

3. Inherited geochemical signature of serpentinites

3.1. Geochemical consequences due to serpentinization and protolith fingerprints

3.1.1. Major elements

Major consequence of serpentinization is the addition of water into a peridotitic system. Serpentine phases can contain over 13 wt.% of water in their crystal structure. However, the L.O.I. is not always correlated with the degree of serpentinization since other phases (e.g. talc, brucite, chlorite, and clay minerals) will influence this budget. For samples described as completely serpentinized in the literature and used in our database, we observe a L.O.I. varying from 1.46 to 22.8 wt.% ($n = 284$; average of 13.15; Fig. 3a). Hence the amount of water cannot be used as a proxy for the degree of serpentinization without a careful description of samples.

The mobility of major elements during serpentinization has been debated off and on in the literature for a long time, and a good summary is given in O'Hanley (1996). Some authors have mentioned a slight change in bulk rock Mg/Si ratio due to seawater-dominated hydration (and not serpentinization itself) of mantle rocks (Niu, 2004; Snow and Dick, 1995). On the other hand, as illustrated in Fig. 3a, serpentinization preserves the (sum oxides)/SiO_2 ratio (with sum oxides = MgO + $Fe_2O_{3(total)}$ + Al_2O_3 + TiO_2 + CaO + Cr_2O_3 + MnO + NiO + Na_2O + K_2O + P_2O_5), as demonstrated by Bogolepov (1970) and Coleman and Keith (1971). Such constancy in the SiO_2/(sum oxides) ratio (average of 0.81; $n = 899$) over a broad range of serpentinization degree argues in favor of no or very minor change in the major element composition. The evidence suggests that the major elements of protolith must be preserved during the hydration processes. Note that the average composition of this database plots close to the serpentine phase composition, and is aligned between talc and brucite poles (Fig. 3a).

By plotting compiled serpentinites in a FeO versus MgO (wt.%) diagram (Fig. 3b), we first observe that the samples are relatively consistent between them in terms of compositions, especially for FeO content (mostly between 6 and 10 wt.%). Moreover, their compositions are consistent with those of abyssal and ophiolitic peridotites (Bodinier and Godard, 2003; Godard et al., 2008; Niu, 2004). Samples are in general refractory, especially a set of samples representative of

mantle wedge serpentinites which plot close to the evolution trend of the stoichiometric variations of olivines. Note that samples, having experienced melt/rock interactions, present FeO enrichment for a constant MgO.

Past studies have documented systematic depletion in Ca during serpentinization (Coleman and Keith, 1971; Iyer et al., 2008; Janecky and Seyfried, 1986; Miyashiro et al., 1969; Palandri and Reed, 2004), while some authors have shown that the precipitation of carbonates, mostly related to seafloor alteration, can increase the Ca content in the bulk rock, in particular in abyssal peridotites (e.g. Seifert and Brunotte, 1996; Shipboard scientific party, 2004). Our compiled data in Fig. 3c and d show low CaO even compared to depleted mantle values (Salters and Stracke, 2004). A CaO depletion trend seems to appear through the compilation of subduction-related serpentinites. Nevertheless it is difficult to assess if this trend is representative of serpentinization-related depletion, or more related to the depletion in CaO of protoliths. In Fig. 3d, we note that serpentinized lherzolite has high CaO (>1.5 wt.%) and could be easily distinguished; however, the difference between serpentinized dunite and harzburgite is not apparent. Most of CaO contents in serpentinites vary between 0.01 and 2 wt.%, which are similar to values observed on anhydrous abyssal and ophiolitic peridotites (Bodinier and Godard, 2003; Niu, 2004). A few samples, described as mainly altered to talc (Paulick et al., 2006), plot outside the array and close to the composition of talc. Such local talc formation can greatly modify the initial major element composition, notably by a non-negligible enrichment in silica. Other well studied examples of metasomatism associated with serpentinization are rodingitization (hydration of gabbroic dikes and recrystallized to a secondary assemblage rich in calcsilicates; Aumento and Loubat, 1971; Bach and Klein, 2009; Bideau et al., 1991; Honnorez and Kirst, 1975), and/or of the formation of tremolite-talc schists (Boschi et al., 2006; Escartin et al., 2003; MacLeod et al., 2002), which could induce a redistribution of CaO and Na_2O during the serpentinization process (e.g. Mével and Stamoudi, 1996). However these rocks are volumetrically insignificant and the formation requires the interaction with mafic rocks, which is different from serpentinites.

Diagram of MgO/SiO_2 versus Al_2O_3/SiO_2 shows that most serpentinites plot at low Al_2O_3/SiO_2 (less than 0.03; Fig. 4a). The majority of samples plot close to the extreme of the mantle fractionation array, and represent the mineralogy of olivine and orthopyroxene. The evidence suggest that most protoliths had experienced partial melting before serpentinization since this late process has no effect on the Al_2O_3/SiO_2 ratio (e.g. Paulick et al., 2006; Snow and Dick, 1995). Refractory protolith for serpentinites are not really surprising since olivine is more easily changed into serpentine phases (for T < 300 °C; Allen and Seyfried, 2003; Martin and Fyfe, 1970; Mével, 2003) compared to pyroxenes which require higher temperature to be destabilized (T > 400 °C; Oelkers and Schott, 2001). Thus, low Al in the protolith could be related to sampling bias due to the predisposition of olivine-rich samples to be serpentinized (Fig. 4b), as well as a sampling bias independently of serpentinization process since in the case of abyssal peridotites, most of recovered samples are harzburgite or dunite. Note that a part of compiled serpentinites fall within the oceanic array (Bodinier and Godard, 2003; Niu, 2004), which is parallel to the terrestrial array but with lower values in MgO/SiO_2. Previous authors explained such a difference between terrestrial array and oceanic array by a loss of MgO during low temperature seafloor weathering (Niu, 2004; Snow and Dick, 1995).

Except talc-dominated samples from the Mid-Atlantic Ridge (Paulick et al., 2006), we did not observe SiO_2 enrichment which could have enhanced talc crystallization, nor a strong influence of brucite fingerprints. Distinction between serpentinized dunite, harzburgite and lherzolite is not trivial. Serpentinized lherzolite and harzburgite mostly has MgO/SiO_2 ratio below 1.1, whereas serpentinized dunite can have higher MgO/SiO_2 values reflecting an increase of olivine (Ol)/orthopyroxene (Opx) ratio from harzburgite to dunite (Fig. 4b). Note that only serpentinites originating from dunites, and/or deriving after Ol-rich harzburgites, plot above the terrestrial array.

Some characteristics vary between samples from different environments. Abyssal serpentinites, with the exception of few serpentinized troctolites, have low Al_2O_3/SiO_2 ratio (<0.035) and MgO/SiO_2 ratio varying between 0.8 and 1.2, and are not really consistent with the field defined for the abyssal peridotites ($0.01 < Al_2O_3/SiO_2 < 0.07$, $0.75 < MgO/SiO_2 < 1.05$; Niu, 2004; Fig. 4a). With few exceptions, compiled mantle wedge serpentinites share the same characteristics as the abyssal serpentinites, despite more refractory compositions for few samples ($0.8 < MgO/SiO_2 < 1.5$ for samples with $Al_2O_3/SiO_2 < 0.06$). The serpentinites with significantly high MgO/SiO_2 (>1.3) were sampled in the Mariana forearc mud volcanoes and contain non-negligible amounts of brucite, a Mg-rich hydrous phase. Subduction-related serpentinites are more widespread and have Al_2O_3/SiO_2 ratio up to 0.1 for samples having MgO/SiO_2 ratio between ~0.7 and ~1.3. We do not observe clear geochemical distinctions concerning both ratios (MgO/SiO_2 and Al_2O_3/SiO_2) for serpentinites having dunitic, harzburgitic, or lherzolitic protolith, although serpentinized dunites on average plot at low Al_2O_3/SiO_2 (Fig. 4b). However, we note that subducted serpentinites on average have less refractory characteristics and/or evidence of refertilization, whereas abyssal and mantle wedge serpentinites seems to be constrained by a Al_2O_3/SiO_2 ratio mostly below 0.03 (Fig. 4a). Such features point in the direction of a relatively complex geological history experienced by subducted serpentinites (see Section 3.1.2.3). Samples having high MgO/SiO_2 are not representative of only the mantle wedge (or suprasubduction zone) serpentinites, especially since serpentinites having the same characteristics have been reported in abyssal contexts (e.g. Godard et al., 2008; Paulick et al., 2006). So, in contrast with the conclusions of the initial study of Hattori and Guillot (2007), our compilation indicates that the MgO/SiO_2 versus Al_2O_3/SiO_2 ratios cannot be used as a discriminating tool to characterize the geological setting of serpentinites. In a TiO_2 versus MgO (wt.%) diagram (Fig. 3e), serpentinites plot below the depleted mantle composition (Salters and Stracke, 2004). We first observe that the subducted serpentinites are relatively consistent with composition of abyssal peridotites defined by Niu (2004). Mantle wedge serpentinites has on average lower TiO_2 contents than abyssal serpentinites. Therefore, Ti contents may be used to distinguish serpentinites of different protoliths and it will be discussed more in detail in Section 3.3.1.

The wide range of variations in L.O.I. (up to 20%) is illustrated in Fig. 4d. Some serpentinites have high water contents due to the formation of secondary brucite, especially in serpentinized dunites. Abyssal samples have L.O.I. close to the observed values for theoretical serpentine minerals (average of 12.38 wt.% ± 2.99; n = 102) whereas

Fig. 3. a.) Ternary plot of (L.O.I. × 10)-SiO_2-(sum oxides = MgO + $Fe_2O_{3(total)}$ + Al_2O_3 + TiO_2 + CaO + Cr_2O_3 + MnO + NiO + Na_2O + K_2O + P_2O_5) for bulk rock compositions of serpentinites compiled in Fig. 2 (oxides are recalculated under anhydrous forms). Degree of serpentinization is defined by relevant authors. We note that serpentinization and associated increasing L.O.I. content is not modifying the major element budget (with the exception of talc-dominated rocks). International standard UB-N composition is after Georem (http://georem.mpch-mainz.gwdg.de). b.) FeO (wt.%), c.) and d.) CaO (wt.%), and e.) TiO_2 (wt.%) versus MgO (wt.%) diagrams for serpentinites compiled in Fig. 2. Compositions are recalculated on a volatile free basis; FeO stands for total Fe content. For each contexts (abyssal, subducted and mantle wedge), nature of primary protoliths (dunite or harzburgite) was distinguished, as well as refertilization processes (marked with a cross inside the symbol) taking place before serpentinization. In panel b, dashed gray lines represent iso-Mg# lines for a Mg# (=100 × Mg/(Mg + Fe) cationic ratio) ranging from 85 to 95 while the black line represents the stoichiometric variations of olivine Fe–Mg compositions (with FeO + MgO = 66.67 in mol%). Estimated composition of the depleted mantle is from Salters and Stracke (2004) and abyssal peridotite compositions are from Niu (2004).

mantle wedge serpentinites have higher L.O.I. and plot toward the brucite composition (average of 14.41 wt.% ± 3.35; n = 431; Fig. 4d). In contrast, subducted serpentinites have lower L.O.I. (average of 11.15 wt.% ± 3.37; n = 381) due to (1) a partial dehydration of these samples during their subduction and prograde metamorphism, or (2) an higher amount of antigorite in these samples (66 atg-

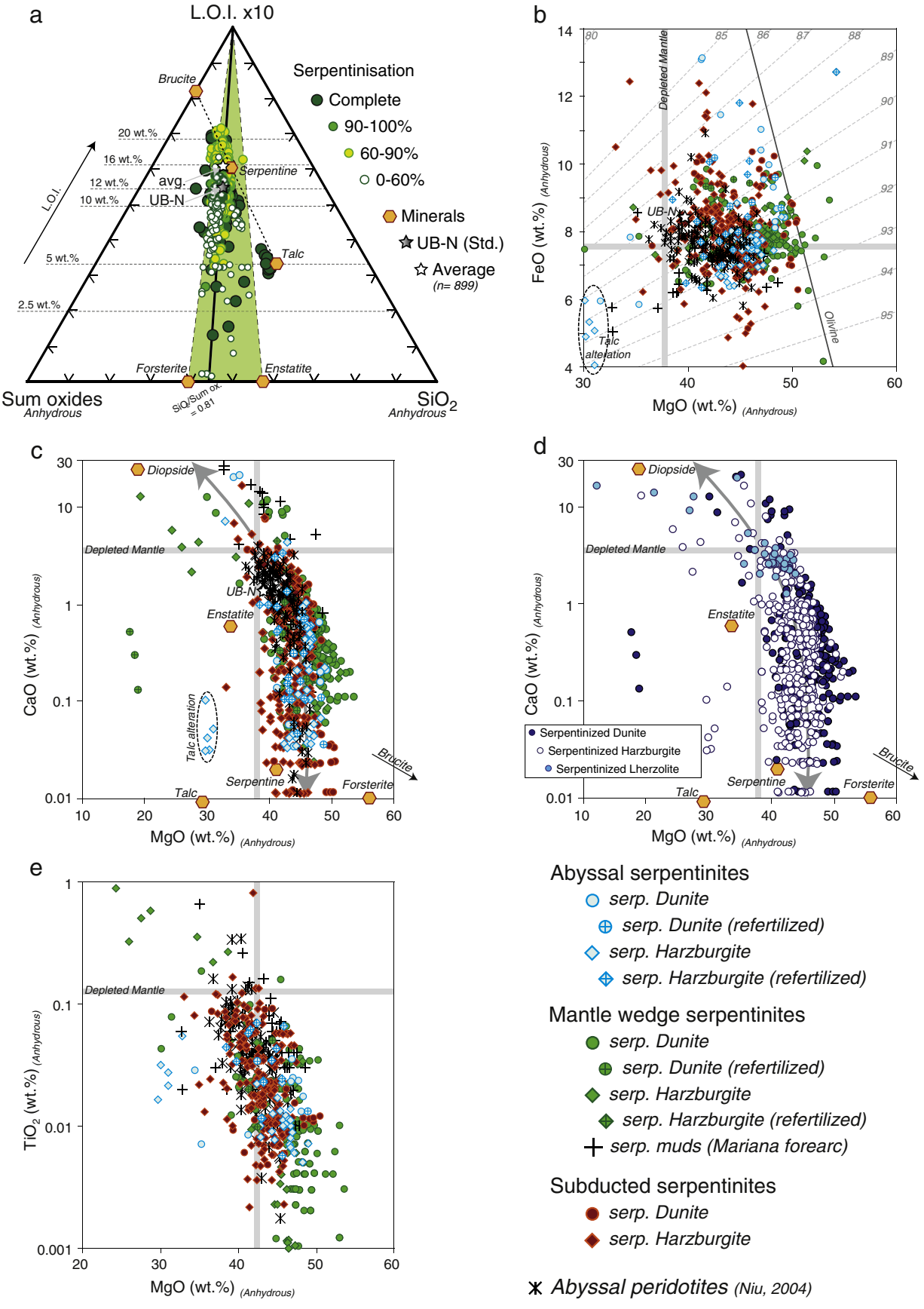

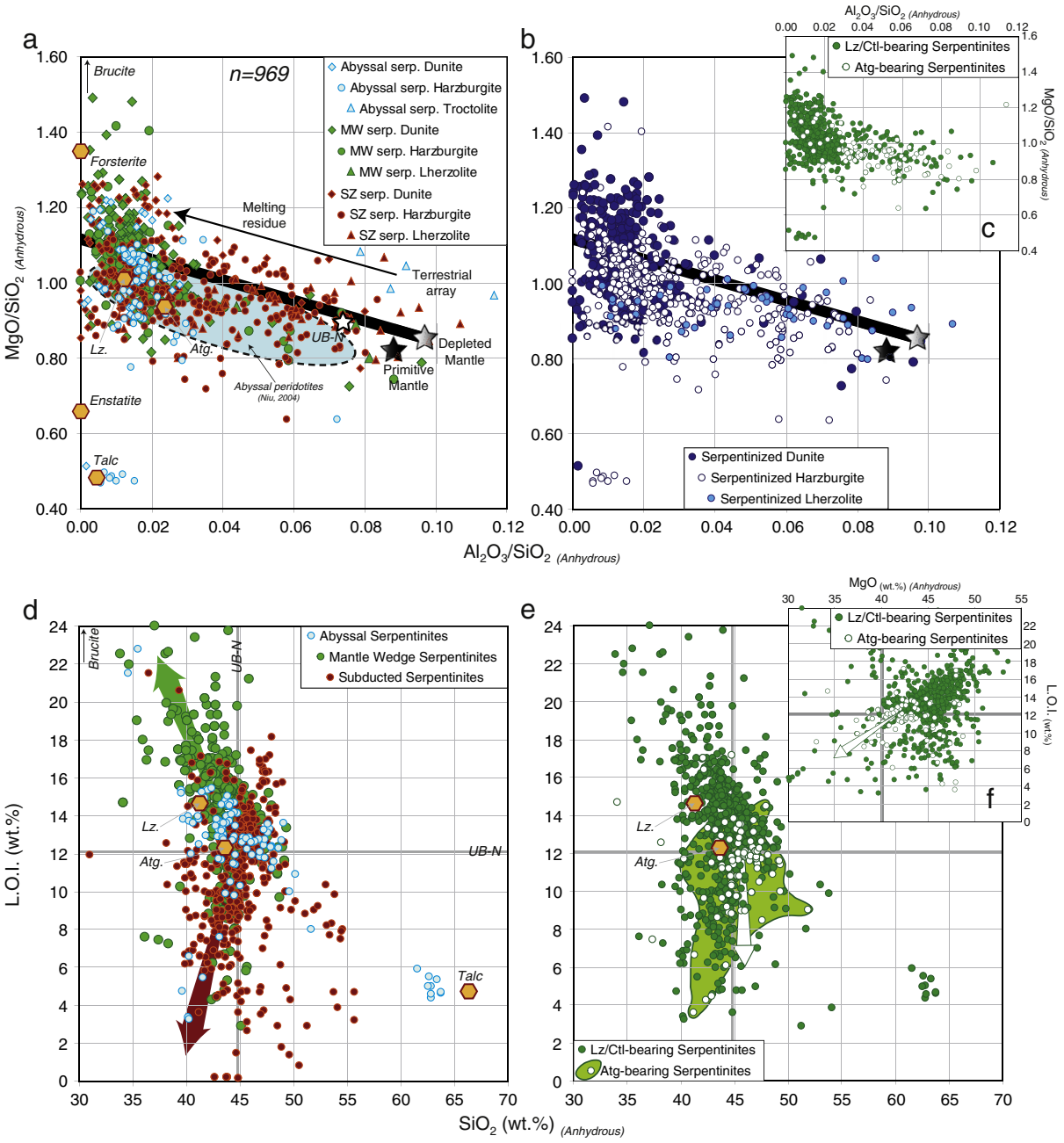

Fig. 4. a.), b.) and c.) MgO/SiO_2 versus Al_2O_3/SiO_2 diagrams for serpentinites compiled in Fig. 2 (n = 969). Compositions are recalculated on a volatile free basis. In panel a, distinctions were made between different geological contexts (abyssal, subducted and mantle wedge serpentinites) while in panel b distinctions were made on the nature of the protoliths (dunite, harzburgite and lherzolite) and in panel c lizardite/chrysotile- and antigorite-bearing serpentinites were individualized. Estimated composition of the depleted mantle is from Salters and Stracke (2004) and of the primitive mantle is from McDonough and Sun (1995). The large black line represents the bulk silicate Earth evolution so-called "terrestrial array" after Jagoutz et al. (1979) and Hart and Zindler (1986). The expected compositional variation due to partial melting effect is shown with the arrow; melting residues have higher MgO/SiO_2 and lower Al_2O_3/SiO_2 whereas melt has lower MgO/SiO_2 and higher Al_2O_3/SiO_2. Gray field in panel a represent compositions of abyssal peridotites after Niu (2004). d.) and e.) L.O.I. (loss on ignition; wt.%) versus SiO_2 (anhydrous forms; wt.%) diagrams. f.) L.O.I. (loss on ignition; wt.%) versus MgO (anhydrous forms; wt.%) diagram. In panel d, distinctions were made between different geological contexts (abyssal, subducted and mantle wedge serpentinites) while in panels e and f distinctions were made between lizardite/chrysotile- and antigorite-bearing serpentinites. International standard UB-N composition is after Georem (http://georem.mpch-mainz.gwdg.de).

samples out of 381 (~17%), against 36 atg-samples out of 431 (~8%) for mantle wedge serpentinites). Antigorite contains less water in its stoichiometric formula. Such decrease in L.O.I., as well as in MgO, in the antigorite structure, experimentally observed by Wunder et al. (2001), is discernible on antigorite-bearing samples in the studied database (L.O.I.: 15.41 ± 3.51 wt.% in lz $[Mg_3Si_2O_5(OH)_4]$-bearing samples (n = 756) and 11.50 ± 2.28 wt.% in atg $[Mg_{48}Si_{34}O_{85}(OH)_{62}]$-bearing samples (n = 103); Fig. 4e, f). Also the relative increase of Al_2O_3/SiO_2 ratios seems related to the formation of antigorite as illustrated in Fig. 4c. We observe that antigorite-bearing serpentinites have mostly $Al_2O_3/SiO_2 > 0.03$; this could be an effect of a preferential incorporation of Al_2O_3 in the antigorite structure (Padrón-Navarta et al., 2008) compared to lizardite and chrysotile (theoretical Al_2O_3 contents from Deer et al. (1992): atg: 1.03, ctl: 0.30, and lz: 0.54 wt.% Al_2O_3). However, looking in detail, we note that most of the antigorite-bearing serpentinites were described in the subducted serpentinite subset, and subsequently, such a feature could be due also to the fact that these samples are less refractory (see above).

3.1.2. Rare earth elements and other trace elements

Abundance of REE in serpentinites is influenced by fluid/rock interactions and it is dependent on other factors such as the REE contents of primary phases and their stability during hydration, the REE content of the percolating fluid, and the affinity for REE of secondary minerals. Experimental studies on seawater–peridotite interactions showed that hydrothermal fluids and serpentinites after harzburgite are enriched in LREE (Allen and Seyfried, 2005; Menzies et al., 1993). Other studies have shown that aerial alteration and weathering can remobilize REE (e.g. Grauch, 1989; Humphris, 1984; Ludden and Thompson, 1979; Négrel et al., 2000; Nesbitt, 1979; Poitrasson et al., 1995). Nevertheless, in the majority of cases, the change in the REE budget is moderate during hydration, and REE still reflect the geochemical signature of the original protolith. We feel confident that REE abundance of serpentinites may be used to distinguish their protoliths: dunite, harzburgite and lherzolite (Fig. 5), at least for abyssal and mantle wedge serpentinites. This is supported by relatively good positive correlations between Yb and many other trace elements (especially for abyssal and mantle wedge serpentinites) suggesting that they are poorly mobile during serpentinization. Menzies et al. (1993) and O'Hanley (1996) explain that REE the lack mobility during the hydration of peridotites by low abundance of clinopyroxene, which is the main reservoir for REE, and resistant against hydration compared to olivine and orthopyroxene. However, clinopyroxene is present in many peridotites and Leblanc and Lbouabi (1988) proposed that complete serpentinization can alter REE signature.

3.1.2.1. Abyssal serpentinites. Serpentinization in abyssal environments is mainly controlled by hydrothermal alteration at ridges, and such effect varies between the sites. Compiled abyssal serpentinites (see Section 2.4) are relatively homogeneous at the first order (with the exception of refertilized samples; Figs. 5a, b, c and 6a, b, c). Samples were divided in three main groups: serpentinites after dunite, harzburgite and troctolite. Note that few to none serpentinized lherzolite are reported in the literature.

We observe that the bulk rock REE compositions are quite variable (Figs. 5a, b, c and 7a, b; LREE in dunite are varying from ~0.01 to ~1 CI-Chondrite and HREE from ~0.05 to ~1 CI-Chondrite, whereas LREE in harzburgite are varying from ~0.001 to ~0.1 CI-Chondrite and HREE from ~0.1 to ~0.5 CI-Chondrite), but REE patterns remain relatively parallel. Such differences in REE can be explained by small differences in the primary mineral assemblages of serpentinite

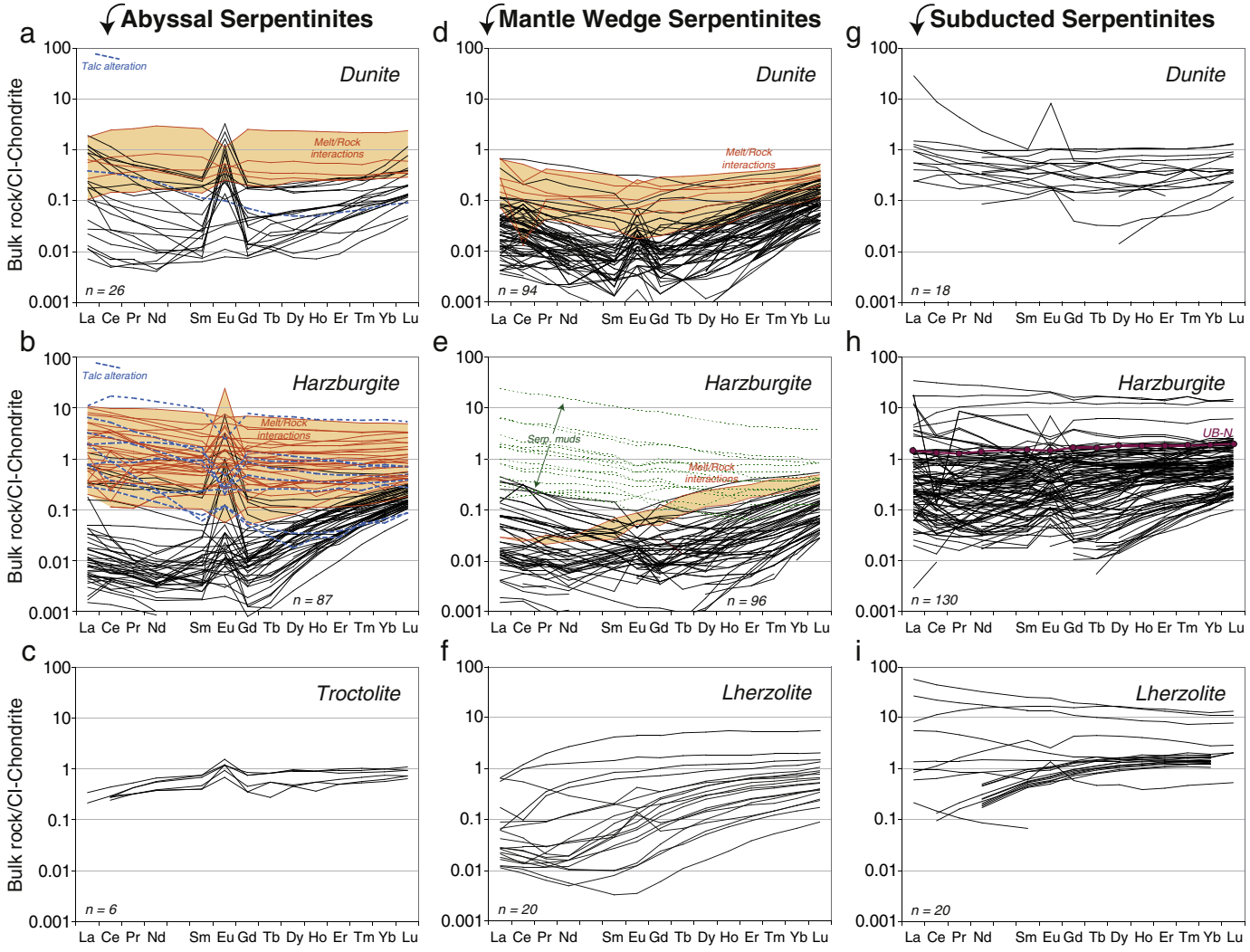

Fig. 5. REE compositions of serpentinites compiled in Fig. 2. a.), b.), and c.) Compositions of abyssal serpentinites derived from dunite, harzburgite and troctolite, respectively. d.), e.), and f.) Compositions of mantle wedge serpentinites derived from dunite, harzburgite and lherzolite, respectively. g.), h.), and i.) Compositions of subducted serpentinites derived from dunite, harzburgite and lherzolite, respectively. Red patterns highlighted by a light red field represent serpentinites having characteristics of a refertilized protolith after melt/rock interactions. In panels a and b, dashed blue patterns represent serpentinites which experienced talc alteration. In panel e, dashed green patterns represent serpentinite muds. International standard UB-N composition reported in panel h is after Georem (http://georem.mpch-mainz.gwdg.de). CI-Chondrite normalizing values are after McDonough and Sun (1995). See text for explanations.

protoliths; clinopyroxene, which is the principal carrier of REE signature, varies in abundance and composition. Generally, abyssal serpentinized dunites (Fig. 5a) have U-shaped REE patterns (below chondritic values) while abyssal serpentinized harzburgites are mostly below 0.1 time chondritic values (with the exception of HREE); they are highly depleted in LREE, despite a slight enrichment from La to Nd, and are gradually enriched in HREE from Gd to Lu. All abyssal serpentinites have positive Eu anomalies with average $(Eu/Eu^*)_N = 14.4$ in serpentinized dunite, and 5.4 in serpentinized harzburgite (Fig. 5b). We must keep in mind that compiled abyssal serpentinites could be biased toward (highly) refractory samples, compared to abyssal peridotites defined by Niu (2004).

The presence of the positive Eu-anomaly (Figs. 5a, b, c and 7c) could be explained by the presence of plagioclase in the protolith reflecting early melt/rock interactions (e.g. Niu et al., 1997). However, as demonstrated by Paulick et al. (2006), most of serpentinites (in particular the most altered) have Sr contents lower than 2 ppm, and do not show systematic correlations between Eu/Eu* and Sr and can even display locally Eu depletions. An alternative explanation is high Eu in hydrothermal fluids due to reactions with plagioclase-bearing rocks, such as oceanic gabbros (e.g. Douville et al., 2002) and/or changes in the percolating fluid chlorinity and in the local redox conditions that will favor LREE and Eu mobility (e.g. Allen and Seyfried, 2005). It is quite difficult to assess the individual effect of seawater-derived and/or hydrothermal fluids on the REE concentrations (except for Eu as seen above). Paulick et al. (2006) observed a decreasing of Lu content with increasing L.O.I. This feature is more marked in serpentinized harzburgites compared to serpentinized dunites and reflects their initial olivine content. We reach the same conclusion in the compiled database. On the other hand, changes in LREE (e.g. La) content and L.O.I. are not correlated. Similar to Eu variations, they are commonly interpreted as the results of chemical interactions with hydrothermal fluids, which are generally LREE-enriched and HREE-depleted (e.g. Douville et al., 2002; Schmidt et al., 2007).

Extended trace element patterns (Fig. 6a, b, c) are characterized by strong enrichments in U, Pb, and Sr, and a small negative anomaly in Y compared to the neighboring elements. Except these few elements, trace element compositions are depleted compared to primitive mantle estimate (McDonough and Sun, 1995); a feature in accord with residual mantle origin of the protoliths. We observe on some samples a decoupling between Nb and Ta, with a preferential enrichment in Ta. Overall, trace element compositions of serpentinites, from both serpentinized dunite and harzburgite (and few troctolite), are in good agreement (with the exception of LREE and Eu) with those observed in depleted peridotites from abyssal and ophiolitic contexts (e.g. Bodinier and Godard, 2003; Niu, 2004; Niu and Hekinian, 1997); this observation confirms the overall moderate mobility for most incompatible elements during serpentinization.

An interesting feature, highlighted by Paulick et al. (2006), is the occurrence of enriched serpentinites having nearly flat REE patterns

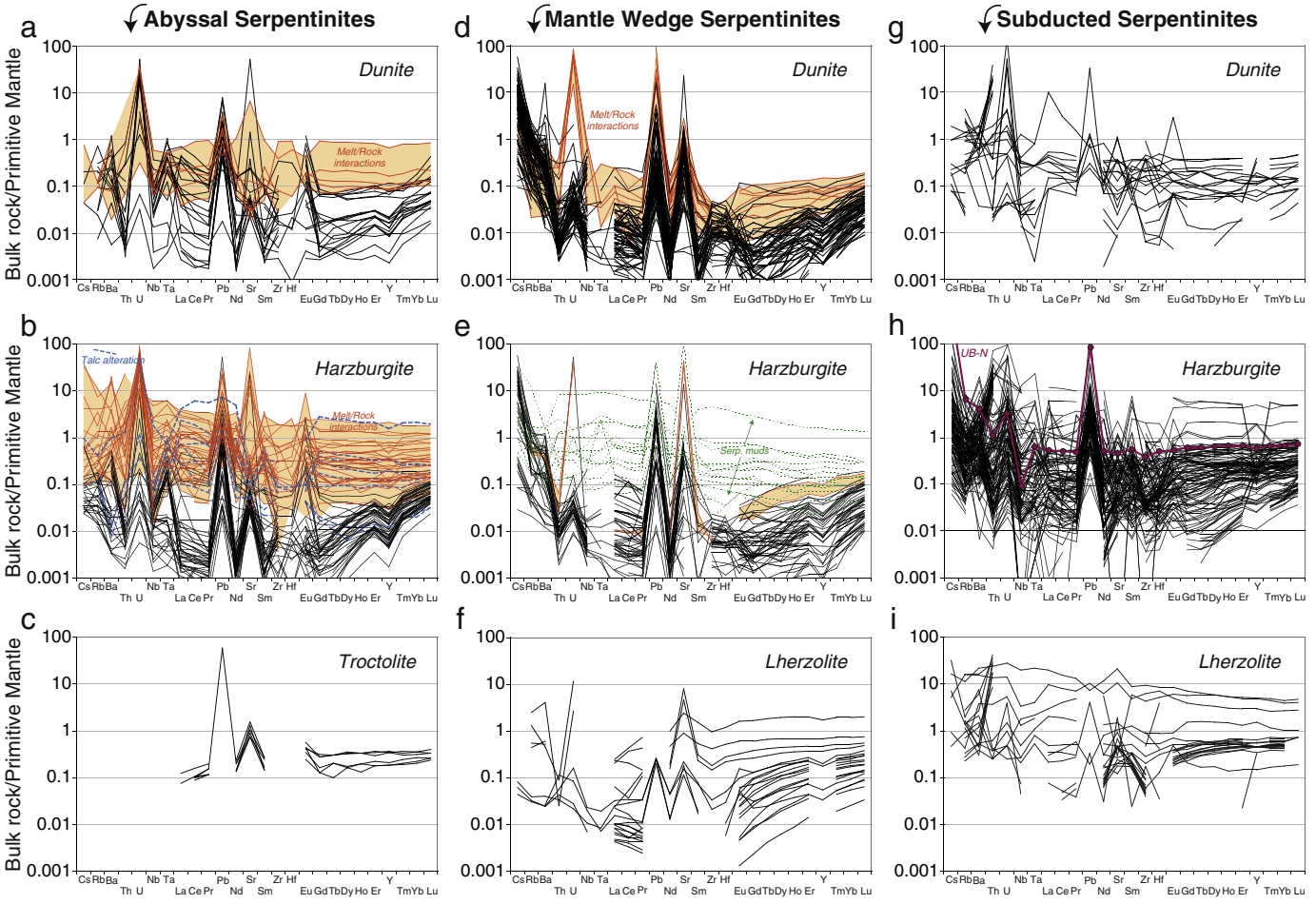

Fig. 6. Extended trace element patterns for serpentinites compiled in Fig. 2. a.), b.), and c.) Compositions of abyssal serpentinites derived from dunite, harzburgite and troctolite, respectively. d.), e.), and f.) Compositions of mantle wedge serpentinites derived from dunite, harzburgite and lherzolite, respectively. g.), h.), and i.) Compositions of subducted serpentinites derived from dunite, harzburgite and lherzolite, respectively. Red patterns highlighted by a light red field represent serpentinites having characteristics of a refertilized protolith after melt/rock interactions. In panels a and b, dashed blue gray patterns represent serpentinites which experienced talc alteration. In panel e, dashed green patterns represent serpentinite muds. International standard UB-N composition reported in panel h is after Georem (http://georem.mpch-mainz.gwdg.de). Primitive mantle normalizing values are after McDonough and Sun (1995). See text for explanations.

(indicated in gray in Fig. 5a, b). These samples are over-enriched in all elements compared to previous serpentinites, and consequently positive anomalies in U, Pb, and Sr are less discernible (Fig. 6a, b). We observe an increase of REE, Th and high field strength elements (HFSE; e.g. Nb, Ta, Zr and Hf; Augustin et al., 2012; Paulick et al., 2006; Fig. 8); over-enrichment in LREE, as well as MREE and HREE, is particularly well-marked on serpentinized harzburgite compared to neighboring serpentinites (Fig. 5b). Note that same observations were made by Niu (2004) on abyssal peridotites. It is admitted that REE and HFSE have a similar behavior and solubility in mafic melts, whereas in aqueous solutions LREE are more easily mobilized than HREE and HFSE. Thus melt–rock interactions will cause an addition in equal proportions of LREE and HFSE (Niu, 2004). In Th versus Gd/Lu and Nb versus La diagrams (Fig. 8a, b), we observe two positive trends: a trend shows LREE enrichment associated with only a minor increase of HFSE, whereas another trend, mainly defined by enriched serpentinites and abyssal peridotites from Niu (2004) presents conjoint enrichment in LREE and HFSE. Previous authors (Augustin et al., 2012; Niu, 2004; Paulick et al., 2006) have interpreted these enrichments as resulting from previous melt/rock interactions, before serpentinization, recorded by the protoliths (for more information, refer to Paulick et al., 2006). This interpretation is motivated by the fact that HFSE are highly immobile and have a low solubility in aqueous solutions and, consequently, observed enrichment cannot be due to hydrothermal processes. Such melt/rock interactions in oceanic peridotites are a common process and have been described so far (e.g. Drouin et al., 2009, 2010; Godard et al., 2008; Seyler et al., 2007; Suhr et al., 2008).

Last, a characteristic alteration with talc predominance was also described in serpentinite samples from the MAR 15°20′N area (ODP Hole 1268A; Paulick et al., 2006). These samples are characterized by a lower content in H_2O (5–6 wt.%) and a higher content in SiO_2 (60–65 wt.%) and FeO (4–5 wt.%) compared to serpentinites. Concerning their trace element compositions, talc-dominated serpentinites present also LREE enrichment, especially on samples deriving after harzburgite (Fig. 5a, b), associated to a negative Eu-anomaly. In contrast to samples that experienced melt/rock interactions, talc-dominated serpentinites are not particularly enriched in HFSE (Fig. 6a, b).

3.1.2.2. Mantle wedge serpentinites. Serpentinites coming from mantle wedge are expected to be highly refractory since this area is believed to have experienced extensive partial melting. Compiled mantle wedge serpentinites (see Section 2.4) are mainly derived after dunite, harzburgite, and lherzolite (Fig. 5d, e, f). In contrast to abyssal serpentinites (see above), we observe a predominance of serpentinites after dunite in the compiled database (Fig. 5d, e). However, it should be noted that this could reflect the over-representation of serpentinites drilled in the Mariana forearc (ODP Legs 125 and 195; Ishii et al., 1992; Kodolányi et al., 2012; Lagabrielle et al., 1992; Parkinson and Pearce, 1998; Savov et al., 2005a,b, 2007) in this compilation of mantle wedge serpentinites, although Savov et al. (2007) observed similarities between Mariana serpentinites and those present in the Franciscan formation and other preserved forearc accretionary sequences (e.g. Bebout, 1995; Bebout and Barton, 2002; Fryer et al., 2000; King et al., 2003, 2006). In spite of this possible sampling bias, systematic characteristics of the mantle wedge serpentinites are generally accepted: preservation of the refractory signature of their protoliths (e.g. Deschamps et al., 2010; Marchesi et al., 2009) and of geochemical evidences of metasomatism by melts and/or fluids taking place before serpentinization (e.g. Deschamps et al., 2010; Parkinson and Pearce, 1998; Savov et al., 2005a,b, 2007).

As observed for abyssal serpentinites, REE compositions of mantle wedge serpentinites are also quite variable, but remain relatively depleted (Figs. 5d, e, f and 7a, b). Serpentinites after dunites (Fig. 5d) have LREE content varying from ~0.005 to ~0.1 CI-Chondrite and HREE from ~0.02 to ~0.2 CI-Chondrite; serpentinites after harzburgites (Fig. 5e) have LREE content varying from ~0.001 to ~0.2 CI-Chondrite and HREE from ~0.02 to ~0.5 CI-Chondrite; and serpentinites after lherzolites (Fig. 5f) have LREE content varying from ~0.01 to ~1 CI-Chondrite and HREE from ~0.1 to ~2 CI-Chondrite. Generally, mantle wedge serpentinized dunites (Fig. 5d) are characterized by U-shaped patterns with smaller positive Eu anomalies compared to abyssal serpentinites ($(Eu/Eu^*)_N = 2.45$ on average). They generally have a small decrease from LREE to MREE ($La/Sm = 4.1$ in average) and a progressive enrichment from MREE to HREE ($Sm/Lu = 0.44$ in average). Mantle wedge serpentinized harzburgites have more heterogeneous REE compositions compared to those from abyssal contexts. No systematic Eu-anomaly can be distinguished. Mantle wedge serpentinites do not display correlations between REE contents and L.O.I., suggesting that they might preserve the REE signature of the mantle protolith (e.g. Savov et al., 2005a,b). Their LREE enriched signature is interpreted as the result of the combination of extensive partial melting and subsequent percolation of LREE-rich fluids or melts through the mantle wedge. As suggested by Savov et al. (2005a, b), such melts or fluids are mainly encountered beneath arcs in intra-oceanic contexts. Their HREE compositions are similar to those observed in ultramafic samples having experienced high degree of melt extraction (e.g. Bodinier and Godard, 2003). Concerning the particular case of serpentinized lherzolite, two types of pattern can be distinguished: (1) those influenced by a mineralogy dominated by clinopyroxene; they have slight enrichment from LREE to MREE, and flat patterns from MREE to HREE; and (2) the second type of pattern is relatively flat from LREE to MREE and slightly enriched from MREE to HREE. Note that only 3 samples (out of 20) indicate a small positive Eu-anomaly.

Mantle wedge spider diagrams (Fig. 6d, e, f) are characterized by Pb and Sr enrichments similar to those of abyssal serpentinites, as well as strong enrichments in Cs and Rb, which were not observed in abyssal contexts. U anomaly is less marked compared to abyssal serpentinites (up to ~0.1 PM values). Positive Eu-anomaly is difficult to discern compared to the neighboring elements. Negative Y-anomaly is present as already observed in the abyssal samples. As expected for mantle wedge derived rocks (which are susceptible to experience mantle melting), most of the trace elements (with the exception of Cs, Rb, Sr and Pb to a lesser extent) are depleted compared to primitive mantle values (McDonough and Sun, 1995). HFSE and Ti (Fig. 7d) are low compared to the depleted mantle estimates (Salters and Stracke, 2004). Low content in HFSE is interpreted as reflecting high degrees of melt extraction (Parkinson and Pearce, 1998; Parkinson et al., 1992). Nb presents a high variation (Savov et al., 2005a,b), especially in serpentinites after dunite; Savov et al. (2005a) and Deschamps et al. (2010) explain this variation by the presence of Nb-bearing oxide phases heterogeneously distributed within samples.

As in the case of abyssal serpentinites, some of the mantle wedge samples present evidence of melt/rock interactions prior to serpentinization process (South Sandwich arc, Pearce et al., 2000; Tso Morari massif, Deschamps et al., 2010). In the case of Tso Morari massif serpentinites, Deschamps et al. (2010) highlighted that studied samples were enriched in elements which are not mobile in aqueous fluids (e.g. Nb or REE) compared to serpentinites coming from Izu–Bonin Mariana arc (Savov et al., 2005a). On the basis of this observation, Deschamps et al. (2010) proposed that such enrichment occurs before the serpentinization, and hence perhaps reflects extensive metasomatism of the mantle protolith (probably by injection of tholeiitic magmas during early intra-oceanic arc stage). These samples, in the case of serpentinized dunite, are characterized by more flat REE patterns (indicated in gray in Fig. 5d) reflecting LREE enrichment. Serpentinites after harzburgite having experienced refertilization (indicated on gray in Fig. 5e) have higher HREE content compared to

other serpentinites, but no flat REE patterns as described previously; LREE are less enriched compared to HREE ($0.07 < (La/Yb)_N < 0.12$). Positive Eu-anomaly is not discernible in these samples. Interestingly, these samples present a huge positive anomaly in U (up to 10 times that of the primitive mantle values). Note also the case of the Caribbean mantle wedge which appears relatively fertile (Saumur et al., 2010) compared to that which is normally described on the literature. The authors propose that this characteristic is due to the short-lived nature of this subduction zone, and consequently to the small volume of igneous rocks produced.

Note the presence within the compilation of serpentinite muds coming essentially from the Mariana forearc (Figs. 5e and 6e; Kodolányi et al., 2012; Savov et al., 2005b). These samples have overall higher trace element compositions compared to serpentinites, with selective enrichment in LREE, and huge variability. Such compositions are easily explained by the presence of fine-grained mafic rock fragments (which are enriched in trace elements) within the serpentinite muds.

3.1.2.3. Subducted (and subduction zones-related) serpentinites. Having experienced complex geological history, subducted serpentinites are not always well constrained in the literature and represent a highly heterogeneous material in terms of origin and geochemical characteristics. In the compiled database (see Section 2.4), we observe that these samples are dominated by serpentinites deriving from harzburgite (more than 70% of the serpentinites; Fig. 5g, h, i).

REE compositions of subducted serpentinites are highly heterogeneous with variability of one to two orders of magnitude (Figs. 5g, h, i and 7a, b). Serpentinites after dunite (Fig. 5g) are mostly characterized by nearly flat REE pattern, with LREE and HREE contents varying from ~0.2 to ~1.5 CI-Chondrite; only one sample displays a positive Eu-anomaly, as well as a strong enrichment in LREE (Zagros suture zone; Aziz et al., 2011). Serpentinized harzburgites have LREE and HREE contents varying from ~0.02 to ~2 CI-Chondrite; few samples are marked by a positive Eu-anomaly and are essentially represented by serpentinites from Feather River ophiolite (Agranier et al., 2007; Li and Lee, 2006). Finally, serpentinites after lherzolite are really heterogeneous, enriched or depleted in LREE (from ~0.1 to ~90 CI-Chondrite) and have HREE content varying from ~1 to ~10 CI-Chondrite. Subducted serpentinite REE patterns distinguish from abyssal and mantle wedge serpentinites which have mostly U-shaped REE patterns.

Subducted serpentinites are enriched in almost every trace elements compared to abyssal and mantle wedge serpentinites. Because of the important heterogeneity and variability of the compiled dataset, it makes no sense to discuss here every chemical anomaly. We observe systematic enrichments only in three elements: Cs, U and above all in Pb (up to ~100 PM values; Fig. 6g, h, i). The important point is that these samples differ by their enrichment compared to abyssal and mantle wedge serpentinites, which represent the possible protoliths for subducted serpentinites before their incorporation into the subduction channel.

Interestingly, we note that the flat REE pattern characteristic of subducted serpentinites is close to the geochemical signature observed for abyssal and mantle wedge serpentinites having experienced melt/rock interactions prior to serpentinization. Thus, the LREE enrichment of subducted serpentinites is probably not due to the serpentinization process itself. Such enriched compositions in subducted serpentinites imply that their mantle protoliths (1) did not experience an influential partial melting event, and/or (2) were refertilized (melt/rock interaction) before serpentinization process, and/or (3) were enriched in a supra-subduction environment by fluids during their hydration. By comparing the geochemical characteristics of compiled subducted serpentinites with data of refertilized serpentinites and abyssal peridotites defined by Niu (2004) (Figs. 7 and 8), we observed similarities. Subducted serpentinites plot on the melt/rock interaction trend on the Th versus Gd/Lu and Nb versus La diagrams (Fig. 8a and b), and present similar enrichments in LREE and HFSE, as discussed in the previous section. In Fig. 8c, d and e, we report serpentinite compositions, as well as data or abyssal peridotites after Niu (2004), in U–Th, Pb–Th, and Pb–U diagrams. Interestingly, we observe that mantle wedge serpentinites plot in the field of the fresh Tonga forearc peridotites defined by Niu (2004), at the most depleted end of the magmatic trends defined by basaltic rocks; all serpentinites are enriched in Pb. Abyssal peridotites and abyssal and mantle wedge serpentinites having experienced melt/rock interactions present strong enrichment in U and deviate from the terrestrial array; a part of the subducted serpentinites present the same behavior. Percolation of silicate melts through mantle peridotite (by reactive porous flow or chromatographic fractionation) is accompanied by enrichment in LREE, as well as in incompatible elements, such as U and Th for example (e.g. Kelemen et al., 1997; Navon and Stolper, 1987). Looking at incompatible elements, it appears that the geochemical signature of subducted serpentinites reflects mostly melt/rock interactions occurring prior to serpentinization; however, we will see later that these rocks experienced also enrichment by fluids during serpentinization.

A scenario to explain trace element enrichments in subducted serpentinites is that they probably mostly derived from the ocean–continent transition (OCT, passive margin). Passive margin and OCT serpentinites must have higher (incompatible) trace element concentrations than abyssal and mantle wedge serpentinites (Kodolányi et al., 2012), due to smaller degrees of partial melting and/or strong refertilization by metasomatizing melts prior to serpentinization. Consequently, the protolith available for serpentinization have less depleted chemical composition compared to other mantle settings. Rifting of continents involves extensional faulting, subcontinental mantle exhumation and magmatism which reflect the ability of the continental lithosphere to localize deformation and melt in the upper part of the lithosphere (Mohn et al., 2012; Müntener et al., 2010). The OCT can form several tens of km wide basins, with a smooth seafloor and dominated by moderate (50%) to highly (95–100%) serpentinized peridotites cored at several ODP sites in the Galicia margin (e.g. Kodolányi et al., 2012; Sutra and Manatschal, 2012). Serpentinization decreases with depth, and gravimetric and seismic profile allows estimation that the serpentinized mantle is about 5 km thick (Afilhado et al., 2008). Olivine is replaced by mesh lizardite-type serpentine and pyroxene is pseudomorphosed by bastite; spinel is sometimes rimmed with plagioclase, indicative of decompression but generally fully replaced by magnetite and chlorite. Locally tectonic breccia and semi-ductile gouge composed of a mixture of gabbro/amphibolite clast and serpentinite in a matrix of calcite and chloritic cataclasite are recovered during drilling. Primary phase chemistry and clinopyroxene trace-element composition indicate slightly depleted

Fig. 7. a.) La/Yb ratio versus Yb contents (ppm) for serpentinites compiled in Fig. 2. Arrows represent the refertilization fingerprint after melt/rock interactions for peridotites. b.) Sm/Yb ratio versus La/Sm ratio. Gray ellipse represents serpentinites deriving from refertilized protoliths. c.) $(Eu/Eu^*)_N$ ratio versus La/Sm ratio ($_N$ = normalized to CI-Chondrite, with $Eu/Eu^* = Eu/((Sm + Gd)/2)$). d.) Ti (ppm) versus Yb (ppm) concentrations. Such a diagram is discriminative between mantle wedge serpentinites having depleted compositions and low Ti content and subducted serpentinites having more fertile compositions. Abyssal peridotites plotted in an intermediary field between both defined previously. Compositions of abyssal peridotites reported for comparison in panels a–d are after Niu (2004). In every graph, estimated composition of the depleted mantle is from Salters and Stracke (2004) and of the primitive mantle is from McDonough and Sun (1995). e.) V (ppm) versus MgO (wt.%; recalculated under anhydrous forms) illustrating melting degrees and oxygen fugacities modeling of peridotite using V–MgO covariations after Lee et al. (2003). Curves represent partial melting trend at 1 log unit intervals, spanning fO_2 from FMQ − 3 to FMQ + 2 (thick solid curve is for FMQ). Dashed lines represent the degree of melt extracted in 10% increment (Lee et al., 2003). Light blue field represent abyssal peridotites and obducted massif or ophiolitic peridotites, assumed to be representative of oceanic mantle, as defined by Frey et al. (1985), Suen and Frey (1987), Bodinier (1988), Bodinier et al. (1988), Fabries et al. (1989) and Burnham et al. (1998).

mantle by less than 10% of partial melting and percolated by mafic melts. Oxygen isotope profiles of serpentinized peridotites show evidence of successive episodes of fluid infiltration (Skelton and Valley, 2000). The earlier event is pervasive and involves high temperature seawater (>175 °C). The absence of antigorite suggests that the temperature is lower than 300 °C at this stage. This serpentinization happens beneath thinned continental crust before rifting and seafloor exhumation of the mantle. Late deformation-channeled infiltration of

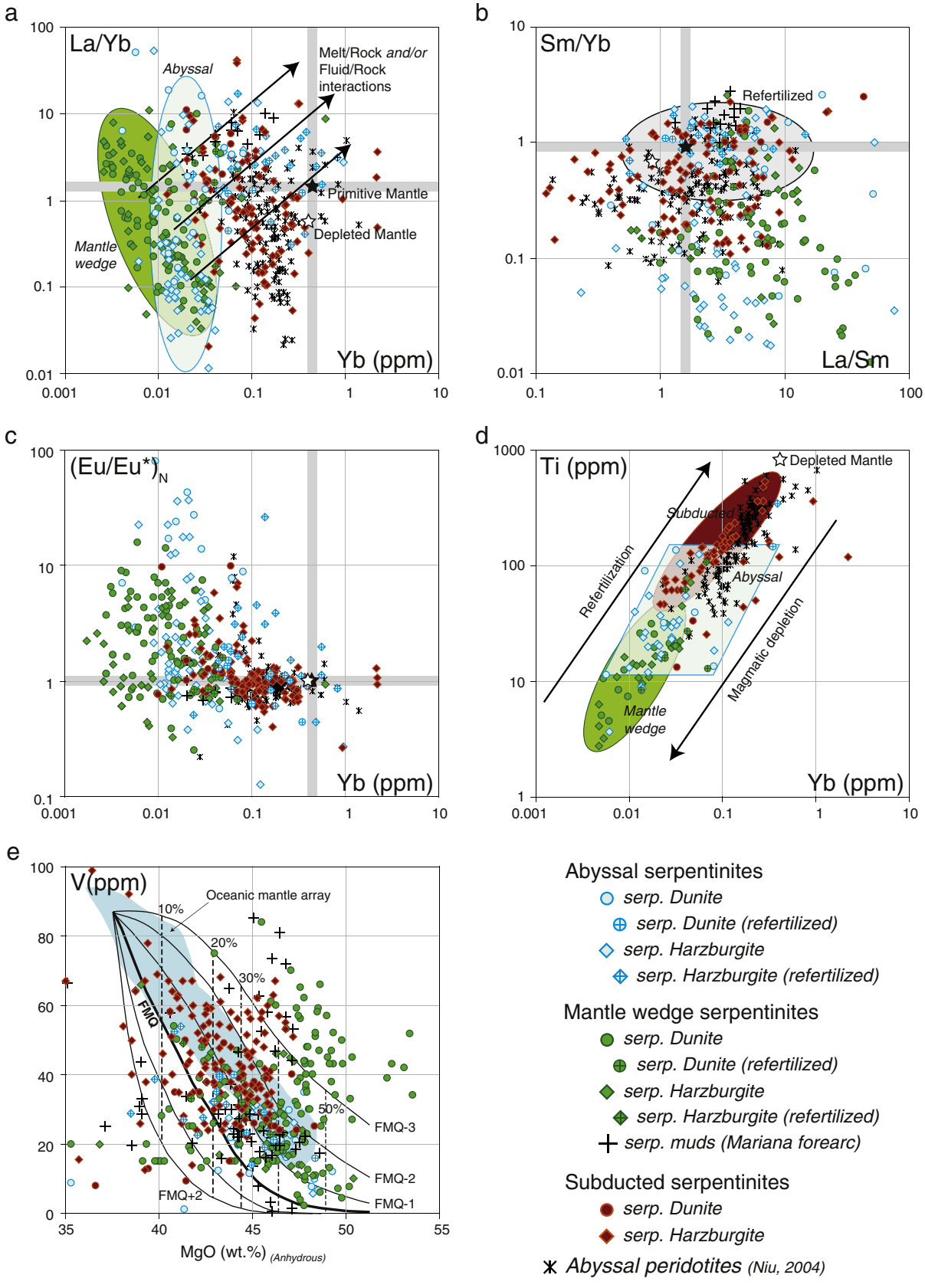

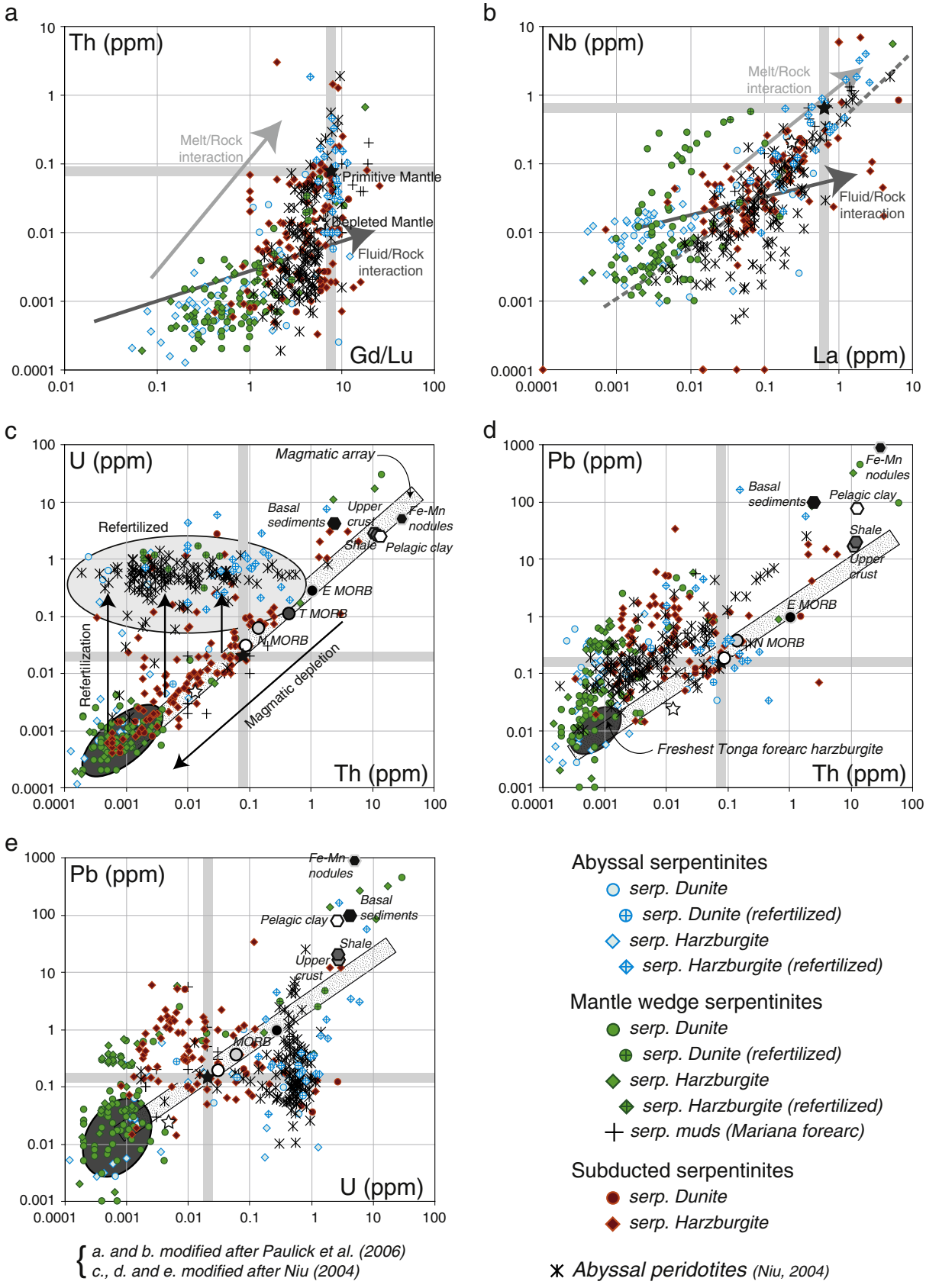

Fig. 8. a.) Th contents (ppm) versus Gd/Lu ratio and b.) Nb versus La contents (ppm) for serpentinites compiled in Fig. 2. Dark gray arrow represents the refertilization fingerprint after melt/rock interactions, whereas light gray arrow represents trend reflecting fluid/rock interactions for peridotites; dashed line represent linear regression for abyssal peridotites (modified after Paulick et al., 2006). c.) U versus Th contents (ppm), d.) Pb versus Th contents (ppm), and e.) Pb versus U contents (ppm) for compiled serpentinites (modified after Niu, 2004). Gray ellipse represents serpentinites deriving from refertilized protoliths. In panels c, d and e, estimates of sedimentary pole are after Li and Schoonmaker (2003), and estimates of MORB compositions are after Klein (2003); shaded area correspond to the magmatic array defined by MORB, OIB, IAB, oceanic gabbros and freshest peridotites; Black field represent freshest Tonga forearc harzburgite (Niu, unpublished data 2004). Compositions of abyssal peridotites after Niu (2004) are reported for comparison. In every graph, estimated composition of the depleted mantle is from Salters and Stracke (2004) and of the primitive mantle is from McDonough and Sun (1995).

cooler sea water (<100 °C) along brittle normal faults accompanies mantle exhumation on the seafloor.

3.2. In situ geochemistry of serpentine phases (lizardite, chrysotile and antigorite)

Numerous in situ studies of the compositions of serpentine minerals were carried out (e.g. Deschamps et al., 2010, 2011, 2012; Kodolányi and Pettke, 2011; Kodolányi et al., 2012; Lafay et al., 2013; Scambelluri et al., 2004a,b; Vils et al., 2008, 2011). These studies were motivated to identify the minerals hosting trace and fluid-mobile elements in bulk serpentinites, to determine the mobility of some elements during subduction-related prograde metamorphism, and to compare the composition between the primary mantle minerals (olivine and pyroxenes) and serpentine phases.

3.2.1. Major elements

Although there are a few stoichiometric differences between lizardite/chrysotile ($Mg_3Si_2O_5(OH)_4$) and antigorite ($Mg_{48}Si_{34}O_{85}(OH)_{62}$), serpentine phases are polytypes and no clear geochemical differences can be distinguished among them with routine microprobe analyses (see O'Hanley, 1996). However, as experimentally demonstrated by Wunder et al. (2001), it is possible to observe some differences between low-grade and high-grade serpentine phases, especially in SiO_2, MgO, and water contents. For example, compared to low-grade serpentine from abyssal serpentinites (e.g. Moll et al., 2007), antigorite from Tso Morari serpentinites (Deschamps et al., 2010) contains slightly higher SiO_2 and lower H_2O and MgO. Such compositions are attributed to partial dehydration during the lizardite/antigorite transition. Additionally, Padrón-Navarta et al. (2008) observed Al enrichment in antigorite from Cerro del Almirez which contribute to the stabilization of antigorite structure at high temperature.

Pseudomorphic serpentine can identify the primary phases (mesh texture after olivine or bastite after pyroxene). Interestingly, the compositional variations of serpentine minerals are often related to the variability of precursor phases (e.g. Deschamps, 2010; Moll et al., 2007). Serpentine after olivine has high MgO (35–45 wt.%) and NiO (up to 0.5 wt.%) contents, whereas serpentines after pyroxene contain lower MgO (on average 25–40 wt.%) and higher Al_2O_3 (up to 4 wt.%) and Cr_2O_3 (up to 1 wt.%) contents. It is difficult to distinguish serpentines formed after orthopyroxene and clinopyroxene using major elements, since Ca is totally removed during serpentinization.

3.2.2. Rare earth elements and moderately incompatible elements

Despite the low concentrations of most trace elements of serpentine minerals, it is possible today to get high-quality data due to the recent progress with in situ analysis technologies (LA-ICP-MS and SIMS). Numerous studies were so far focused on the behavior of selected elements such as Li, Be, B, Cl and As, but recently, increasing database on trace elements, notably REE, allows better understanding of geochemical changes between primary and serpentine phases.

Deschamps et al. (2010) showed that some moderately incompatible elements together with REE could be useful to discriminate serpentines after olivine, orthopyroxene and clinopyroxene. Serpentinized orthopyroxenes are richer in compatible elements such as Sc, Co, V, Zn, Cr, Y and Ti. Serpentine after olivine displays nearly flat REE (La_N/Yb_N ~ 0.93) patterns with concentrations varying from 0.01 to 1 time CI-Chondrite (Fig. 9a), whereas serpentine after orthopyroxene shows higher HREE contents and is characterized by variable LREE/HREE ratios ($0.22 < La_N/Yb_N < 3.77$; Fig. 9c) probably related to geochemical compositions of primary orthopyroxene. Looking at REE patterns of serpentine after clinopyroxene (Fig. 9e), it is obvious that the REE compositions are mainly inherited from clinopyroxene; such patterns are rich in HREE and clearly depleted in LREE (La_N/Yb_N ~ 0.11). However, if it is clear that the composition of serpentine phases after clinopyroxene is controlled by that of the primary minerals, this scenario is not really convincing for serpentine formed after olivine and orthopyroxene. As noted by Deschamps et al. (2010), serpentine interpreted as deriving from olivine is not preferentially enriched in Ni for example. This could be explained by the incorporation of this element into the Fe-oxide phases which formed during serpentinization of olivine. But the most controversial point concerns the relative enrichment in REE of serpentine after olivine compared to fresh olivine. Some authors (Deschamps et al., 2012; Lafay et al., 2013) proposed that a redistribution and equilibration with surrounding matrix occur during serpentinization of primary phases. According to experimental observations (e.g. Allen and Seyfried, 2003), olivine is preferentially altered to serpentine at low temperature (<300 °C) and can experience a (L)REE-enrichment due to homogenization with the surrounding matrix composed of olivines and pyroxenes. Such a scenario can explain the similarities between REE compositions of serpentine after olivine and after orthopyroxene. These geochemical exchanges occur at a very local scale, and explain why the geochemical composition at the scale of the bulk rock samples is not impacted. Further work will confirm (or not) if mostly lithophile trace elements can be used to characterize the primary phases of serpentines.

We observed no significant differences in the trace element compositions, and more specifically, in the REE budget of lizardite and antigorite, except for a slight depletion in REE in antigorite compared to lizardite (Fig. 9). This is illustrated by the analysis of antigorite patches, which formed after lizardite (Queyras Alps, Lafay et al., 2013). This antigorite has lower REE compositions (nearly 10 times less) compared to the surrounding lizardite mesh matrix. This feature could be related to either (1) the inherent geochemical signature of antigorite phase due to its stoichiometric composition, or (2) the release of some mobile elements during the lizardite/antigorite transition as it was demonstrated for some fluid-mobile elements (Kodolányi and Pettke, 2011; Kodolányi et al., 2012; Lafay et al., 2013; Vils et al., 2011). This debated point needs to be more investigated in the future.

3.3. Determination of serpentinization environments using geochemical compositions

Abyssal and mantle wedge serpentinites derive from (strongly) depleted mantle protoliths, and it is not always obvious to distinguish the geological settings in which they were formed when they are sampled in accretionary zones. Moreover, refertilized samples from abyssal and mantle wedge contexts present geochemical characteristics close to those observed in subducted serpentinites. By combining observations of different geochemical features, it is possible to determine the tectonic setting of the mantle rock protolith of serpentinites.

3.3.1. Inherited signature of serpentinite protoliths

The geochemistry of mantle rocks is commonly thought to reflect increasing degrees of melt extraction, from passive margins to mature oceans to subduction zones (Bonatti and Michael, 1989). However, it is quite difficult to determine the geological setting of serpentinites using only major elements (Fig. 4a); for example high MgO/SiO_2 values has been reported for abyssal peridotites (Godard et al., 2008; Paulick et al., 2006) similar to those observed for mantle wedge serpentinites in Himalaya or Mariana forearc. Moreover, numerous processes prior to serpentinization could also modify the compositions of peridotites, such as melt/rock interactions at ridges (e.g. Paulick et al., 2006) or within the mantle wedge (e.g. Pearce et al., 2000). On the other hand, trace element, and particularly REE as discussed above (e.g. Fig. 5), compositions of serpentinites can be used to decipher the nature of the protolith and the interaction(s) with fluid/melt, when compared with petrologically and geodynamically well constrained samples. In this perspective, we hope that our compiled database will be helpful for future studies.

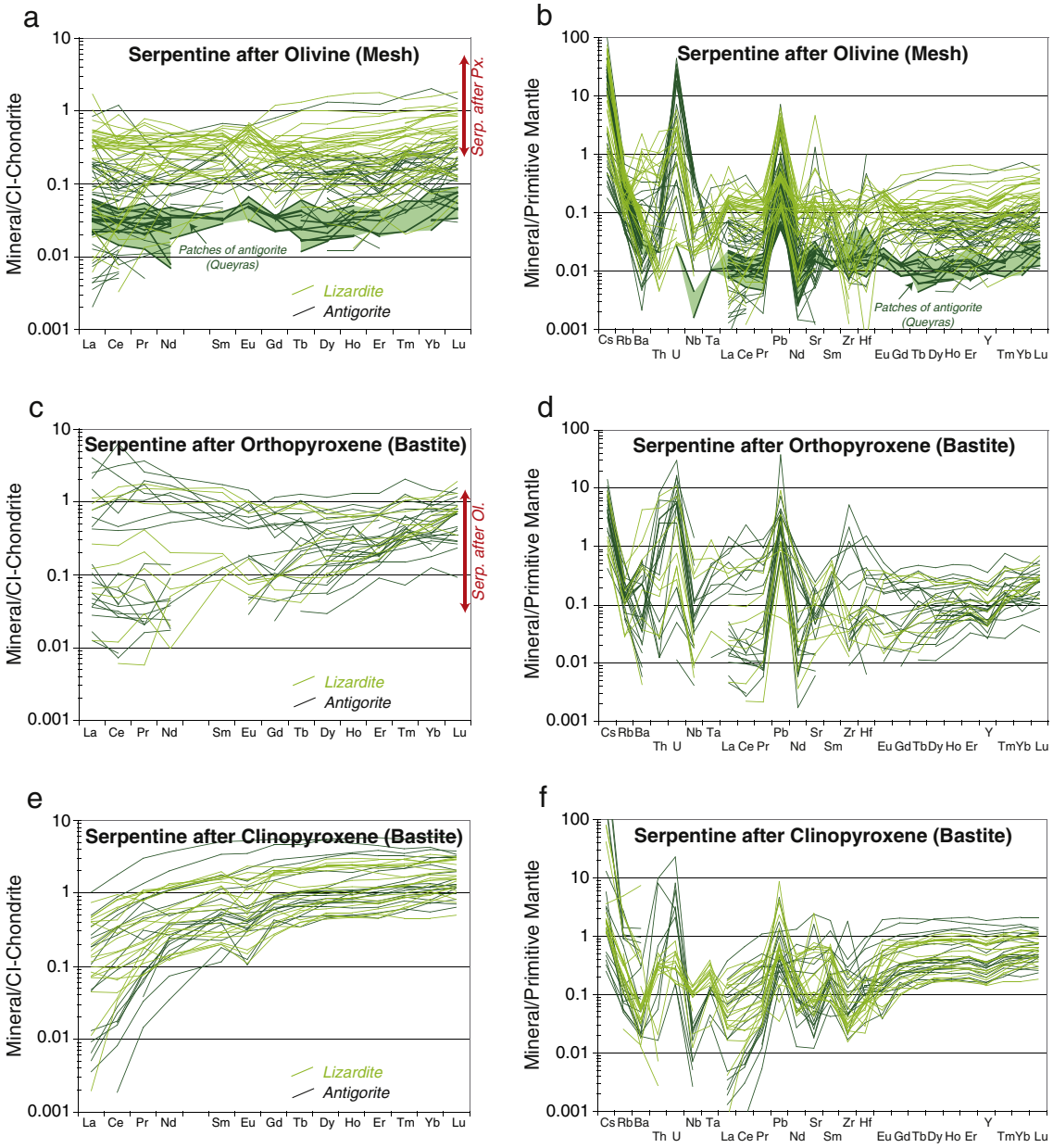

Fig. 9. REE and extended trace element patterns for serpentine phases after a.) and b.) olivine (mesh), c.) and d.) orthopyroxene and e.) and f.) clinopyroxene (bastite). Serpentine compositions are from Deschamps et al. (2010, 2012), Lafay et al. (2013). A distinction was made between lizardite (±chrysotile) (light green patterns) and antigorite (dark green patterns). Thick solid lines highlighted by light green field represent antigorite patches from the Queyras (Lafay et al., 2013). CI-Chondrite and primitive mantle normalizing values are after McDonough and Sun (1995). See text for explanations.

Among trace elements, Ti appears to be a useful tracer in identifying the protolith of serpentinites (Figs. 3e and 7d). It is widely accepted that mantle wedge peridotites, which experienced extensive partial melting, have (highly) refractory compositions. Several authors (e.g. Arai and Ishimaru, 2008) have demonstrated that peridotites in this environment are Ti-depleted; for example, peridotites from serpentinite seamounts in Mariana forearc are characterized by low bulk rock Ti (10–25 ppm; Ishii et al., 1992; Parkinson et al., 1992). Such characteristics will be preserved during serpentinization because essentially no Ti mobility was observed; moreover, refertilized samples from mantle wedge or abyssal context display only limited enrichment in Ti. By plotting compiled serpentinites in a Ti versus Yb diagram, we observe a positive trend defined by all compiled serpentinites, and reflecting refertilization and depletion processes. The diagram shows distinct fields for mantle wedge ($2 < Ti < 50$ ppm), subducted serpentinites ($Ti > 50$ ppm), and abyssal serpentinites (10–130 ppm).

3.3.2. Chromian spinels

A good proxy to determine the geological setting of formation of ultramafic mantle rocks is the concentration of Cr, Al and Ti in Cr-spinel cores (Arai, 1992; Dick and Bullen, 1984; Irvine, 1967), when they are not altered to ferroan chromite or Cr-bearing magnetite. It is accepted that high values of Cr# ($= Cr/(Cr + Al)$) reflect high degrees of melting (Dick and Bullen, 1984; Hellebrand et al., 2001). Thus, abyssal peridotites (and related serpentinites) formed in slow spreading context contain generally chromian spinels having low Cr# ($0.20 < Cr# < 0.60$; Michael and Bonatti, 1985), whereas subduction-related rocks (including mantle wedge rocks) present chromian spinels with higher values of Cr# (>0.40 on average; Dick and Bullen, 1984; Ozawa, 1994; Parkinson and Arculus, 1999). For example, Mariana forearc serpentinites have Cr-spinels with Cr# up to 0.82 (Ishii et al., 1992), and Tso Morari (Ladakh, Himalaya) serpentinites have Cr-spinels with Cr# up to 0.84 (Guillot et al.,

2001). However, it is important to keep in mind that Cr# of chromian spinels could be modified by late stage processes, such as metasomatism and metamorphism, as observed in Slovenska Bistrica (De Hoog et al., 2009) and Dominican Republic (Saumur and Hattori, 2013) ultramafic complex serpentinites.

3.3.3. Redox conditions

Serpentinization plays a role in redox conditions of the mantle which change the oxidation state of redox-sensitive elements. It is recognized that, for a constant amount of Fe remaining, the ratios of $((Fe_2O_3 \times 100)/(Fe_2O_3 + FeO))$ in bulk rock increase with the degree of serpentinization. Ferrous Fe in primary silicates phases oxidize to ferric Fe which is incorporated in serpentine phases and magnetite (e.g. Andreani et al., 2013; Evans et al., 2013). An attempt was made using this database to determinate redox conditions for the protoliths of serpentinites formed. In order to estimate these conditions, we used the V–MgO diagram proposed by Lee et al. (2003), since we know that V records fO_2 during mantle melting (e.g. Lee et al., 2003, 2005). Most data plot between the FMQ+2 and over the FMQ−3 trends (Fig. 7e). However, in detail, we note that abyssal serpentinites fall mainly between FMQ and FMQ−2, and are generally in the oxygen fugacity of the oceanic mantle peridotites close to the fayalite-magnetite-quartz buffer (Bodinier, 1988; Bodinier et al., 1988; Burnham et al., 1998; Fabries et al., 1989; Frey et al., 1985; Suen and Frey, 1987). Compiled subducted serpentinites plot also between the same trends, although mostly of the data seems to be between FMQ−1 and FMQ−2.

Mantle wedge above subduction zones are generally more oxidized than upper mantle in other tectonic contexts (e.g. Parkinson and Arculus, 1999). The occurrence of As(V) in serpentinites in the Himalaya support this notion (Hattori et al., 2005). In the V–MgO diagram, mantle wedge serpentinites data are more heterogeneous and it is difficult to evaluate their redox conditions. However, the fO_2 of the asthenospheric mantle is homogeneous with low fO_2 (Lee et al., 2005; Wang et al., 2007). If we neglect data plotting above the FMQ−3 trend, we observe that, on average, mantle wedge serpentinites have more oxidizing characteristics than serpentinites from abyssal environments and subduction zones. Refertilized samples, from mantle wedge and abyssal settings, plot mostly between FMQ−1 and FMQ+1. However, Fe^{3+} is mainly controlled by metasomatic processes; consequently, the fO_2 value obtained using the V content, and reflecting principally oxygen fugacity records during melting event (Lee et al., 2005), could differ and be lower than the fO_2 values determined thermodynamically in peridotites from subduction zones.

3.3.4. Platinum group elements (PGE)

Harzburgites are generally considered to be residual mantle peridotites after partial melting. Therefore, serpentinites with the pseudomorphic textures of harzburgite are safely assumed to have originated from residual mantle peridotites. Many serpentinites, however, do not retain the pseudomorphic textures. It is a challenge in identification of such serpentinites. Some serpentinites are hydration products of dunite.

Dunite may form as cumulates of mafic magmas. Dunite also forms as a reaction product of primitive mafic melt with peridotites where pyroxene is replaced by olivine. Dunite may form as the result of high degrees of partial melting after fusion of clinopyroxene and orthopyroxene (e.g. Bernstein et al., 2007; Kubo, 2002). Such highly refractory dunite forms through influx fusion in mantle wedges. It is not easy to identify the protoliths of serpentinites formed from dunite based on major and minor element data because any dunite has similar bulk rock compositions. The abundance of platinum group elements (PGE) provides useful information in identifying the two types because PGE signatures are different. PGE are fractionated during partial melting and Ir-type PGE (IPGE; Ir, Os, Ru) remain in the residual mantle peridotites during partial melting (e.g. Brenan et al., 2005). Therefore, melt contains less IPGE, whereas the residual mantle peridotites contain high contents of IPGE.

Among PGE, Pd is mobile in hydrothermal fluids, which causes enrichment and depletion of Pd in serpentinites, and serpentinites commonly show a scatter in the concentrations of Pd. However, IPGE, especially Ir are not mobile during hydrothermal alteration and even intense metasomatism (Wang et al., 2008), which make these as good indicators for evaluating the protoliths of ultramafic rocks. Therefore, the concentration ratios of IPGE to Pt may be used to identify the protoliths of ultramafic rocks (e.g. Guillot et al., 2001; Hattori et al., 2010). The compilation of data in Fig. 10 shows that most serpentinites contain high IPGE, similar to primitive mantle values, suggesting that these serpentinites in subduction zones are residual mantle peridotites. There are, however, ultramafic massifs of cumulate origin based on low concentrations of IPGE.

Good examples of ultramafic rocks include the basal ultramafic rocks of the Nidar ophiolite and Drakkarpo unit in the western Himalayas (Hattori and Guillot, 2007), dunite and garnet-bearing ultramafic rocks in the Dominican Republic (Hattori et al., 2010) and Pohorje complex in eastern Alps of Slovenia (De Hoog et al., 2011), ultramafic massif in the Schistes Lustres near the Pelvas d'Abries (Hattori, unpublished data) and serpentinized dunite that extruded to the seafloor in the Mariana forearc (Hattori and Ishii, unpublished data). These studies suggest that cumulate ultramafic rocks, dunites and wehrlites may form large bodies and massifs of several km in size.

4. Serpentinites: a sink/source vector for fluid-mobile elements

4.1. Fluid-mobile enrichments in bulk serpentinites and related serpentine phases

High contents of FME characterize subduction-related magmas (e.g. Leeman, 1996; Noll et al., 1996; Ryan et al., 1995). The origin of these enrichments has been extensively discussed. Recent studies

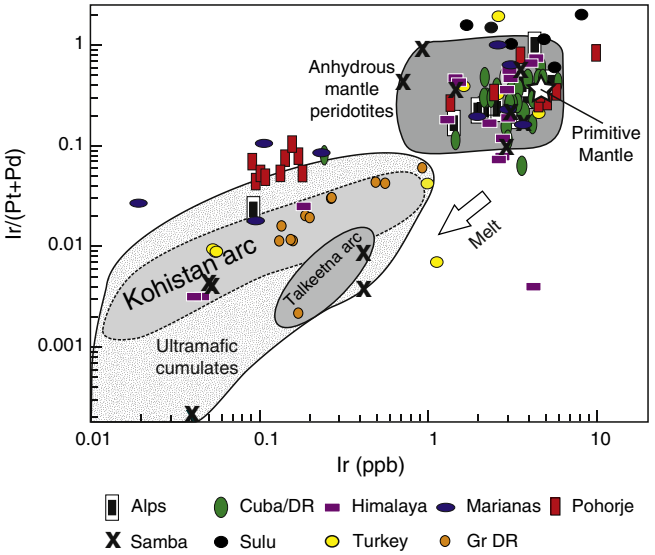

Fig. 10. Ir versus Ir/(Pt + Pd) ratios of ultramafic rocks in subduction zones. Data sources: Alpine serpentinites (Hattori and Guillot, 2007) plus unpublished data of Schistes Lustres near the Pelvas d'Abries; serpentinites from Dominican Republic (DR) and Cuba (Saumur et al., 2010); Himalayan serpentinites near the Tso Morari UHP unit (Hattori and Guillot, 2007); Mariana forearc serpentinites (Unpublished data of Hattori, Ishii, 2006); ultramafic rocks from the Pohorje complex (De Hoog et al., 2011); serpentinites and partially hydrated pyroxene-bearing rocks in the Sanbagawa metamorphic belt (Samba; Hattori et al., 2010); ultramafic massifs in the Sulu UHP belt (Xie et al., in press); and ultramafic rocks from the Anatolia ophiolite, Turkey (Aldanmaz and Koprubasi, 2006).

point to a significant role of serpentinites as sink and source of these elements during subduction (e.g. Deschamps et al., 2011; Hattori and Guillot, 2003, 2007; Kodolányi et al., 2012). FME, such as light elements (B, Li), semi volatile and chalcophile elements (As, Sb, Pb), and large ion lithophile elements (LILE; Sr, Rb, Cs, Ba, Th and U), are preferentially enriched into fluids relative to mineral phases during metamorphic or dehydration reactions. FME are selectively (over-) enriched in serpentinites (e.g. Deschamps et al., 2010, 2011, 2012; Hattori and Guillot, 2007; Kodolányi et al., 2012; Li and Lee, 2006; Savov et al., 2005a,b; Tenthorey and Hermann, 2004) and as such they can be used as tracers for serpentinization processes, from ridges to subduction zone, during secondary serpentinization and prograde metamorphism in the slab and hydration of mantle wedge.

In contrast to the major, minor and moderately incompatible trace element composition of serpentinites, and associated serpentine minerals, is mainly controlled by the composition of their mantle protoliths (see previous part), such is not the case for fluid-mobile elements. The (re-)distribution of FME is mostly controlled by (i) the nature and chemical compositions of hydrating fluids (hydrothermal, seawater, or slab-derived fluids), and (ii) the redox state, duration, and temperature of fluid/rock interaction. On spider diagrams, whatever their protoliths and geological settings, bulk serpentinites (Fig. 6) and associated serpentine minerals (Fig. 9b, d, f) have positive anomalies in Cs, U, Pb, Sr, and to a lesser extent Rb. However, from one geodynamic setting to another, the sequence of FME-enrichment during serpentinization can be different as discussed below.

4.1.1. Light elements: boron and lithium

Serpentinites are probably the most important sink for B in subducting slab (e.g. Agranier et al., 2007; Benton et al., 2001; Bonatti et al., 1984; Boschi et al., 2008; Deschamps et al., 2011; Lee et al., 2008; Pabst et al., 2011; Pelletier et al., 2008; Scambelluri et al., 2004a,b; Spivack and Edmond, 1987; Thompson and Melson, 1970; Vils et al., 2008). B is abundant in seawater (4.6 ppm; Jean-Baptise et al., 1991; Quinby-Hunt and Turekian, 1983) compared to depleted and/or primitive mantle (0.06 and 0.3 ppm respectively), as a consequence, seawater/mantle peridotite interactions will enrich the protolith in B during serpentinization. Experimental work has shown that B is mostly incorporated in serpentinites at temperatures below 300 °C (Seyfried and Dibble, 1980). Our compiled dataset indicates that, regardless of geological settings, bulk rock B contents are limited to about 100 ppm (Fig. 11a). Although the number of data is limited, this maximum value may reflect the structural capacity of serpentine minerals. We do not observe important difference in terms of B-enrichment between abyssal, mantle wedge, and subducted bulk serpentinites. Moreover, as noted by Agranier et al. (2007) and Vils et al. (2008), significant correlations are not observed between the B concentrations and L.O.I. In situ analyses suggest that B is mainly stored in serpentine phases: up to 140 ppm B in abyssal serpentines (Bonatti et al., 1984; Vils et al., 2008, 2011); up to 200 ppm in mantle wedge serpentines (Deschamps et al., 2010; Kodolányi et al., 2012; Pabst et al., 2011); and up to 120 ppm in subducted serpentines (Deschamps et al., 2012; Lafay et al., 2013).

Lithium is enriched in serpentinites (e.g. Agranier et al., 2007; Benton et al., 2004; Decitre et al., 2002; De Hoog et al., 2009; Parkinson and Pearce, 1998; Savov et al., 2005a,b) and such characteristic is in agreement with elevated Li content in seawater (Li and Lee, 2006). Lithium concentrations in bulk serpentinites vary from ~0.1 to ~20 ppm (Fig. 11b). In situ analyses of serpentine phases from natural rock samples and experimental products have demonstrated that serpentine minerals can host large amounts of Li (Deschamps et al., 2010, 2012; Kodolányi et al., 2012; Lafay et al., 2013; Vils et al., 2008, 2011; Wunder et al., 2010). However, in contrast to B, the Li content of serpentine seems partly controlled by protolith minerals. Some authors have proposed that the Li enrichment could be due partly to processes occurring prior to serpentinization (e.g. Kodolányi et al., 2012; Vils et al., 2008), and serpentinization itself should decrease the Li content of the bulk samples (Pelletier et al., 2008; Vils et al., 2008). For example, Kodolányi et al. (2012) observed that serpentines formed after olivine in some samples are depleted in Li compared to the mineral protolith (olivine or pyroxene), whereas bastite pseudomorphs have higher concentrations of Li than original orthopyroxene, for the same samples. On this basis, these authors concluded that serpentinization itself does not fully control the bulk Li budget, at least in oceanic environments, and that the observed Li abundance in serpentinites is likely related to the event before serpentinization, such as melt/rock interaction.

4.1.2. Chalcophile elements: arsenic, antimony, and lead

Because of their high mobility in fluids, these elements represent potential tracers of the nature of fluids during serpentinization. Little data exist today on As and Sb concentrations in serpentinites (Fig. 11g, h); nevertheless it appears that they are moderately to highly enriched in these elements compared to primitive and depleted mantle ($0.1 < As < 10$ ppm; $0.001 < Sb < 1$ ppm; De Hoog et al., 2009; Deschamps et al., 2010, 2011, 2012; Hattori and Guillot, 2003, 2007; Savov et al., 2005a, 2007), independently of the geological settings. As and Sb are largely incorporated by serpentine phases (Deschamps et al., 2010, 2011, 2012), although sulfides can also host a minor fraction (Hattori et al., 2005). Hattori et al. (2005) showed that As(V) is transferred by aqueous fluids from the slab to the mantle wedge, and is incorporated into serpentinites under oxidized conditions at shallow depths (~25 km). The mantle wedge serpentinites from the Tso Morari massif (Himalaya) are distinguished by exceptionally high enrichments in As and Sb in bulk serpentinites (up to ~100 and ~10 ppm respectively; Hattori and Guillot, 2003, 2007), as well as in the serpentine minerals (average $As_{mineral} = 22$ ppm, and $Sb_{mineral} = 6$ ppm; Deschamps et al., 2010), compared to the mantle wedge serpentinites from the Mariana (average As = 0.55 ppm and Sb = 0.055 ppm; Savov et al., 2005a) and subducted serpentinites from the Slovenska Bistrica ultramafic complex (average As = 3.43 ppm and Sb = 0.095; De Hoog et al., 2009). This extreme enrichment of As in serpentinites from the Tso Morari massif reflects high As contents of subducted sediments. The northern margin of the Indian continent was overlain by shallow water sediments formed from Archean granitic rocks (Deschamps et al., 2010; Hattori and Guillot, 2007). This scenario was confirmed by high ^{87}Sr of serpentinites (Hattori and Guillot, 2007) and Pb-isotope systematics (Deschamps et al., 2010). In parallel, the same influence of As- and Sb-rich fluids deriving from (meta)sediments was shown in the case of subducted serpentinites from the Greater Caribbean (Deschamps et al., 2011).

All serpentinites are characterized by high Pb relative to neighboring elements on spider diagrams (Fig. 6). Pb concentrations are usually between 0.01 and 10 ppm (Fig. 11i), and no clear distinctions can be made between abyssal, mantle wedge, and subducted serpentinites. Part of the Pb anomaly may have a protolith origin (e.g. Godard et al., 2008) and it appears that the positive Pb-anomaly is less marked on abyssal and mantle wedge serpentinites that have experienced melt/rock interactions. However, strong Pb enrichments (higher than primitive mantle values) are mainly an effect of fluid percolation during serpentinization. Li and Lee (2006) observed high Pb concentrations associated with low Ce/Pb ratios in Feather River ophiolite serpentinites. Ce/Pb ratio can be fractionated during aqueous fluid/rock interaction (as the aqueous solubility of Pb is much greater than that of Ce), and consequently serpentinization could generate low Ce/Pb ratios. In situ analyses have confirmed that serpentine phases hold an important amount of Pb, but cannot explain totally and sufficiently the bulk Pb content. The same conclusions were reached also for U and Sr; these observations may reveal the role of carbonates to the whole rock budget (Deschamps et al., 2010; Kodolányi et al., 2012), since carbonates are known to host Sr, U, and Pb (e.g. Olivier and Boyet, 2006).

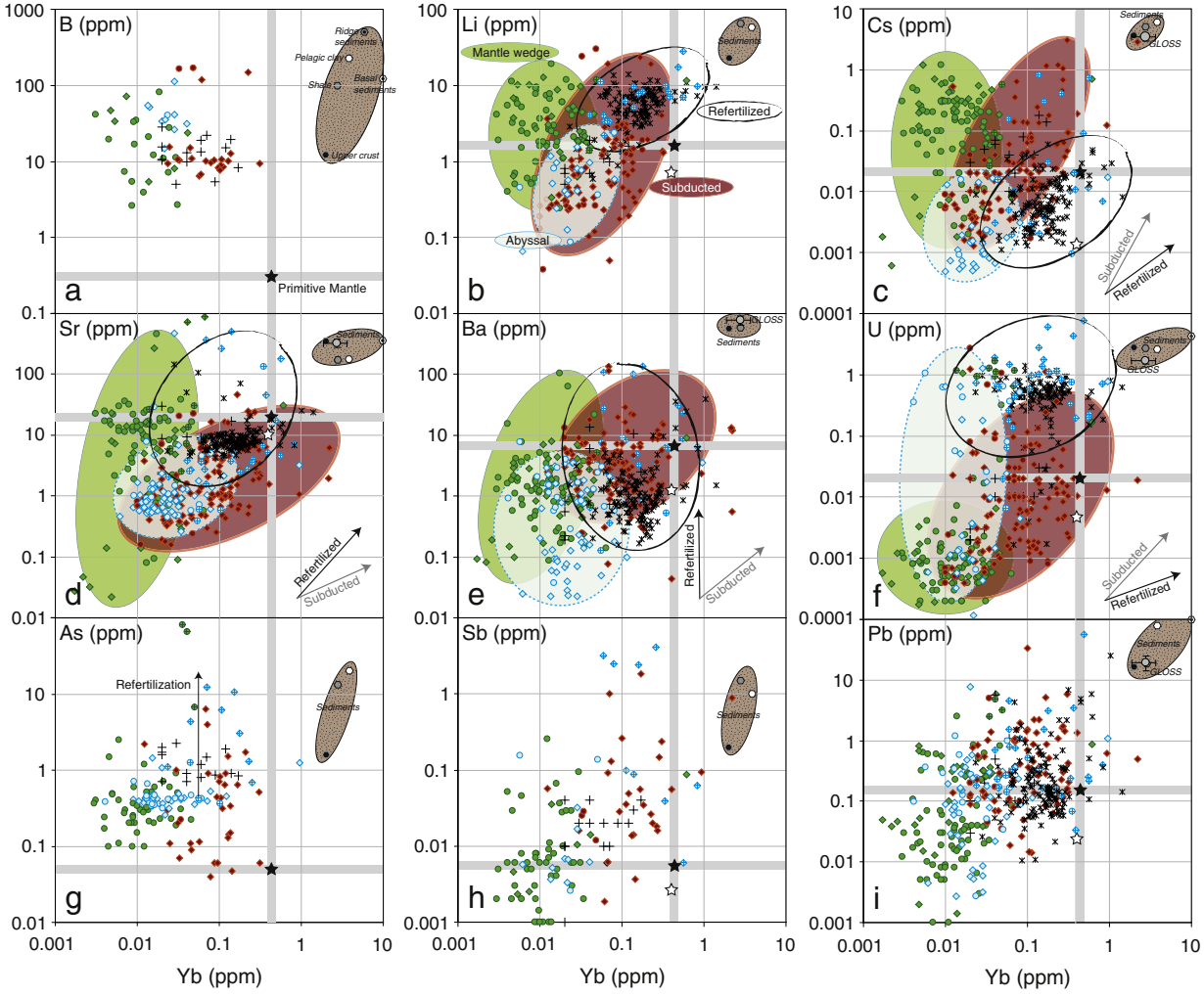

Fig. 11. a.) B, b.) Li, c.) Cs, d.) Sr, e.) Ba, f.) U, g.) As, h.) Sb and i.) Pb versus Yb (ppm) compositions for serpentinites compiled in Fig. 2. Symbols are the same as those used in the previous figs. In every graph, estimated composition of the depleted mantle is from Salters and Stracke (2004) and of the primitive mantle is from McDonough and Sun (1995). Compositions of sedimentary poles are from Li and Schoonmaker (2003) and estimated composition of global subducted sediments (GLOSS) is after Plank and Langmuir (1998).

4.1.3. Uranium and thorium

The bulk rock geochemistry of serpentinites is characterized by positive anomaly in U, and no significant enrichment in Th. Relative to other trace elements with similar compatibility during partial melting in the mantle, these two elements, and especially U, are systematically enriched. This is consistent with the soluble nature of U in fluids (Bailey and Ragnarsdottir, 1994). The origin of the U enrichment is however difficult to assess in subducted serpentinites since two possible processes can explain this feature. Seawater/rock interaction during serpentinization could lead to the observed U enrichment; seawater has U contents of about 3.2 ppb whereas reduced submarine hydrothermal fluids exhibit low U concentrations (e.g. Schmidt et al., 2007) relative to seawater due to uptake of U in the basement rocks. Another possible cause for the enrichment of U is melt/rock interaction (cf. Fig. 8c), as observed for abyssal peridotites (Niu, 2004) and refertilized abyssal and mantle wedge serpentinites which deviate from the terrestrial array. Part of the subducted serpentinites presents the same behavior. However, in Fig. 11f (U versus Yb content), we note that subducted serpentinites overlap both the fields of abyssal serpentinites and of refertilized serpentinites and sediments. Therefore, we speculate that U content in subducted serpentinites could also be controlled by percolation of sediment-deriving fluids; this point will be discussed in the next section.

4.1.4. Uptake and release of fluid-mobile elements: timing (and thermometry) of serpentinization

Although the number of in situ studies of the FME distribution in serpentine minerals is still limited, these studies suggest that different stages of serpentinization control the uptake and release of FME during subduction. It is strongly influenced by the lizardite/antigorite transition (around 300–400 °C; Lafay et al., 2013), and of late antigorite breakdown (600–700 °C; Ulmer and Trommsdorff, 1995; Wunder and Schreyer, 1997). However, the scenarios discussed below should be considered as tentative (and centered on few FME) and need to be supported by further geochemical studies.

In situ analyses on serpentine minerals in the serpentinites from Tso Morari (Himalaya) by Deschamps et al. (2010) have demonstrated that antigorite after olivine is preferentially enriched in As and Sb, and to a lesser extent in B and U, yet antigorite formed after primary orthopyroxene concentrates Pb, Cs, Li, and Ba. This was explained by different temperatures of serpentinization of primary minerals, associated with the differential mobility of FME released from the slab, a process that is temperature-dependent (Bebout, 2007; Bebout et al., 1999). Therefore, according to observations on natural samples (Mével, 2003) and experimental works (Allen and Seyfried, 2003; Godard et al., 2013; Martin and Fyfe, 1970), it appears that olivine is easily destabilized at low temperatures (<300 °C), and serpentinization of olivine (which take place at shallow depth) will consequently incorporate

elements (e.g. As and Sb) released from the slab in the earliest stage of subduction. Then, due to the downward movement of the serpentinites in the mantle wedge, and the associated increase in temperature, orthopyroxene will be transformed into serpentine at temperatures above 400 °C (Allen and Seyfried, 2003; Martin and Fyfe, 1970), and preferentially incorporate elements released later, and at deeper levels, from the slab (e.g. Pb, Cs, Li, Ba).

Another case of differential incorporation of FME was discussed by Kodolányi et al. (2012). They observed that serpentine which formed after orthopyroxene hosts about half the B compared to serpentine formed after olivine in abyssal (Mid-Atlantic Ridge, 15°20′N) and Mariana forearc serpentinites. Thus, they conclude that, in this case, serpentinization started at temperatures above 300–350 °C, and for these conditions orthopyroxene is destabilized to serpentine while olivine remains stable. High-T serpentinization of orthopyroxene will consume a certain amount of B from the fluid and then the remaining olivine will be serpentinized at lower T by a fluid substantially depleted in B.

Last, numerous studies have emphasized the role of the lizardite/antigorite transition on the mobility of FME, especially for B, and to a lesser extent Li and Cl (Deschamps et al., 2011; Kodolányi and Pettke, 2011; Kodolányi et al., 2012; Lafay et al., 2013; Vils et al., 2011). This mineralogical change occurs around 300–400 °C (Fig. 1a; e.g. Lafay et al., 2013). It appears that in subducted serpentinites, low temperature serpentine polymorphs (lizardite, chrysotile) are generally characterized by higher concentrations in B and Li than the high temperature serpentine phase (antigorite). Additionally, Kodolányi and Pettke (2011) observed that antigorite formed after chrysotile is less enriched in B, Cl, and Sr; they explain this loss by fluid-assisted chrysotile-to-antigorite transformation which can remobilize some FME. However, the lizardite-chrysotile/antigorite change is nearly conservative in a simplified CMSH-system, and consequently only a very limited amount of H_2O will be released (Wunder et al., 2001). During this change due to the increasing grade of metamorphism, light elements, and more specifically B, will be liberated together with a fluid phase in a limited quantity. Moreover, as B will be released in larger quantity than Li (Kodolányi and Pettke, 2011; Vils et al., 2011), the lizardite-to-antigorite transition can fractionate B from Li, and is likely to produce fluids with a particularly high B/Li signature.

4.2. Serpentinite fingerprints in subduction geochemical cycle

Many of the fluid-mobile elements (and sometimes associated isotopes) can be used to trace recycling of hydrous materials into the mantle during subduction (Fig. 12), and it is widely accepted that serpentinization will play a major role for the recycling of water and FME (e.g. Hattori and Guillot, 2003; Leeman, 1996; Rüpke et al., 2004; Sharp and Barnes, 2004; Straub and Layne, 2003). In the following, we will review the behavior of FME in serpentinites, from ridges to subduction zones, the transfer of FME into mantle wedge, and their probable role in arc magmatism.

4.2.1. From ridge to forearc environments: incorporation of serpentinites within subduction zones and related FME enrichments

Fluid/rock interactions associated to serpentinization at slow-spreading ridge have important consequences for geochemical cycles in the ocean as well as for elemental fluxes to subduction zones. As mentioned before, and despite the preservation of some geochemical characteristics of the primary rocks, serpentinization causes notable enrichment of FME in hydrated ultramafic rocks. Consequently, subduction of serpentinized oceanic lithosphere will transport into the mantle a non-negligible amount of FME. Subducted serpentinites can derive from abyssal peridotites/serpentinites, and/or (serpentinized) ultramafic rocks from the OCT. Yet, once incorporated into the accretionary prism, and before their exhumation, they will experience a complex geological history (e.g. secondary serpentinization at the trench; e.g. Deschamps et al., 2011) and various chemical interactions with slab-lithologies, (meta)sediments, and aqueous fluids, along the entire prograde path, and these processes may play a role in producing FME enrichments (Deschamps et al., 2011; Lafay et al., 2013).

FME show minor differences in their behavior among abyssal, mantle wedge, and subducted serpentinites (Fig. 11). Mantle wedge serpentinites are enriched in Li, Cs, and partly in Sr compared to abyssal serpentinites which are distinguished by higher concentrations of

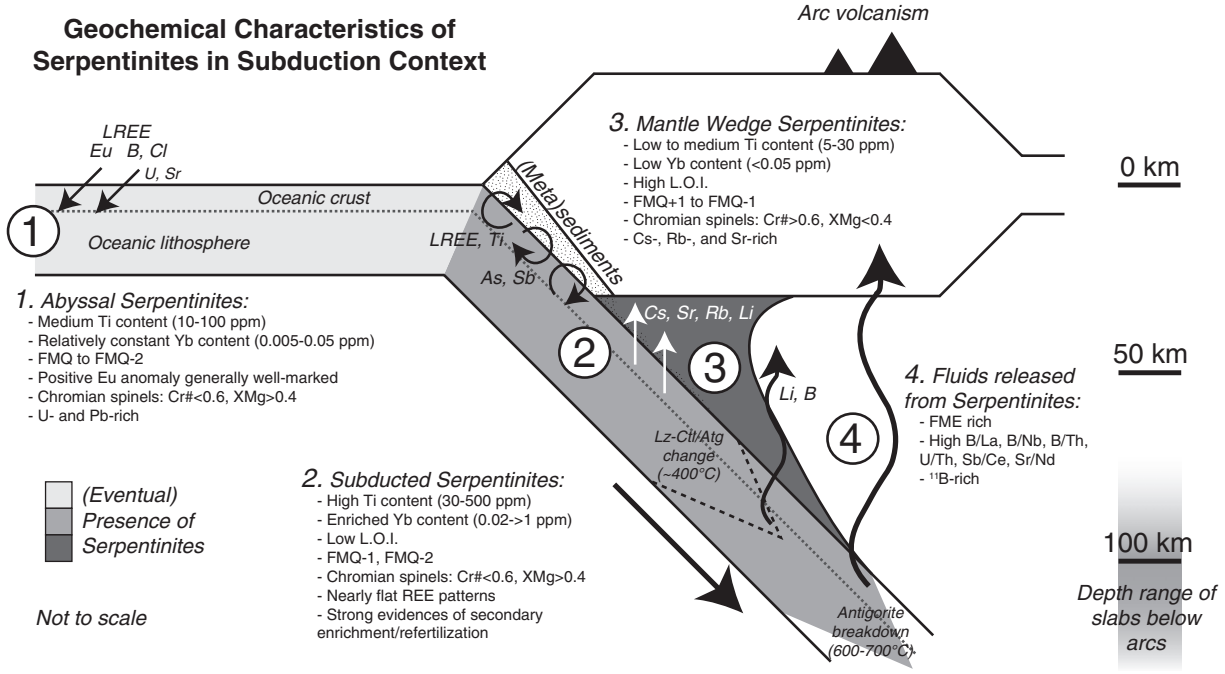

Fig. 12. Schematic cross section of a subduction zone context illustrating the main geochemical characteristics of different serpentinites present in this environment (abyssal, subducted and mantle wedge). Principal transfer of fluid-mobile elements is also noted, as well as geochemical signature of fluids released during dehydration of serpentinites and late "antigorite breakdown" due to the prograde metamorphism.

U. Enrichment in B, As, Sb, and Pb are similar for two types of serpentinites. The concentrations of nearly all the FME in subducted serpentinites overlap those of abyssal and mantle wedge serpentinites. As discussed above (Section 3), subducted serpentinites are enriched in all other trace elements compared with abyssal and mantle wedge serpentinites, and they also show the evidence for melt/rock interactions prior to serpentinization. By comparing subducted serpentinites with refertilized (mantle wedge and abyssal) serpentinites (see above) and abyssal peridotites (Niu, 2004), we observe also differences in the sequence of FME enrichment: the compositional trends defined by subducted serpentinites are different from those in refertilized serpentinites and abyssal peridotites. With the exception of Li which composition is controlled by the protolith, all FME abundance of subducted serpentinites evolves toward sedimentary compositions (Fig. 11). Therefore, we suggest that subducted serpentinites have experienced a complex geological history, notably including first refertilization, and addition of FME induced by (meta)sedimentary-related fluids during subduction.

A second serpentinization can occur during the early stages of subduction, and is mainly controlled by sediment-derived fluids as shown by Deschamps et al. (2011, 2012) on the basis of As and Sb enrichments, and Pb-isotope compositions of bulk serpentinites and associated serpentine phases. On the basis of the study of the accretionary prism of Queyras (Western Alps), Lafay et al. (2013) envisaged two stages for serpentinization. (i) The first stage is associated with the reactivation of normal faults that formed earlier at spreading ridges and/or formation of new bending normal faults at the outer rise/trench zone when the serpentinized oceanic lithosphere enters into the subduction zone (e.g. Ranero et al., 2003, 2005); subsequently such faulting could favor the accumulation of sediments and the infiltration of sediment-derived fluids into the slab. (ii) The second scenario, which seems more realistic and efficient, implies that sediment-derived fluids percolate throughout the serpentinites within the subduction channel, where (meta)sediments and serpentinites are more or less intimately mixed. This last scenario is confirmed by field observations where serpentinites wrap (meta)sediment blocks for example (e.g. Guillot et al., 2009), as well as by numerical models (e.g. Gerya and Stöckhert, 2002; Gorczyk et al., 2007). In this environment, serpentinites will store a non-negligible amount of FME. Moreover, it is assumed that serpentinites can act as sponges by acquiring and bringing at deeper depth a sedimentary signature (Deschamps et al., 2011; Lafay et al., 2013) until they are released by dehydration of serpentinites, during antigorite breakdown as discussed below.

4.2.2. Fluid transfers from the slab to the mantle wedge

The dehydration of the subducting slab (which experiences increasing pressure and temperature triggering prograde metamorphic changes and dehydration) liberates a significant amount of fluids into the mantle wedge (Hyndman and Peacock, 2003; Schmidt and Poli, 1998, 2003; Tatsumi and Eggins, 1995), which as a result experiences serpentinization.

Due to high degrees of melting and melt extraction of the mantle protoliths, mantle wedge serpentinites are characterized by low to very low trace element concentrations. Relative to other elements with similar compatibility (Figs. 6d, e, f and 11), mantle wedge serpentinites are characterized by generally strong bulk-rock enrichment in Cs, Rb, Sr, Ba, Pb, and Li. These high contents in FME, notably in alkali elements, probably reflect the elevated concentrations of these elements in the mantle wedge hydrating fluids. Compared with the hydrothermal fluids serpentinizing the abyssal mantle at ridges, these fluids are especially rich in Cs, Rb, and Sr which suggest that they originate from sediment dehydration during shallow subduction, for instance beneath forearcs (e.g. Bebout and Barton, 2002; Hyndman and Peacock, 2003; Iwamori, 1998; Scambelluri et al., 2004b; Schmidt and Poli, 1998, 2003; You et al., 1996). Several studies support this hypothesis. Kodolányi et al. (2012) and Aziz et al. (2011) point out that mantle wedge serpentinites from different forearc systems display the same LILE enrichments, indicating interaction with sediment-derived fluids having high LILE contents (Ba/Th (up to 1200), U/Th (up to 90), Ba/La (up to 285), Sr/Ce (up to 420), and Ba/Rb (up to 125) in mantle wedge serpentinites). Stable isotope ($\delta^{18}O$ and δD) measurements on serpentinites from Mariana forearc also indicate that the fluids responsible for serpentinization could be ultimately derived from the sediments in the subducting slab (Alt and Shanks, 2006). Alt and Shanks (2006) estimate that serpentinization took place within the mantle wedge over temperatures of about 300–375 °C, and that percolating fluids were released from the slab at a temperature lower than 200 °C.

4.2.3. Serpentinite dehydration and its relation with arc magmatism

Although it is widely accepted today that the FME-rich signature observed in arc magmas is explained by the subducted sediments and altered oceanic crust, an increasing number of observations indicates that serpentinites have a role in the process (e.g. Singer et al., 2007; Stern et al., 2006; Tonarini et al., 2007). Hattori and Guillot (2003) have proposed a relation between location of active arc volcanoes on the surface, and the depth of slab below the volcanic front, which is generally between 80 and 140 km depth (Figs. 1a and 12). This depth interval corresponds to the maximum pressure of the stability field of antigorite (Ulmer and Trommsdorff, 1995; Wunder and Schreyer, 1997). The release of water from serpentinites occurs later, deeper, and produces a greater amount of water than most of the hydrous slab-constitutive lithologies that releases water continuously during their subduction history (Rüpke et al., 2002, 2004). As observed before, mantle wedge and subducted serpentinites are FME-rich, and they will release also large amount of FME during antigorite breakdown, since they are not compatible with newly formed olivine (Tenthorey and Hermann, 2004), as well as halogens (e.g. F, Cl, Br, and I; John et al., 2011) and noble gas (e.g. Ne, Ar, Kr and Xe; Kendrick et al., 2011). Moreover, according to the model of "sponge" serpentinites which could act as a temporary reservoir (Deschamps et al., 2011), once incorporated into serpentinites, FME become immobile (with the exception of B, and to a lesser extent Li partially released at the lizardite/antigorite transition) and can be transferred downward until antigorite breakdown (~600–700 °C). This contrast with the well known devolatilization of FME usually observed for subducted sedimentary rocks (e.g. Bebout et al., 1999, 2007) and altered oceanic crust during prograde metamorphism (e.g. Bebout, 2007; Marschall et al., 2007).

When serpentine phases are destabilized, FME-rich aqueous fluids released from serpentinites will migrate upward, through the anhydrous mantle wedge, will trigger partial melting, and subsequently FME can be incorporated into the arc magmas. Enrichments in As, Sb, Pb, and B, elements which are hosted by serpentinites (Fig. 11), are commonly observed in arc magmas (e.g. Leeman, 1996; Noll et al., 1996; Ryan et al., 1995). The elevated B concentrations observed in some arc lavas (high B/La ~5–50) have been interpreted as evidence of mantle wedge metasomatism by serpentinite-derived fluids (e.g. Ishikawa et al., 2001; Singer et al., 2007). These observations must be related to the conclusions of Savov et al. (2007) who propose that dehydration of serpentinites leads to loss of over 80% of B and 9% of Li. B and Li can be easily traced using their isotopes which have specific signature (e.g. Benton et al., 2001, 2004; Ishikawa et al., 2001; Singer et al., 2007), notably due to isotopic fractionation during dehydration (Wunder et al., 2010). In this context, B concentrations and isotope compositions could be valuable tracers of serpentinite influence upon arc magma geochemical compositions, as it is the case for Pb-isotope compositions in subducted sediments which influence isotope compositions of arc magmas. It is accepted that the B isotope compositions of arc magmas cannot be solely explained by the influence of fluids released from oceanic crust or sediments upon the arc magma mantle source, and therefore subducted and/or mantle wedge

serpentinites play a non-negligible role in this context (e.g. Benton et al., 2001; Scambelluri and Tonarini, 2012; Straub and Layne, 2002; Tonarini et al., 2007, 2011). Note that chlorine (which was not presented in this study due to the small amount of reliable data) and particularly Cl-isotope also allow tracing of serpentinite-derived fluids (e.g. Barnes and Straub, 2010; Barnes et al., 2008; Bonifacie et al., 2008). Another probable influence of serpentinites on the formation of subduction-related volcanic rocks relates to the observed depletion of high-field-strength elements (HFSE; Nb, Ta, Zr, Hf, and Ti) compared to large-ion lithophile elements (LILE; Rb, Ba). Garrido et al. (2005) propose that dehydration of antigorite produce chlorite-harzburgite which may scavenge HFSE from the released fluids, due to the formation of F–OH–Ti–clinohumite; this last phase can retain HFSE during melt generation and/or transport. A last point discussed by Niu (2004) concerns the high U/Pb ratio observed on abyssal peridotites, refertilized abyssal and mantle wedge serpentinites, and partly on subducted serpentinites. If such characteristics are preserved during subduction, it is possible that these rocks could contribute to compositional heterogeneities in the Earth's mantle, and notably to the HIMU isotopic signatures observed on some oceanic island basalts (Niu, 2004).

Few studies exist today about the nature and geochemical compositions of fluids released during dehydration of serpentinites (Garrido et al., 2005; Scambelluri et al., 1995; Scambelluri et al., 2001a,b, 2004a, 2004b; Tatsumi and Nakamura, 1986; Tenthorey and Hermann, 2004), and to our knowledge, only few field geological evidence of dehydrations of serpentinites, with the transition from serpentine phases to anhydrous mantle minerals is documented (Cerro del Almirez massif, Spain; e.g. Marchesi et al., 2013-this volume; Padrón-Navarta et al., 2011; Scambelluri et al., 2001a; Trommsdorff et al., 1998; Tso Morari, Himalaya; e.g. Guillot et al., 2001; Hattori and Guillot, 2007).

5. Summary

We compiled >900 available geochemical data of abyssal, mantle wedge, and subducted serpentinites in order to evaluate the geochemical evolution of these rocks during their subduction history as well as their roles in the global geochemical cycle. A summary of the geochemical characteristics of serpentinites, depending on the context in which they were formed, is given in Fig. 12.

(1) Abyssal and mantle wedge serpentinites are characterized by refractory compositions. No evidence of mobility (with the exception of Ca) is observed for major elements and most trace elements. Thus, REE and IPGE can be used to characterize the initial protolith. However, we observe samples having high LREE that likely reflect processes before serpentinization, such as melt/rock interactions.
(2) Subducted serpentinites are characterized by less refractory compositions, and notable enrichments in REE. Such compositions could reflect a magmatic refertilization process, and/or could be related to the intrinsic nature of the protolith (such as an ocean–continent transition mantle).
(3) Based on a selected geochemical features (REE patterns, Ti and PGE contents, Cr# of chromian spinel), it is possible to estimate the nature of the initial protolith for serpentinites, as well as the geological settings in which they were formed.
(4) All serpentinites, whatever the geological settings, are characterized by moderate to strong enrichments in fluid-mobile elements (such as B, Li, As, Sb, Pb, U, Cs, Sr, Ba) during serpentinization. In detail, FME enrichment in subducted serpentinites is characterized by a strong influence of sediment-derived fluids, and result from late chemical interactions probably within the subduction channel.
(5) Serpentinites must be taken into account for the interpretation of fluid-mobile element compositions, as well as isotopic signature (B, Li, Pb), of arc magmas.

Acknowledgments

FD is grateful to B. Reynard for encouraging him to write this contribution. The research project was supported by CNRS INSU. This paper has been greatly improved by M. Scambelluri, C. Marchesi and an anonymous reviewer.

Appendix A. Supplementary data

Supplementary data to this article can be found online at http://dx.doi.org/10.1016/j.lithos.2013.05.019.

References

Afilhado, A., Matias, L., Shiobara, H., Hirn, A., Mendes-Victor, L., Shimamura, H., 2008. From unthinned continent to ocean: the deep structure of the West Iberia passive continental margin at 38°N. Tectonophyics 458, 9–50.
Agranier, A., Lee, C.-T.A., Li, Z.-X.A., Leeman, W.P., 2007. Fluid mobile element budgets in serpentinized oceanic lithospheric mantle: insights from B, As, Li, Pb, PGEs and Os isotopes in the Feather River Ophiolite, California. Chemical Geology 245, 230–241.
Agrinier, P., Cannat, M., 1997. Oxygen-isotope constraints on serpentinization processes in ultramafic rocks from the Mid-Atlantic Ridge (23°N). In: Karson, J.A., Cannat, M., Miller, D.J., Elthon, D. (Eds.), Proceedings of the Ocean Drilling Program, Scientific Results, 153, pp. 381–388.
Aldanmaz, E., Koprubasi, N., 2006. Platinum-group-element systematics of peridotites from ophiolite complexes of northwest Anatolia, Turkey: implications for mantle metasomatism by melt percolation in a supra-subduction zone environment. International Geology Review 48, 420–442.
Allen, D.E., Seyfried Jr., E., 2003. Compositional controls on vent fluids from ultramafic-hosted hydrothermal systems at mid-ocean ridges: an experimental study at 400 °C, 500 bars. Geochimica et Cosmochimica Acta 67 (8), 1531–1542.
Allen, D.E., Seyfried Jr., E., 2005. REE controls in ultramafic-hosted MOR hydrothermal systems: an experimental study at elevated temperature and pressure. Geochimica et Cosmochimica Acta 69, 675–683.
Alt, J.C., Shanks III, W.C., 2006. Stable isotope compositions of serpentinite seamounts in the Mariana forearc: serpentinization processes, fluid sources and sulphur metasomatism. Earth and Planetary Science Letters 242, 272–285.
Amstutz, A., 1951. Sur l'évolution des structures alpines. Archives des Sciences 4, 323–329.
Andreani, M., Mével, C., Boullier, A.-M., Escartin, J., 2007. Dynamic control on serpentine crystallization in veins: constraints on hydration processes in oceanic peridotites. Geochemistry, Geophysics, Geosystems. http://dx.doi.org/10.1029/2006GC001373.
Andreani, M., Muñoz, M., Marcaillou, C., Delacour, A., 2013. μXANES study of iron redox state in serpentine during oceanic serpentinization. Lithos. 178, 70–83.
Anselmi, B., Mellini, M., Viti, C., 2000. Chlorine in the Elba, Monti Livornesi and Murlo serpentines: evidence for sea–water interaction. European Journal of Mineralogy 12, 137–146.
Arai, S., 1992. Chemistry of chromian spinel in volcanic rocks as a potential guide to magma chemistry. Mineralogical Magazine 56, 173–784.
Arai, S., 1994. Characterization of spinel peridotites by olivine–spinel compositional relationships: review and interpretation. Chemical Geology 113, 191–204.
Arai, S., Ishimaru, S., 2008. Insights into petrological characteristics of the lithosphere of mantle wedge beneath arcs through peridotite xenoliths: a review. Journal of Petrology 49 (4), 665–695.
Arai, S., Abe, N., Ishimaru, S., 2007. Mantle peridotites from the Western Pacific. Gondwana Research 11, 180–199.
Arcay, D., Tric, E., Doin, M.-P., 2005. Numerical simulations of subduction zones: effect of slab dehydration on the mantle wedge dynamics. Physics of the Earth and Planetary Interiors 149 (1–2), 133–153.
Augustin, N., Paulick, H., Lackschewitz, K.S., Eisenhauer, A., Garbe-Schönberg, D., Kuhn, T., Botz, R., Schmidt, M., 2012. Alteration at the ultramafic-hosted Logatchev hydrothermal field: constraints from trace element and Sr–O isotope data. Geochemistry, Geophysics, Geosystems. http://dx.doi.org/10.1029/2011GC003903.
Aumento, F., Loubat, H., 1971. The Mid-Atlantic Ridge near 45°N. XVI. Serpentinized ultramafic intrusions. Canadian Journal of Earth Sciences 8, 631–663.
Aziz, N.R.H., Aswad, K.J.A., Koyi, H.A., 2011. Contrasting settings of serpentinite bodies in the northwestern Zagros Suture Zone, Kurdistan region, Iraq. Geological Magazine 148, 819–837.
Bach, W., Klein, F., 2009. The petrology of seafloor rodingites: insights from geochemical reaction path modelling. Lithos 112, 103–117.
Bach, W., Garrido, C.J., Paulick, H., Harvey, J., Rosner, M., 2004. Seawater–peridotite interactions: first insights from ODP Leg 209, MAR 15°N. Geochemistry, Geophysics, Geosystems 5. http://dx.doi.org/10.1029/2004GC000744.
Bailey, E.H., Ragnarsdottir, K.V., 1994. Uranium and thorium solubilities in subduction zone fluids. Earth and Planetary Science Letters 124, 119–129.
Ballhaus, C., Berry, R.F., Green, D.H., 1991. High pressure experimental calibration of the olivine–orthopyroxene–spinel oxygen geobarometer: implications for the oxidation state of the upper mantle. Contributions to Mineralogy and Petrology 107, 27–40.

Barnes, J.D., Straub, S.M., 2010. Chlorine stable isotope variations in Izu–Bonin tephra: implications for serpentinites subduction. Chemical Geology 272, 62–74.

Barnes, J.D., Sharp, Z.D., Fischer, T.P., 2008. Chlorine isotope variations across the Izu–Bonin–Mariana arc. Geology 36 (11), 883–886.

Bebout, G., 1995. The impact of subduction-zone metamorphism on mantle-ocean chemical cycling. Chemical Geology 126 (2), 191–218.

Bebout, G.E., 2007. Metamorphic chemical geodynamics of subduction zones. Earth and Planetary Science Letters 260, 373–393.

Bebout, G.E., Barton, M.D., 1989. Fluid flow and metasomatism in a subduction zone hydrothermal system: Catalina Schist terrane, California. Geology 17, 976–980.

Bebout, G.E., Barton, M.D., 2002. Tectonic and metasomatic mixing in a subduction-zone melange: insights into the geochemical evolution of the slab-mantle interface. Chemical Geology 187, 79–106.

Bebout, G.E., Ryan, J.G., Leeman, W.P., Bebout, A.E., 1999. Fractionation of trace elements by subduction-zone metamorphism — effect of convergent-margin thermal evolution. Earth and Planetary Science Letters 171, 63–81.

Bebout, G.E., Bebout, A.E., Graham, C.M., 2007. Cycling of B, Li, and LILE (K, Cs, Rb, Ba, Sr) into subduction zones: SIMS evidence from micas in high-P/T metasedimentary rocks. Chemical Geology 239, 284–304.

Benton, L.D., Ryan, J.G., Tera, F., 2001. Boron isotopes systematics of slab fluids as inferred from a serpentine seamount, Mariana forearc. Earth and Planetary Science Letters 187, 273–282.

Benton, L.D., Ryan, J.G., Savov, I.P., 2004. Lithium abundance and isotope systematics of forearc serpentinites, Conical Seamount, Mariana forearc: insights into the mechanics of slab-mantle exchange during subduction. Geochemistry, Geophysics, Geosystems 5 (8). http://dx.doi.org/10.1029/2004GC000708.

Bernstein, S., Kelemen, P.B., Hanghoj, K., 2007. Consistent olivine Mg# in cratonic mantle reflects Archean mantle melting to the exhaustion of orthopyroxene. Geology 35, 459–462.

Bideau, D., Hébert, R., Hékinian, R., Cannat, M., 1991. Metamorphism of deep-seated rocks from the Garrett ultrafast transform (East Pacific Rise) near 13°25′S. Journal of Geophysical Research 96 (B6), 10,079–10,099.

Bird, P., 2003. An updated digital model of plate boundaries. Geochemistry, Geophysics, Geosystems 4 (3). http://dx.doi.org/10.1029/2001GC000252.

Blanco-Quintero, I., Proenza, J.A., Garcia-Casco, A., Tauler, E., Gali, S., 2011. Serpentinites and serpentinites within a fossil subduction channel: La Corea mélange, Eastern Cuba. Geologica Acta 9, 389–405.

Bodinier, J.-L., 1988. Geochemistry and petrogenesis of the Lanzo Peridotite Body, Western Alps. Tectonophysics 149, 67–88.

Bodinier, J.-L., Godard, M., 2003. Orogenic, ophiolitic, and abyssal peridotites. Treatise on Geochemistry. In: Carlson, R.W. (Ed.), Mantle and Core. Treatise on Geochemistry, vol. 2. Elsevier Science Ltd., pp. 103–170.

Bodinier, J.-L., Dupuy, C., Dostal, J., 1988. Geochemistry and petrogenesis of Eastern Pyrenean peridotites. Geochimica et Cosmochimica Acta 52, 2893–2907.

Bogolepov, V.G., 1970. Problem of serpentinization of ultrabasic rocks. International Geology Review 12, 421–432.

Boillot, G., Grimaud, S., Mauffret, A., Mougenot, D., Kornprobst, J., Mergoil-Daniel, J., Torrent, G., 1980. Ocean–continent boundary off the Iberian margin: a serpentinite diapir west of the Galicia Bank. Earth and Planetary Science Letters 48, 23–34.

Bonatti, E., 1976. Serpentinite protrusions in the oceanic crust. Earth and Planetary Science Letters 32, 107–113.

Bonatti, E., Michael, P.J., 1989. Mantle peridotites from continental rifts to ocean basins to subduction zones. Earth and Planetary Science Letters 91, 297–311.

Bonatti, E., Lawrence, J.R., Morandi, N., 1984. Serpentinization of oceanic peridotites: temperature dependence of mineralogy and boron content. Earth and Planetary Science Letters 70, 88–94.

Bonifacie, M., Busigny, V., Mével, C., Philippot, P., Agrinier, P., Jendrzejewski, N., Scambelluri, M., Javoy, M., 2008. Chlorine isotopic composition in seafloor serpentinites and high-pressure metaperidotites. Insights into oceanic serpentinization and subduction processes. Geochimica et Cosmochimica Acta 72, 126–139.

Boschi, C., Früh-Green, G.L., Delacour, A., Karson, J.A., Kelley, D.S., 2006. Mass transfer and fluid flow during detachment faulting and development of an oceanic core complex, Atlantis Massif (MAR 30°N). Geochemistry, Geophysics, Geosystems. http://dx.doi.org/10.1029/2005GC001074.

Boschi, C., Dini, A., Fruh-Green, G.L., 2008. Isotopic and element exchange during serpentinization and metasomatism at the Atlantis Massif (MAR 30 degrees N): insights from B and Sr isotope data. Geochimica et Cosmochimica Acta 72, 1801–1823.

Bostock, M.G., Hyndman, R.D., Rondenay, S., Peacock, S.M., 2002. An inverted continental Moho and serpentinization of the forearc mantle. Nature 417, 536–538.

Brenan, J.M., McDonough, W.F., Ash, R., 2005. An experimental study of the solubility and partitioning of iridium, osmium and gold between olivine and silicate melt. Earth and Planetary Science Letters 237, 855–872.

Bromiley, G.D., Pawley, A.R., 2003. The stability of antigorite in the systems $MgO–SiO_2–H_2O$ (MSH) and $MgO–Al_2O_3–SiO_2–H_2O$ (MASH): the effects of Al^{3+} substitution on high-pressure stability. American Mineralogist 88, 99–108.

Burnham, O.M., Rogers, N.W., Pearson, D.G., van Calsteren, P.W., Hawkesworth, C.J., 1998. The petrogenesis of the eastern Pyrenean peridotites: an integrated study of their whole-rock geochemistry and Re–Os isotope composition. Geochimica et Cosmochimica Acta 62, 2293–2310.

Cagnioncle, A.-M., Parmentier, E.M., Elkins-Tanton, L.T., 2007. Effect of solid flow above a subducting slab on water distribution and melting at convergent plate boundaries. Journal of Geophysical Research 112 (B09402). http://dx.doi.org/10.1029/2007JB004934.

Canil, D., 1992. Orthopyroxene stability along the peridotite solidus and the origin of cratonic lithosphere beneath southern Africa. Earth and Planetary Science Letters 111, 83–95.

Cannat, M., 1993. Emplacement of mantle rocks in the seafloor at Mid-Atlantic Ridges. Journal of Geophysical Research 98, 4163–4172.

Cannat, M., Mével, C., Maia, M., Deplus, C., Durand, C., Gente, P., Agrinier, P., Belarouchi, A., Dubuisson, G., Hulmer, E., Reynolds, J., 1995. Thin crust, ultramafic exposures, and rugged faulting patterns at the Mid-Atlantic Ridge (22°24°N). Geology 23, 49–52.

Cannat, M., Fontaine, F., Escartín, J., 2010. Serpentinization at slow-spreading ridges: extent and associated hydrogen and methane fluxes, in diversity of hydrothermal systems on slow spreading ocean ridge. AGU Geophysical Monograph, Ridges 188, 241–264.

Carlson, R.L., 2001. The abundance of ultramafic rocks in Atlantic Ocean crust. Geophysical Journal International 144, 37–48.

Chalot-Prat, F., Ganne, J., Lombard, A., 2003. No significant element transfer from the oceanic plate to the mantle wedge during subduction and exhumation of the Tethys lithosphere (Western Alps). Lithos 69, 69–103.

Coleman, R.G., 1977. Ophiolites Ancient Oceanic Lithosphere? Springer-Verlag, Berlin Heidelberg New York (229 pp.).

Coleman, R.G., Keith, T.E., 1971. A chemical study of serpentinization — Burro Mountain, California. Journal of Petrology 12, 311–328.

Contreras-Reyes, E., Grevemeyer, I., Flueh, E.R., Scherwath, M., 2007. Alteration of the subducting oceanic lithosphere at the southern central Chile trench/outer rise. Geochemistry, Geophysics, Geosystems 8. http://dx.doi.org/10.1029/2007GC001632.

Currie, C., Wang, K., Hyndman, R.D., He, J., 2004. The thermal effects of steady state slab-driven mantle flow above a subducting plate: the Cascadia subduction zone and backarc. Earth and Planetary Science Letters 223, 35–48.

Davies, J.H., 1999. Simple analytic model for subduction zone thermal structure. Geophysical Journal International 139 (3), 823–828.

De Hoog, J.C.M., Janák, M., Vrabec, M., Froitzheim, N., 2009. Serpentinised peridotites from an ultrahigh-pressure terranes in the Pohorje Mts. (Eastern Alps, Slovenia): geochemical constraints on petrogenesis and tectonic setting. Lithos 109, 209–222.

De Hoog, J.C.M., Janák, M., Vrabec, M., Hattori, K.H., 2011. Ultramafic cumulates of oceanic affinity in an intracontinental subduction zone: ultrahigh-pressure garnet peridotites from Pohorje (Eastern Alps, Slovenia). In: Dobrzhinetskaya, L., Cuthbert, S., Faryad, W. (Eds.), Ultrahigh Pressure Metamorphism. Elsevier, Amsterdam. http://dx.doi.org/10.1016/B978-0-12-385144-4.00012-6.

Decitre, S., Deloule, E., Reisberg, L., James, R., Agrinier, P., Mével, C., 2002. Behaviour of Li and its isotopes during serpentinization of oceanic peridotites. Geochemistry, Geophysics, Geosystems 3 (1). http://dx.doi.org/10.1029/2001GC000178.

Deer, W.A., Howie, R.A., Zussman, J., 1992. An Introduction to the Rock-forming Minerals, 2nd edition. Longman Scientific & Technical, Harlow.

Delacour, A., Früh-Green, G.L., Frank, M., Gutjahr, M., Kelley, D.S., 2008. Sr- and Nd-isotope geochemistry of the Atlantis Massif (30°N, MAR): implications for fluid fluxes and lithospheric heterogeneity. Chemical Geology 254, 19–35.

Deschamps, F., 2010. Caractérisation in situ des serpentines en contexte de subduction: De la nature à l'expérience. Unpublished doctoral dissertation Université Joseph Fourier, Grenoble (402 pp. (oai: tel.archives-ouvertes.fr:tel-00464129)).

Deschamps, F., Guillot, S., Godard, M., Chauvel, C., Andreani, M., Hattori, K., 2010. In situ characterization of serpentinites from forearc mantle wedges: timing of serpentinization and behavior of fluid-mobile elements in subduction zones. Chemical Geology 269, 262–277.

Deschamps, F., Guillot, S., Godard, M., Andreani, M., Hattori, K., 2011. Serpentinites act as sponges for fluid-mobile elements in abyssal and subduction zone environments. Terra Nova 23, 171–178.

Deschamps, F., Godard, M., Guillot, S., Chauvel, C., Andreani, M., Hattori, K., Wunder, B., France, L., 2012. Behavior of fluid-mobile elements in serpentines from abyssal to subduction environments: examples from Cuba and Dominican Republic. Chemical Geology 312–313, 93–117.

DeShon, H.R., Schwartz, S.Y., 2004. Evidence for serpentinization of the forearc mantle wedge along the Nicoya Peninsula. Geophysical Research Letters 31. http://dx.doi.org/10.1029/2004GL021179.

Dick, H.J.B., Bullen, T., 1984. Chromian spinel as a petrogenetic indicator in abyssal and alpine type peridotites and spatially associated lavas. Contributions to Mineralogy and Petrology 86, 54–76.

Dick, H.J.B., Lin, J., Schouten, H., 2003. An ultraslow-spreading class of ocean ridge. Nature 426, 405–412.

Douville, E., Charlou, J.L., Oelkers, E.H., Bienvenu, P., Jove Colon, C.F., Donval, J.P., Fouquet, Y., Pricur, D., Appriou, P., 2002. The rainbow vent fluids (36°14′N, MAR): the influence of ultramafic rocks and phase separation on trace element content in mid-Atlantic ridge hydrothermal fluids. Chemical Geology 184, 37–48.

Downes, H., Macdonald, R., Upton, B.G.J., Cox, K.G., Bodinier, J.-L., Mason, P.R.D., James, D., Hill, P.G., Hearn Jr., B.C., 2004. Ultramafic xenoliths from the Bearpaw Mountains, Montana, USA: evidence for multiple metasomatic events in the lithospheric mantle beneath the Wyoming craton. Journal of Petrology 45, 1631–1662.

Drouin, M., Godard, M., Ildefonse, B., Bruguier, O., Garrido, C., 2009. In situ geochemistry of olivine-rich troctolites (IODP Hole U1309D, Atlantis Massif, Mid-Atlantic Ridge, 30°N): a record of magmatic impregnation in the lower oceanic lithosphere. Chemical Geology 264, 71–88.

Drouin, M., Ildefonse, B., Godard, M., 2010. A microstructural imprint of melt impregnation in slow-spread lithosphere: olivine-rich troctolites from the Atlantis Massif (Mid-Atlantic Ridge 30°N, IODP Hole U1309D). Geochemistry, Geophysics, Geosystems 11. http://dx.doi.org/10.1029/02009GC002995.

Eberle, M.A., Grasset, O., Sotin, C., 2002. A numerical study of the interaction between the mantle wedge, subducting slab, and overriding plate. Physics of the Earth and Planetary Interiors 134 (3–4), 191–202.

Epp, D., Suyenaga, W., 1978. Thermal contraction and alteration of the oceanic crust. Geology 6, 726–728.
Escartin, J., Hirth, G., Evans, B., 1997. Effects of serpentinization on the lithospheric strength and the style of normal faulting at slow-spreading ridges. Earth and Planetary Science Letters 151, 181–189.
Escartin, J., Mével, C., MacLeod, C.J., McCaig, A.M., 2003. Constraints on deformation conditions and the origin of oceanic detachments: the mid-Atlantic ridge core complex at 15–45°N. Geochemistry, Geophysics, Geosystems 4, 1–37. http://dx.doi.org/10.1029/2002GC000472.
Evans, B.W., Johannes, W., Oterdoom, H., Trommsdorf, V., 1976. Stability of chrysotile and antigorite in the serpentine multisystem. Schweizerische Mineralogische und Petrographische Mitteilungen 56, 79–93.
Evans, B.W., Hattori, K., Baronnet, A., 2013. Serpentinite: what, why, where? Elements 9, 99–106.
Fabries, J., Bodinier, J.-L., Dupuy, C., Lorand, J.-P., Benkerrou, C., 1989. Evidence for modal metasomatism in the orogenic spinel lherzolite body from Caussou (northeastern Pyrenees, France). Journal of Petrology 30, 199–228.
Francis, T.J.G., 1981. Serpentinization faults and their role in the tectonics of slow spreading ridges. Journal of Geophysical Research 86 (B12), 11,616–11,622.
Frey, F.A., Suen, J.C., Stockman, H.W., 1985. The Ronda high temperature peridotite: geochemistry and petrogenesis. Geochimica et Cosmochimica Acta 49, 2469–2491.
Früh-Green, G.L., Plas, A., Lécuyer, C., 1996. 14. Petrologic and stable isotope constraints on hydrothermal alteration and serpentinization of the EPR shallow mantle at Hess Deep (site 895). In: Mevel, C., Gillis, K.M., Allan, J.F., Meyer, P.S. (Eds.), Proceedings of the Ocean Drilling Program, Scientific Results, 147, pp. 255–291.
Fryer, P., 1992. 36. A synthesis of Leg 125 drilling of serpentine seamounts on the Mariana and Izu–Bonin forearcs. In: Fryer, P., Pearce, J.A., Stokking, L.B., et al. (Eds.), Proceedings of the Ocean Drilling Program, Scientific Results, 125, pp. 593–614.
Fryer, P., Fryer, G.J., 1987. Origin of non-volcanic seamounts in a forearc environment. Seamounts, Islands and Atolls: In: Keating, B., Fryer, P., Batiza, R. (Eds.), A.G.U. Geophysical Monograph, 43, pp. 61–69.
Fryer, P., Salisbury, M.H., 2006. Leg 195 synthesis: site 1200 — serpentinite seamounts of the Izu Bonin/Mariana convergent plate margin (ODP Leg 125 and 195 drilling results). In: Shinohara, M., Salisbury, M.H., Richter, C. (Eds.), Proceedings of the Ocean Drilling Program, Scientific Results, 195, pp. 1–30.
Fryer, P., Ambos, E.L., Hussong, D.M., 1985. Origin and emplacement of Mariana forearc seamounts. Geology 13, 774–777.
Fryer, P., Lockwood, J., Becker, N., Todd, C., Phipps, S., 2000. Significance of serpentine and blueschist mud volcanism in convergent margin settings. In: Dilek, Y., et al. (Ed.), Ophiolites and Oceanic Crust: New Insights from Field Studies and Ocean Drilling Program: Special Papers Geological Society of America, 349, pp. 35–51.
Fukao, Y., Hori, S., Ukawa, M., 1983. A seismological constraint on the depth of basalt–eclogite transition in a subducting oceanic crust. Nature 303, 413–415.
Furukawa, Y., 1993. Depth of the decoupling plate interface and thermal structure under arcs. Journal of Geophysical Research 98, 20,005–20,013.
Garrido, C.J., López Sánchez-Vizcaíno, V., Gómez-Pugnaire, M.T., Trommsdorff, V., Alard, O., Bodinier, J.-L., Godard, M., 2005. Enrichment of HFSE in chlorite-harzburgite produced by high-pressure dehydration of antigorite-serpentinite: Implications for subduction magmatism. Geochemistry, Geophysics, Geosystems 6 (1). http://dx.doi.org/10.1029/2004GC000791.
Gerya, T.V., Stöckhert, B., 2002. Exhumation rates of high pressure metamorphic minerals in subduction channels: the effect of rheology. Geophysical Research Letters 29, 1261. http://dx.doi.org/10.1029/2001GL014307.
Gerya, T.V., Yuen, D., 2003. Rayleigh–Taylor instabilities from hydration and melting propel "cold plumes" at subduction zones. Earth and Planetary Science Letters 212, 47–62.
Gerya, T.V., Stöckhert, B., Perchuk, A.L., 2002. Exhumation of high-pressure metamorphic rocks in a subduction channel: a numerical simulation. Tectonics 21, 1056. http://dx.doi.org/10.1029/2002TC001406.
Gill, J., 1981. Orogenic Andesites and Plate Tectonics. Springer-Verlag, New York (390 pp.).
Godard, M., Lagabrielle, Y., Alard, O., Harvey, J., 2008. Geochemistry of the highly depleted peridotites drilled at ODP Sites 1272 and 1274 (Fifteen-Twenty Fracture Zone, Mid-Atlantic Ridge): implications for mantle dynamics beneath a slow spreading ridge. Earth and Planetary Science Letters 267, 410–425.
Godard, M., Luquot, L., Andreani, M., Gouze, P., 2013. Incipient hydration of mantle lithosphere at ridges: A reactive-percolation experiment. Earth and Planetary Science Letters 371–372, 92–102.
Gorczyk, W., Guillot, S., Gerya, T.V., Hattori, K.H., 2007. Asthenospheric upwelling, oceanic slab retreat and exhumation of UHP mantle rocks: insights from Greater Antilles. Geophysical Research Letters 34. http://dx.doi.org/10.1029/2007GL031059.
Grauch, R.I., 1989. Rare earth elements in metamorphic rocks. In: Lipin, B.R., McKay, G.A. (Eds.), Geochemistry and Mineralogy of Rare Earth Elements. Reviews in Mineralogy and Geochemistry, vol. 21. Mineralogical Society of America, Washington, D. C., pp. 147–167.
Green II, H.W., 2007. Shearing instabilities accompanying high-pressure phase transformations and the mechanics of deep earthquakes. Proceedings of the National Academy of Sciences 104, 9133–9138.
Guillot, S., Hattori, K.H., De Sigoyer, J., 2000. Mantle wedge serpentinization and exhumation of eclogites: insights from eastern Ladakh, northwest Himalaya. Geology 28, 199–202.
Guillot, S., Hattori, K.H., de Sigoyer, J., Nägler, T., Auzende, A.-L., 2001. Evidence of hydration of the mantle wedge and its role in the exhumation of eclogites. Earth and Planetary Science Letters 193, 115–127.
Guillot, S., Hattori, K.H., Agard, P., Schwartz, S., Vidal, O., 2009. Exhumation processes in oceanic and continental subduction contexts: a review. Special volume, Subduction Zone Geodynamics. Frontiers in Earth Sciences 175–205.
Hacker, B., Abers, G., Peacock, S., 2003. Subduction factory 1. Theoretical mineralogy densities, seismic wave speeds, and H_2O contents. Journal of Geophysical Research 108 (B1). http://dx.doi.org/10.1029/2001JB001127.
Hart, S.R., Zindler, A., 1986. In search of a bulk-Earth composition. Chemical Geology 57 (3–4), 247–267.
Hattori, K.H., Guillot, S., 2003. Volcanic fronts form as a consequence of serpentinite dehydration in the forearc mantle wedge. Geology 31 (6), 525–528.
Hattori, K.H., Guillot, S., 2007. Geochemical character of serpentinites associated with high- to ultrahigh-pressure metamorphic rocks in the Alps, Cuba, and the Himalayas: recycling of elements in subduction zones. Geochemistry, Geophysics, Geosystems 8 (9). http://dx.doi.org/10.1029/2007GC001594.
Hattori, K., Takahashi, Y., Guillot, S., Johanson, B., 2005. Occurrence of arsenic (V) in forearc mantle serpentinites based on X-ray absorption spectroscopy study. Geochimica et Cosmochimica Acta 69, 5585–5596.
Hattori, K.H., Wallis, S., Enami, T., Mizukami, T., 2010. Subduction of mantle wedge peridotites: evidence from the Higashi-akaishi ultramafic body in the Sanbagawa metamorphic belt. Island Arc 19, 192–207.
Hellebrand, E., Snow, J.E., Dick, H.J.B., Hofmann, A.W., 2001. Coupled major and trace elements as indicators of the extent of melting in mid-ocean-ridge peridotites. Nature 410, 677–681.
Hemley, J.J., Montoya, J.W., Christ, C.L., Hostetler, P.B., 1977. Mineral equilibria in the $MgO–SiO_2–H_2O$ system: I talc–chrysotile–forsterite–brucite stability relations. American Journal of Science 277, 322–351.
Hermann, J., Müntener, O., Scambelluri, M., 2000. The importance of serpentinite mylonites for subduction and exhumation of oceanic crust. Tectonophysics 327, 225–238.
Hilairet, N., Reynard, B., 2009. Stability and dynamics of serpentinite layer in subduction zone. Tectonophysics 465, 24–29.
Hilairet, N., Reynard, B., Wang, Y., Daniel, I., Merkel, S., Nishiyama, N., Petitgirad, S., 2007. High-pressure creep of serpentine, interseismic deformation, and initiation of subduction. Science 318, 1910–1913.
Hirth, G., Guillot, S., 2013. Rheology and tectonic significance of serpentinite. Elements 9, 107–113.
Hirth, G., Kohlstedt, D., 1996. Water in the oceanic upper mantle: implications for rheology, melt extraction and the evolution of the lithosphere. Earth and Planetary Science Letters 144 (1–2), 93–108.
Honnorez, J., Kirst, P., 1975. Petrology of rodingites from the equatorial Mid-Atlantic fracture zones and their geotectonic significance. Contributions to Mineralogy and Petrology 49, 233–257.
Humphris, S.E., 1984. The mobility of rare earth elements in the crust. In: Henderson, P. (Ed.), Rare Earth Element Geochemistry, pp. 317–342.
Hyndman, R.D., Peacock, S.M., 2003. Serpentinization of the forearc mantle. Earth and Planetary Science Letters 212, 417–432.
Hyndman, R.D., Currie, C.A., Mazzotti, S.P., 2005. Subduction zone backarcs, mobile belts, and orogenic heat. GSA Today 15 (2), 4–10.
Irvine, T.N., 1967. Chromian spinel as a petrogenetic indicator; part II, petrologic applications. Canadian Journal of Earth Sciences 4, 71–103.
Ishii, T., Robinson, P.T., Maekawa, H., Fiske, R., 1992. 27. Petrological studies of peridotites from diapiric serpentinite seamounts in the Izu–Ogasawara–Mariana forearc, Leg 125. In: Fryer, P., Pearce, J.A., Stokking, L.B., et al. (Eds.), Proceedings of the Ocean Drilling Program, Scientific Results, 125, pp. 445–485.
Ishikawa, T., Tera, F., Nakazawa, T., 2001. Boron isotope and trace element systematics of three volcanic zones in the Kamchatka arc. Geochimica et Cosmochimica Acta 24, 4523–4537.
Iwamori, H., 1998. Transportation of H_2O and melting in subduction zone. Earth and Planetary Science Letters 160, 65–80.
Iyer, K., Austrheim, H., John, T., Jamtveit, B., 2008. Serpentinization of the oceanic lithosphere and some geochemical consequences: constraints from the Leka Ophiolite Complex, Norway. Chemical Geology 249, 66–90.
Jagoutz, E., Palme, H., Baddenhausen, H., Blum, K., Cendales, M., Dreibus, G., Spettel, B., Lorenz, V., Vanke, H., 1979. The abundance of major, minor and trace elements in the earth's mantle as derived from primitive ultramafic nodules. Geochimica et Cosmochimica Acta 11 (2), 2031–2050.
Janecky, D.R., Seyfried Jr., W.E., 1986. Hydrothermal serpentinisation of peridotite within the oceanic crust: experimental investigations of mineralogy and major element chemistry. Geochimica et Cosmochimica Acta 50, 1357–1378.
Jean-Baptise, P., Charlou, J.L., Stievenard, M., Donval, J.P., Bougault, H., Mével, C., 1991. Helium and methane measurements in hydrothermal fluids from the Mid-Atlantic ridge: the Snake Pit site at 23°N. Earth and Planetary Science Letters 106, 17–28.
John, T., Scambelluri, M., Frische, M., Barnes, J., Bach, W., 2011. Dehydration of subducting serpentinite: implications for halogen mobility in subduction zones and the deep halogen cycle. Earth and Planetary Science Letters 308, 65–76.
Jöns, N., Bach, W., Klein, F., 2010. Magmatic influence on reaction paths and element transport during serpentinisation. Chemical Geology 274, 196–211.
Kamiya, S., Kobayashi, Y., 2000. Seismological evidence for the existence of serpentinized wedge mantle. Geophysical Research Letters 27, 819–822.
Karson, J.A., Lawrence, R.M., 1997. Tectonic setting of serpentinite exposures on the western median valley wall of the MARK area in the vicinity of site 920. In: Karson, J.A., Cannat, M., Miller, D.J., Elthon, D. (Eds.), Proceedings of the Ocean Drilling Program, Scientific Results, 153. Ocean Drilling Program, College Station, TX, pp. 5–21.
Karson, J.A., Kelley, D.S., Williams, E.A., Yoerger, D.R., Jakuba, M., 2006. Detachment shear zone of the Atlantis Massif core complex, Mid-Atlantic Ridge, 30°N. Geochemistry, Geophysics, Geosystems 7. http://dx.doi.org/10.1029/2005GC001109.

Kawakatsu, H., Watada, S., 2007. Seismic evidence for deep-water transportation in the mantle. Science 316, 1468–1471.
Kelemen, P.B., Hirth, G., Shimizu, N., Spiegelman, M., Dick, H.J.B., 1997. A review of melt migration processes in the adiabatically upwelling mantle beneath oceanic spreading ridges. Philosophical Transactions of the Royal Society, London A 355, 283–318.
Kelemen, P.B., Hart, S.R., Bernstein, S., 1998. Silica enrichment in the continental upper mantle via melt/rock reaction. Earth and Planetary Science Letters 164, 387–406.
Kelemen, P.B., Rilling, J.L., Parmentier, E.M., Mehl, L., Hacker, B., 2003. Thermal structure due to solid-state flow in the mantle wedge beneath arcs. In: Eiler, J. (Ed.), Inside the Subduction Factory, Geophysical Monograph Series, 138. AGU, Washington D.C., pp. 293–309.
Kendrick, M.A., Scambelluri, M., Honda, M., Phillips, D., 2011. High abundances of noble gas and chlorine delivered to the mantle by serpentinite subduction. Nature Geoscience 4, 807–812.
Keppler, H., 1996. Constraints from partitioning experiments on the composition of subduction-zone fluids. Nature 380, 237–240.
Kerrick, D.M., 2002. Serpentinite seduction. Science 298, 1344–1345.
King, R.L., Kohn, M., Eiler, J., 2003. Constraints on the petrologic structure of the subduction zone slab-mantle interface from Franciscan Complex exotic ultramafic blocks. Geological Society of America Bulletin 115 (9), 1097–1109.
King, R.L., Bebout, G.E., Moriguti, T., Nakamura, E., 2006. Elemental mixing systematics and Sr–Nd isotope geochemistry of mélange formation: obstacles to identification of fluid sources to arc volcanics. Earth and Planetary Science Letters 246, 288–304.
Klein, E.M., 2003. Geochemistry of the igneous crust. Treatise on Geochemistry, Vol. 3: The Crust. In: Rudnick, R.L. (Ed.), Treatise on Geochemistry. Elsevier Science Ltd., pp. 433–463.
Kodolányi, J., Pettke, T., 2011. Loss of trace elements from serpentinites during fluid-assisted transformation of chrysotile to antigorite — an example from Guatemala. Chemical Geology 284, 351–362.
Kodolányi, J., Pettke, T., Spandler, C., Kamber, B.S., Gméling, K., 2012. Geochemistry of ocean floor and fore-arc serpentinites: constraints on the ultramafic input to subduction zones. Journal of Petrology 53, 235–270.
Kong, L.S., Solomon, S.C., Purdy, G.M., 1992. Microearthquake characteristics of a mid-ocean ridge along axis high. Journal of Geophysical Research 97, 1659–1685.
Korenaga, J., Karato, S.-I., 2008. A new analysis of experimental data on olivine rheology. Journal of Geophysical Research 113 (B02403). http://dx.doi.org/10.1029/2007JB005100.
Kubo, K., 2002. Dunite formation processes in highly depleted peridotite: case study of the Iwanaidake peridotite, Hokkaido, Japan. Journal of Petrology 43, 423–448.
Lafay, R., Deschamps, F., Schwartz, S., Guillot, S., Godard, M., Debret, B., Nicollet, C., 2013. High-pressure serpentinites, a trap-and-release system controlled by metamorphic conditions: example from the Piedmont zone of the western Alps. Chemical Geology 343, 38–54.
Lagabrielle, Y., Karpoff, A.-M., Cotton, J., 1992. 18. Mineralogical and geochemical analyses of sedimentary serpentinites from conical seamount (Hole 778A): implications for the evolution of serpentine seamounts. In: Fryer, P., Pearce, J.A., Stokking, L.B., et al. (Eds.), Proceedings of the Ocean Drilling Program, Scientific Results, 125, pp. 325–342.
Lallemand, S., 1999. La subduction océanique. Gordon & Breach Science Publishers, London (208 pp.).
Leblanc, M., Lbouabi, M., 1988. Native silver mineralization along a rodingite tectonic contact between serpentinite and quartz diorite (Bou Azzer, Morocco). Economic Geology 83, 1379–1391.
Lee, C.-T.A., Brandon, A.D., Norman, M., 2003. Vanadium in peridotites as a proxy of Paleo-fO_2 during partial melting: prospects, limitations and implications. Geochimica et Cosmochimica Acta 67, 3045–3064.
Lee, C.-T.A., Leeman, W.P., Canil, D., Li, Z.-X.A., 2005. Similar V/Sc systematics in MORB and arc basalts: implications for the oxygen fugacities of their mantle source regions. Journal of Petrology 46, 2313–2336.
Lee, C.-T.A., Oka, M., Luffi, P., Agranier, A., 2008. Internal distribution of Li and B in serpentinites from the Feather River Ophiolite, California, based on laser ablation inductively coupled plasma mass spectrometry. Geochemistry, Geophysics, Geosystems. http://dx.doi.org/10.1029/2008GC002078.
Leeman, W.P., 1996. Boron and other fluid-mobile elements in volcanic arc lavas: implications for subduction processes. In: Bebout, G.E., et al. (Ed.), Subduction Top to Bottom: American Geophysical Union Geophysical Monograph, 96, pp. 269–276.
Li, Z.-X.A., Lee, C.-T.A., 2006. Geochemical investigation of serpentinized oceanic lithospheric mantle in the Feather River Ophiolite, California: implications for the recycling rate of water by subduction. Chemical Geology 235, 161–185.
Li, Y.H., Schoonmaker, J., 2003. 7.01 Chemical composition and mineralogy of marine sediments. Treatise on Geochemistry, Vol. 7: Sediments, Diagenesis, and Sedimentary Rocks. In: Mackenzie, F.T. (Ed.), Treatise on Geochemistry. Elsevier Science Ltd., pp. 1–35.
Li, X.-P., Rahn, M., Bucher, K., 2004. Serpentinites of the Zermatt-Saas ophiolite complex and their texture evolution. Journal of Metamorphic Geology 22, 159–177.
Ludden, J.N., Thompson, G., 1979. An evaluation of the behavior of the rare earth elements during the weathering of sea-floor basalt. Earth and Planetary Science Letters 43, 85–92.
MacLeod, C.J., Escartín, J., Banks, G.J., Irving, D.H.B., Lilly, R.M., Niu, Y.-L., Banerji, D., McCaig, A., Allerton, S., Smith, D.K., 2002. Direct geological evidence for oceanic detachment faulting: the Mid-Atlantic Ridge, 15°45′N. Geology 30, 879–882.
MacLeod, C., Searle, R.C., Murton, B.J., Casey, J.F., Mallows, C., Unsworth, S.C., Achenbach, K.L., Harris, M., 2009. Life cycle of oceanic core complexes. Earth and Planetary Science Letters 287, 333–344.
Marchesi, C., Garrido, C.J., Godard, M., Proenza, J.A., Gervilla, F., Blanco-Moreno, J., 2006. Petrogenesis of highly depleted peridotites and gabbroic rocks from the Mayari-Baracoa Ophiolitic Belt (eastern Cuba). Contributions to Mineralogy and Petrology 151, 717–736.
Marchesi, C., Garrido, C.J., Godard, M., Belley, F., Ferré, E., 2009. Migration and accumulation of ultra-depleted subduction-related melts in the Massif du Sud ophiolite (New Caledonia). Chemical Geology 266, 171–186.
Marchesi, C., Garrido, C.J., Padrón-Navarta, J.A., López Sánchez-Vizcaíno, V., Gómez-Pugnaire, M.T., 2013. Element mobility from seafloor serpentinization to high-pressure dehydration of antigorite in subducted serpentinites: insights from the Cerro del Almirez ultramafic massif (southern Spain). Lithos. http://dx.doi.org/10.1016/j.lithos.2012.11.025.
Marschall, H.R., Altherr, R., Rüpke, L., 2007. Squeezing out the slab — modelling the release of Li, Be and B during progressive high pressure metamorphism. Chemical Geology 239, 323–335.
Martin, B., Fyfe, W.S., 1970. Some experimental and theoretical observations on the kinetics of hydration reactions with particular reference to serpentinization. Chemical Geology 6, 185–202.
McDonough, W.F., Sun, S.-S., 1995. The composition of the Earth. Chemical Geology 120, 223–253.
Melekhova, E., Schmidt, M.W., Ulmer, P., Pettke, T., 2007. The composition of liquids coexisting with dense hydrous magnesium silicates at 11–13.5 GPa and the end-points of the solidi in the $MgO–SiO_2–H_2O$ system. Geochimica et Cosmochimica Acta 71, 3348–3360.
Menzies, M., Long, A., Ingram, G., Tatnell, M., Janecky, D.R., 1993. MORB peridotite–seawater interaction: experimental constraints on the behaviour of trace elements, $^{87}Sr/_{86}Sr$ and $^{143}Nd/^{144}Nd$ ratios. In: Prichard, H.M., Alabaster, T., Harris, N.B.W., Neary, C.R. (Eds.), Magmatic processes and plate tectonics: Geological Society Special Publications, 76, pp. 309–322.
Mével, C., 2003. Serpentinization of abyssal peridotites at mid-ocean ridges. Comptes Rendus Géoscience 335, 825–852.
Mével, C., Stamoudi, C., 1996. Hydrothermal alteration of the upper mantle section at Hess Deep. In: Mével, C., Gillis, K., Allan, J. (Eds.), Proceedings of the Ocean Drilling Program, Scientific Results, 147, pp. 293–309.
Mibe, K., Fujii, T., Yasuda, A., 2002. Composition of aqueous fluid coexisting with mantle minerals at high pressure and its bearing on the differentiation of the Earth's mantle. Geochimica et Cosmochimica Acta 66, 2273–2285.
Michael, P.J., Bonatti, E., 1985. Peridotite composition from the North Atlantic; regional and tectonic variations and implications for partial melting. Earth and Planetary Science Letters 73, 91–104.
Michael, P.J., Langmuir, C.H., Dick, H.J.B., Snow, J.E., Goldstein, S.L., Graham, D.W., Lehnert, K., Kurras, G., Jokat, W., Mühe, R., Edmonds, H.N., 2003. Magmatic and amagmatic seafloor generation at the ultraslow-spreading Gakkel ridge, Arctic Ocean. Nature 423, 956–961.
Miyashiro, A., Shido, F., Ewing, M., 1969. Composition and origin of serpentinites from the Mid-Atlantic Ridge near 24 and 30°N. Contributions to Mineralogy and Petrology 23, 117–127.
Mohn, G., Manatschal, G., Beltrando, M., Masini, E., Kusznir, N., 2012. Necking of continental crust in magma-poor rifted margins: evidence from the fossil Alpine Tethys margins. Tectonics 31. http://dx.doi.org/10.1029/2011TC002961.
Moll, M., Paulick, H., Suhr, G., Bach, W., 2007. Data report: microprobe analyses of primary phases (olivine, pyroxene, and spinel) and alteration products (serpentine, iowaite, talc, magnetite, and sulfides) in Holes 1268A, 1272A, and 1274A. In: Kelemen, J., Kikawa, E., Miller, D.J. (Eds.), Proceedings of the Ocean Drilling Program, Scientific Results 209, pp. 1–13. http://dx.doi.org/10.2973/odp.proc.sr.209.003.2007.
Morishita, T., Hara, K., Nakamura, K., Sawaguchi, T., Tamura, A., Arai, S., Okino, K., Takai, K., Kumagai, H., 2009. Igneous, alteration and exhumation processes recorded in abyssal peridotites and related fault rocks from an oceanic core complex along the Central Indian Ridge. Journal of Petrology 50, 1299–1325.
Morris, J., Leemann, W., Tera, F., 1990. The subducted component in island arc lavas: constraints from Be isotopes and B-Be systematics. Nature 344, 31–36.
Mottl, M.J., Wheat, C.G., Fryer, P., Gharib, J., Martin, J.B., 2004. Chemistry of springs across the Mariana forearc shows progressive devolatilization of the subducting plate. Geochimica et Cosmochimica Acta 68, 4915–4933.
Müntener, O., Manastchal, G., Desmurs, L., Pettke, L., 2010. Plagioclase peridotites in ocean–continent transitions: refertilized mantle domains generated by melt segregation in the shallow mantle lithosphere. Journal of Petrology 51, 255–294.
Nakamura, Y., Kushiro, I., 1974. Composition of the gas phase in $Mg_2SiO_4–SiO_2–H_2O$ at 15 kbar. Carnegie Institution of Washington Yearbook 73, 255–258.
Navon, O., Stolper, E., 1987. Geochemical consequences of melt percolation: the upper mantle as a chromatographic column. Journal of Geology 95, 285–307.
Négrel, P., Guerrot, C., Cocherie, A., Azaroual, M., Brach, M., Fouillac, C., 2000. Rare earth elements, neodymium and strontium isotopic systematics in mineral waters: evidence from the Massif Central, France. Applied Geochemistry 15, 1345–1367.
Nesbitt, H.W., 1979. Mobility and fractionation of rare earth elements during weathering of a granodiorite. Nature 279, 207–210.
Niu, Y., 2004. Bulk-rock major and trace element compositions of abyssal peridotites: implications for mantle melting, melt extraction and post-melting processes beneath mid-ocean ridges. Journal of Petrology 45, 2423–2458.
Niu, Y., Hekinian, R., 1997. Spreading rate dependence of the extent of mantle melting beneath ocean ridges. Nature 385, 326–329.
Niu, Y., Langmuir, C.H., Kinzler, R.J., 1997. The origin of abyssal peridotites: a new perspective. Earth and Planetary Science Letters 152, 251–265.
Noll Jr., P.D., Newsom, H.E., Leeman, W.P., Ryan, J.G., 1996. The role of hydrothermal fluids in the production of subduction zone magmas: evidence from siderophile and chalcophile trace elements and boron. Geochimica et Cosmochimica Acta 60, 587–611.

O'Hanley, D.S., 1991. Fault-related phenomena associated with hydration and serpentine recrystallisation during serpentinisation. Canadian Mineralogist 29, 21–35.
O'Hanley, D.S., 1996. Serpentinites, records of tectonic and petrological history. Oxford Monographs on Geology and Geophysics no 34.
Oelkers, H., Schott, J., 2001. An experimental study of enstatite dissolution rates as a function of pH, temperature, and aqueous Mg and Si concentration, and the mechanism of pyroxene/pyroxenoid dissolution. Geochimica et Cosmochimica Acta 65, 1219–1231.
Olivier, N., Boyet, M., 2006. Rare earth and trace elements of microbialites in Upper Jurassic coral- and sponge-microbialite reefs. Chemical Geology 230, 105–123.
Ozawa, K., 1994. Melting and melt segregation in the mantle wedge above a subduction zone; evidence from the chromite-bearing peridotites of the Miyamori ophiolite complex, northeastern Japan. Journal of Petrology 35, 647–678.
Pabst, S., Zack, T., Savov, I.P., Ludwig, T., Rost, D., Vicenzi, E., 2011. Evidence for boron incorporation into the serpentine crystal structure. American Mineralogist 96, 1112–1119.
Padrón-Navarta, J.A., López Sánchez-Vizcaíno, V., Garrido, C.J., Gómez-Pugnaire, M.T., Jabaloy, A., Capitani, G.C., Mellini, M., 2008. Highly ordered antigorite from Cerro del Almirez HP–HT serpentinites, SE Spain. Contributions to Mineralogy and Petrology 156, 679–688.
Padrón-Navarta, J.A., López Sánchez-Vizcaino, V., Garrido, C.J., Gómez-Pugnaire, M.T., 2011. Metamorphic record of high-pressure dehydration of antigorite serpentinite to chlorite harzburgite in a subduction setting (Cerro del Almirez, Nevado-Filábride complex, Southern Spain). Journal of Petrology 52, 2047–2078.
Palandri, J.L., Reed, M.H., 2004. Geochemical models of metasomatism in ultramafic systems: serpentinization, rodingitization, and sea floor carbonate chimney precipitation. Geochimica et Cosmochimica Acta 68, 1115–1133.
Parkinson, I.J., Arculus, R.J., 1999. The redox state of subduction zone: insights from arc peridotites. Chemical Geology 160, 409–423.
Parkinson, I.J., Pearce, J.A., 1998. Peridotites from the Izu–Bonin–Mariana forearc (ODP Leg 125): evidence for mantle melting and melt–mantle interaction in a supra-subduction zone setting. Journal of Petrology 39 (9), 1577–1618.
Parkinson, I.J., Pearce, J.A., Thirlwall, M.F., Johnson, K.T.M., Ingram, G., 1992. Trace element geochemistry of peridotites from the Izu–Bonin–Mariana forearc, Leg 125. Proceedings of Ocean Drilling Program, Scientific Results 125, 487–506.
Paulick, H., Bach, W., Godard, M., De Hoog, J.C.M., Suhr, G., Harvey, J., 2006. Geochemistry of abyssal peridotites (Mid-Atlantic Ridge, 15°20′N, ODP Leg 209): implications for fluid/rock interaction in slow spreading environments. Chemical Geology 234, 179–210.
Pawley, A., Holloway, J.R., 1993. Water sources for subduction zone volcanism — new experimental constraints. Science 260, 664–667.
Peacock, S.M., 1987a. Serpentinization and infiltration metasomatism in the Trinity peridotite, Klamath province, northern California: implications for subduction zones. Contributions to Mineralogy and Petrology 95, 55–70.
Peacock, S.M., 1987b. Thermal effects of metamorphic fluids in subduction zones. Geology 15, 1057–1060.
Peacock, S.M., 1990. Fluid processes in subduction zones. Science 258, 329–337.
Peacock, S.M., 1993. Large-scale hydration of the lithosphere above subducting slabs. Chemical Geology 108, 49–59.
Peacock, S.M., Wang, K., 1999. Seismic consequences of warm versus cool subduction metamorphism: examples from southwest and northeast Japan. Science 286, 937–939.
Pearce, J.A., Barker, P.F., Edwards, S.J., Parkinson, I.J., Leat, P.T., 2000. Geochemistry and tectonic significance of peridotites from the South Sandwich arc-basin system, South Atlantic. Contributions to Mineralogy and Petrology 139, 36–53.
Pelletier, L., Müntener, O., Kalt, A., Vennemann, T.W., Belgya, T., 2008. Emplacement of ultramafic rocks into the continental crust monitored by light and other trace elements: an example from the Geisspfad body (Swiss–Italian Alps). Chemical Geology 255, 143–159.
Pereira, M.D., Peinado, M., Blanco, J.A., Yenes, M., 2008. Geochemical characterization of serpentinites at Cabo Ortegal, northwestern Spain. The Canadian Mineralogist 46, 317–327.
Plank, T., Langmuir, C.H., 1993. Tracing trace elements from sediment input to volcanic output at subduction zones. Nature 362, 163–165.
Plank, T., Langmuir, C.H., 1998. The chemical composition of subducting sediments and its consequences for the crust and mantle. Chemical Geology 145, 325–394.
Poitrasson, F., Pin, C., Duthou, J.L., 1995. Hydrothermal remobilization of rare earth elements and its effect on Nd isotopes in rhyolite and granite. Earth and Planetary Science Letters 130, 1–11.
Poli, S., Schmidt, M.W., 1995. H_2O transport and release in subduction zones: experimental constraints on basaltic and andesitic systems. Journal of Geophysical Research 100 (B11), 22,299–22,314.
Prichard, H.M., 1979. A petrographic study of the process of serpentinisation in ophiolites and the oceanic crust. Contributions to Mineralogy and Petrology 63, 231–241.
Quinby-Hunt, M.S., Turekian, K.K., 1983. Distribution of elements in sea water. Eos 64, 130–132.
Ranero, C., Morgan, J.P., McIntosh, K., Reichert, C., 2003. Bending-related faulting and mantle serpentinization at the Middle America trench. Nature 425, 367–373.
Ranero, C., Villaseñor, A., Morgan, J.P., Weinrebe, W., 2005. Relationship between bend-faulting at trenches and intermediate-depth seismicity. Geochemistry, Geophysics, Geosystems 6. http://dx.doi.org/10.1029/2005GC000997.
Rüpke, L.H., Morgan, J.P., Hort, M., Connolly, J.A.D., 2002. Are the regional variations in Central American arc lavas due to differing basaltic versus peridotitic slab sources of fluids? Geology 30, 1035–1038.
Rüpke, L.H., Morgan, J.P., Hort, M., Connolly, J.A.D., 2004. Serpentine and the subduction zone water cycle. Earth and Planetary Science Letters 223, 17–34.
Ryan, J.G., Morris, J., Tera, F., Leeman, W.P., Tsvetkov, A., 1995. Cross-arc geochemical variations in the Kurile arc as a function of slab depth. Science 270, 625–627.
Sakai, R., Kusakabe, M., Noto, M., Ishii, T., 1990. Origin of waters responsible for serpentinization of the Izu–Ogasawara–Mariana forearc seamounts in view of hydrogen and oxygen isotope ratios. Earth and Planetary Science Letters 100, 291–303.
Salters, V.J.M., Stracke, A., 2004. Composition of the depleted mantle. Geochemistry, Geophysics, Geosystems 5 (5). http://dx.doi.org/10.1029/2003GC000597.
Saumur, B.-M., Hattori, K.H., 2013. Zoned Cr-spinel in forearc serpentinites along the northern Caribbean Margin, Dominican Republic. Mineralogical Magazine 77, 117–136.
Saumur, B.-M., Hattori, K.H., Guillot, S., 2010. Contrasting origins of serpentinites in a subduction complex, northern Dominican Republic. Geological Society of America Bulletin 122, 292–304.
Savov, I.P., Ryan, J.G., D'Antonio, M., Kelley, K., Mattie, P., 2005a. Geochemistry of serpentinized peridotites from the Mariana Forearc Conical Seamount, ODP Leg 125: implications for the elemental recycling at subduction zones. Geochemistry, Geophysics, Geosystems 6 (4). http://dx.doi.org/10.1029/2004GC000777.
Savov, I.P., Guggino, S., Ryan, J.G., Fryer, P., Mottl, M.J., 2005b. Geochemistry of serpentinite muds and metamorphic rocks from the Mariana forearc, ODP Sites 1200 and 778–779, South Chamorro and Conical Seamounts. In: Shinohara, M., Salisbury, M.H., Richter, C. (Eds.), Proceedings of the Ocean Drilling Program, Scientific Results, 195, pp. 1–49.
Savov, I.P., Ryan, J.G., D'Antonio, M., Fryer, P., 2007. Shallow slab fluid release across and along the Mariana arc-basin system: insights from geochemistry of serpentinized peridotites from the Mariana fore arc. Journal of Geophysical Research 112. http://dx.doi.org/10.1029/2006JB004749.
Scambelluri, M., Tonarini, S., 2012. Boron isotope evidence for shallow fluid transfer across subduction zones by serpentinized mantle. Geology 40, 907–910.
Scambelluri, M., Müntener, O., Hermann, J., Piccardo, G.B., Trommsdorff, V., 1995. Subduction of water into the mantle: history of an alpine peridotite. Geology 23 (5), 459–462.
Scambelluri, M., Bottazzi, P., Trommsdorff, V., Vannucci, R., Hermann, J., Gòmez-Pugnaire, M.T., Lòpez-Sànchez Vizcaìno, V., 2001a. Incompatible element-rich fluids released by antigorite breakdown in deeply subducted mantle. Earth and Planetary Science Letters 192, 457–470.
Scambelluri, M., Rampone, E., Piccardo, G.B., 2001b. Fluid and element cycling in subducted serpentinite: a trace-element study of the Erro–Tobbio high pressure ultramafites (Western Alps, NW Italy). Journal of Petrology 42 (1), 55–67.
Scambelluri, M., Fiebig, J., Malaspina, N., Müntener, O., Pettke, T., 2004a. Serpentinite subduction: implications for fluid processes and trace-element recycling. International Geology Review 46, 595–613.
Scambelluri, M., Müntener, O., Ottolini, L., Pettke, T.T., Vannucci, R., 2004b. The fate of B, Cl and Li in the subducted oceanic mantle and in the antigorite breakdown fluids. Earth and Planetary Science Letters 222, 217–234.
Schmidt, M.W., Poli, S., 1998. Experimentally based water budgets for dehydrating slabs and consequences for arc magma generation. Earth and Planetary Science Letters 163, 361–379.
Schmidt, M.W., Poli, S., 2003. Generation of mobile components during subduction of oceanic crust. In: Rudnick, R.L. (Ed.), Treatise on Geochemistry, Vol. 3: The Crust. Elsevier Science Ltd., pp. 567–593.
Schmidt, K., Koschinsky, A., Garbe-Schönberg, D., Carvalho (de), L.M., Seifert, R., 2007. Geochemistry of hydrothermal fluids from the ultramafic-hosted Logatchev hydrothermal field, 15°N on the Mid-Atlantic Ridge: temporal and spatial investigation. Chemical Geology 242, 1–21.
Schwartz, S., Allemand, P., Guillot, S., 2001. Numerical model of the effect of serpentinites on the exhumation of eclogitic rocks: insights from the Monviso ophiolitic massif (Western Alps). Tectonophysics 42, 193–206.
Seifert, K., Brunotte, D., 1996. Geochemistry of serpentinized mantle peridotite from site 897 in the Iberia Abyssal Plain. In: Whitmarsh, R.B., Sawyer, D.S., Klaus, A., Masson, D.G. (Eds.), Proceedings of the Ocean Drilling Program, Scientific Results, 149. Ocean Drilling Program, College Station, TX, pp. 413–424.
Seyfried Jr., W.E., Dibble Jr., W.E., 1980. Seawater–peridotite interaction at 300 °C and 500 bars: implications of the origin of oceanic serpentinites. Geochimica et Cosmochimica Acta 44, 309–321.
Seyler, M., Lorand, J.P., Dick, H.J.B., Drouin, M., 2007. Pervasive melt percolation reactions in ultra-depleted refractory harzburgites at the Mid-Atlantic Ridge, 15°2′N: ODP Hole 1274A. Contribution to Mineralogy and Petrology 153, 303–319.
Sharp, Z.D., Barnes, J.D., 2004. Water-soluble chlorides in massive seafloor serpentinites: a source of chloride in subduction zones. Earth and Planetary Sciences Letters 226, 243–254.
Shipboard Scientific Party, 2004. Leg 209 summary: drilling mantle peridotite along the Mid-Atlantic Ridge from 14° to 16°N: Sites 1268–1275. In: Kelemen, P.B., Kikawa, E., Miller, D.J., et al. (Eds.), Proceedings of ODP, Initial Reports 209. Ocean Drilling Program, College Station TX, pp. 1–139.
Singer, B.S., Jicha, B.R., Leeman, W.P., Rogers, N.W., Thirlwall, M.F., Ryan, J., Nicolaysen, K.E., 2007. Along-strike trace element and isotopic variation in Aleutian Island arc basalt: subduction melts sediments and dehydrates serpentine. Journal of Geophysical Research 112 (B06206). http://dx.doi.org/10.1029/2006JB004897.
Sinton, J.M., Detrick, R.S., 1992. Mid-ocean ridge magma chambers. Journal of Geophysical Research 97, 197–216.
Skelton, A.D.L., Valley, J.W., 2000. The relative timing of serpentinisation and mantle exhumation at the ocean–continent transition, Iberia: constraints from oxygen isotopes. Earth and Planetary Sciences 178, 327–338.

Smith, D., 1979. Hydrous minerals and carbonates in peridotite inclusions from the Green Knobs and Buell Park kimberlitic diatremes on the Colorado Plateau. The Mantle Sample: Inclusions in Kimberlites and Other Volcanics: In: Boyd, F.R., Meyer, H.O.A. (Eds.), Geophysical Monograph, American Geophysical Union, pp. 345–356.
Smith, D., Riter, J.C.A., Merzman, S.A., 1999. Erratum to "Water–rock interactions, orthopyroxene growth, and Si-enrichment in the mantle: evidence in xenoliths from the Colorado Plateau, southwestern United States". Earth and Planetary Science Letters 167, 347–356.
Snow, J.E., Dick, H.J.B., 1995. Pervasive magnesium loss by marine weathering of peridotite. Geochimica et Cosmochimica Acta 59, 4219–4235.
Sobolev, S.V., Chaussidon, M., 1996. H_2O concentrations in primary melts from supra-subduction zones and mid-ocean ridges: implications for H_2O storage and recycling in the mantle. Earth and Planetary Science Letters 137, 45–55.
Spivack, A.J., Edmond, J., 1987. Boron isotope exchange between seawater and oceanic crust. Geochimica et Cosmochimica Acta 51, 1033–1043.
Stalder, R., Ulmer, P., 2001. Phase relations of a serpentine composition between 5 and 14 GPa: significance of clinohumite and phase E as water carriers into the transition zone. Contributions to Mineralogy and Petrology 140, 670–679.
Stern, R.J., 2002. Subduction zones. Reviews of Geophysics 40 (4), 1012. http://dx.doi.org/10.1029/2001RG000108.
Stern, R.J., Kohut, E., Blomer, S.H., Leybourne, M., Fouch, M., Vervoort, J., 2006. Subduction factory processes beneath the Guguan cross-chain, Mariana Arc: no role for sediments, are serpentinites important? Contributions to Mineralogy and Petrology 151, 202–221.
Straub, S.M., Layne, G.D., 2002. The systematics of boron isotopes in Izu arc front volcanic rocks. Earth and Planetary Science Letters 198, 25–39.
Straub, S.M., Layne, G.D., 2003. Decoupling of fluids and fluid-mobile elements during shallow subduction; evidence from halogene-rich andesite melt inclusions from the Izu arc volcanic front. Geochemistry, Geophysics, Geosystems 4 (7). http://dx.doi.org/10.1029/2002GC000349.
Suen, C.J., Frey, F.A., 1987. Origins of the mafic and ultramafic rocks in the Ronda peridotite. Earth and Planetary Science Letters 85, 183–202.
Suhr, G., Kelemen, P., Paulick, H., 2008. Mid-Atlantic Ridge: tracking the fate of melts percolating in peridotite as the lithosphere is intercepted. Geochemistry, Geophysics, Geosystems 9. http://dx.doi.org/10.1029/2007GC001726.
Sutra, E., Manatschal, G., 2012. How does the continental crust thin in a hyperextended rifted margin? Insights from the Iberia margin. Geology 40, 139–142.
Tatsumi, Y., 1986. Formation of the volcanic front in subduction zones. Geophysical Research Letters 17, 717–720.
Tatsumi, Y., 2005. The subduction factory: how it operates in the evolving Earth. GSA Today 15 (7), 4–10.
Tatsumi, Y., Eggins, S., 1995. Subduction Zone Magmatism. Blackwell, Malden, Mass.(211 pp.).
Tatsumi, Y., Nakamura, N., 1986. Composition of aqueous fluid from serpentinite in the subducted lithosphere. Geochemical Journal 20, 191–196.
Tatsumi, Y., Hamilton, D.L., Nesbitt, R.W., 1986. Chemical characteristics of fluid phase released from a subducted lithosphere and origin of arc magmas: evidence from high-pressure experiments and natural rocks. Journal of Volcanology and Geothermal Research 29, 293–309.
Tenthorey, E., Hermann, J., 2004. Composition of fluids during serpentinite breakdown in subduction zones: evidence for limited boron mobility. Geology 32 (10), 865–868.
Thompson, G., Melson, W.G., 1970. Boron contents of serpentinites and metabasalts in the oceanic crust: implications for the boron cycle in the oceans. Earth and Planetary Science Letters 8, 61–65.
Tonarini, S., Agostini, S., Doglioni, C., Innocenti, F., Manetti, P., 2007. Evidence for serpentinite fluid in convergent margin systems: the example of El Salvador (Central America) arc lavas. Geochemistry, Geophysics, Geosystems 8 (9). http://dx.doi.org/10.1029/2006GC001508.
Tonarini, S., Leeman, W.P., Leat, P.T., 2011. Subduction erosion of forearc mantle wedge implicated in the genesis of the South Sandwich Island (SSI) arc: evidence from boron isotope systematics. Earth and Planetary Science Letters 301, 275–284.
Trommsdorff, V., López Sánchez-Vizcaíno, V., Gómez-Pugnaire, M.T., Müntener, O., 1998. High pressure breakdown of antigorite to spinifex-textured olivine and orthopyroxene, SE Spain. Contributions to Mineralogy and Petrology 132, 139–148.
Ulmer, P., Trommsdorff, V., 1995. Serpentine stability to mantle depths and subduction-related magmatism. Science 268 (5212), 858–861.
Ulrich, M., Picard, C., Guillot, S., Chauvel, C., Cluzel, D., Meffre, S., 2010. Multiple melting stages and refertilization as indicators for ridge to subduction formation: the New Caledonia ophiolite. Lithos 115, 223–236.
van Keken, P.E., Kiefer, B., Peacock, S.M., 2002. High-resolution models of subduction zones: Implications for mineral dehydration reactions and the transport of water into the deep mantle. Geochemistry, Geophysics, Geosystems 3 (10), 1056. http://dx.doi.org/10.1029/2001GC000256.
van Keken, P.E., Hacker, B.R., Syracuse, E.M., Abers, G.A., 2011. Subduction factory: 4. Depth-dependent flux of H_2O from subducting slabs worldwide. Journal of Geophysical Research 116. http://dx.doi.org/10.1029/2010JB007922.
Vils, F., Pelletier, L., Kalt, A., Müntener, O., Ludwig, T., 2008. The lithium, boron and beryllium content of serpentinized peridotites from ODP Leg 209 (Sites 1272A and 1274A): implications for lithium and boron budgets of oceanic lithosphere. Geochimica et Cosmochimica Acta 72, 5475–5504.
Vils, F., Müntener, O., Kalt, A., Ludwig, T., 2011. Implications of the serpentine phase transition on the behaviour of beryllium and lithium-boron of subducted ultramafic rocks. Geochimica et Cosmochimica Acta 75, 1249–1271.
Viti, C., Mellini, M., 1998. Mesh textures and bastites in the Elba retrograde serpentinites. European Journal of Mineralogy 10, 1341–1359.
Wang, J., Hattori, K.H., Kilian, R., Stern, C.R., 2007. Metasomatism of sub-arc mantle peridotites below southern South America: reduction of fO_2 by slab-melt. Contributions to Mineralogy and Petrology 153, 607–624.
Wang, J., Hattori, K.H., Stern, C., 2008. Metasomatic origin of garnet orthopyroxenites in the subcontinental lithospheric mantle underlying Pali Aike volcanic field, southern South America. Mineralogy and Petrology 94, 243–258.
Wicks, F.J., Whittaker, E.J.W., 1977. Serpentine texture and serpentinisation. Canadian Mineralogist 15, 459–488.
Wunder, B., Schreyer, W., 1997. Antigorite: high-pressure stability in the system MgO–SiO_2–H_2O (MSH). Lithos 41, 213–227.
Wunder, B., Wirth, R., Gottschalk, M., 2001. Antigorite: pressure and temperature dependence of polysomatism and water content. European Journal of Mineralogy 13, 485–495.
Wunder, B., Deschamps, F., Watenphul, A., Guillot, S., Meixner, A., Romer, R.L., Wirth, R., 2010. The effect of chrysotile-nanotubes on the serpentine-fluid Li-isotopic fractionation. Contributions to Mineralogy and Petrology 159, 781–790.
Xie, Z., Hattori, K., Wang, J., 2013. Origins of ultramafic rocks in the Sulu ultrahigh-pressure terrane, Eastern China. Lithos. 178, 158–170.
You, C.-F., Castillo, P.R., Gieskes, J.M., Chan, L.H., Spivack, A.J., 1996. Trace element behavior in hydrothermal experiments: implications for fluid processes at shallow depths in subduction zones. Earth and Planetary Science Letters 140, 41–52.